

THEORETICAL AND EXPERIMENTAL INVESTIGATION OF HETEROJUNCTION INTERFACES

FINAL REPORT FOR THE PERIOD
September 1, 1976 through June 30, 1983

AB-A235 896

CONTRACT NO. N00014-76-C-1109

Prepared for

Office of Naval Research
800 N. Quincy Street
Arlington, VA 22217

Principal Investigator: E.A. Kraut
Co-Principal Investigator: R.W. Grant
Key Personnel: J.R. Waldrop, S.P. Kowalczyk

NOVEMBER 1983

DTIC
S DEC 1 1983
A

Approved for public release; distribution unlimited

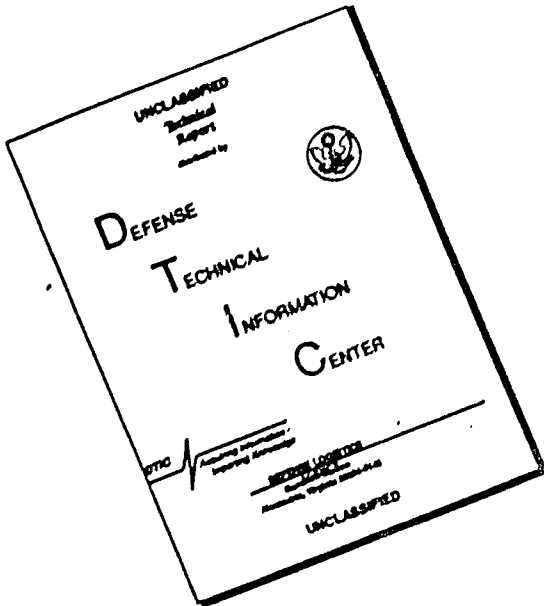
DTIC FILE COPY



Rockwell International

83 12 14 024

DISCLAIMER NOTICE



**THIS DOCUMENT IS BEST
QUALITY AVAILABLE. THE COPY
FURNISHED TO DTIC CONTAINED
A SIGNIFICANT NUMBER OF
PAGES WHICH DO NOT
REPRODUCE LEGIBLY.**

UNCLASSIFIED

SECURITY CLASSIFICATION OF THIS PAGE (When Data Entered)

REPORT DOCUMENTATION PAGE		READ INSTRUCTIONS BEFORE COMPLETING FORM															
1. REPORT NUMBER	2. GOVT ACCESSION NO.	3. RECIPIENT'S CATALOG NUMBER															
4. TITLE (and Subtitle) "THEORETICAL AND EXPERIMENTAL STUDY OF HETEROJUNCTION BANDMATCHING"		5. TYPE OF REPORT & PERIOD COVERED 9/1/76 - 6/30/83 FINAL REPORT															
7. AUTHOR(s) E.A. KRAUT, R.W. GRANT, J.R. WALDROP and S.P. KOWALCZYK		6. PERFORMING ORG. REPORT NUMBER MRDC41099.1FR															
8. CONTRACT OR GRANT NUMBER(s) N00014-76-C-1109		9. PERFORMING ORGANIZATION NAME AND ADDRESS MICROELECTRONICS RESEARCH AND DEVELOPMENT CENTER 3370 Miraloma Avenue Anaheim, CA 92803															
11. CONTROLLING OFFICE NAME AND ADDRESS		10. PROGRAM ELEMENT, PROJECT, TASK AREA & WORK UNIT NUMBERS															
		12. REPORT DATE November 1983															
		13. NUMBER OF PAGES 69															
14. MONITORING AGENCY NAME & ADDRESS(if different from Controlling Office)		15. SECURITY CLASS. (of this report) UNCLASSIFIED															
		15a. DECLASSIFICATION/DOWNGRADING SCHEDULE															
16. DISTRIBUTION STATEMENT (of this Report) Unlimited																	
<p style="text-align: right;">This document has been approved for public release and sale; its distribution is unlimited.</p>																	
17. DISTRIBUTION STATEMENT (of the abstract entered in Block 20, if different from Report)																	
18. SUPPLEMENTARY NOTES																	
19. KEY WORDS (Continue on reverse side if necessary and identify by block number) <table style="width: 100%; border-collapse: collapse;"> <tr> <td style="width: 33%;">Heterojunction</td> <td style="width: 33%;">XPS</td> <td style="width: 33%;">Interface dipoles</td> </tr> <tr> <td>Band discontinuities</td> <td>Ge</td> <td></td> </tr> <tr> <td>Core-level binding energies</td> <td>GaAs</td> <td></td> </tr> <tr> <td>Interface potential</td> <td>ZnSe</td> <td></td> </tr> <tr> <td>Semiconductor interface</td> <td>AlAs</td> <td></td> </tr> </table>			Heterojunction	XPS	Interface dipoles	Band discontinuities	Ge		Core-level binding energies	GaAs		Interface potential	ZnSe		Semiconductor interface	AlAs	
Heterojunction	XPS	Interface dipoles															
Band discontinuities	Ge																
Core-level binding energies	GaAs																
Interface potential	ZnSe																
Semiconductor interface	AlAs																
20. ABSTRACT (Continue on reverse side if necessary and identify by block number) <p>This is the final report for Contact # N00014-76-C-1109 which covered the period 9/1/76 through 6/30/83, and was entitled "Theoretical and Experimental Study of Heterojunction Bandmatching". A technique based on the use of x-ray photoelectron spectroscopy was developed to measure heterojunction band discontinuities with an uncertainty of ± 0.04 eV and changes in band discontinuities for a specific heterojunction interface with an uncertainty of ± 0.01 eV. This technique was used to investigate Ge-GaAs, GaAs-AlAs, ZnSe-GaAs.</p>																	

UNCLASSIFIED

SECURITY CLASSIFICATION OF THIS PAGE (When Data Entered)

and ZnSe-Ge heterojunctions. It was discovered that microscopic dipoles present at abrupt heterojunction interfaces can substantially affect observed band discontinuities. Variations in heterojunction band discontinuities as functions of crystallographic orientation, growth sequence, and growth conditions were observed. It was established that heterojunction band discontinuities depend on microscopic properties of the interface and cannot be predicted from individual semiconductor properties alone. Based on electrostatic considerations, it was shown that polar heterojunction interfaces cannot be atomically abrupt but must require at least two interfacial transition planes to be consistent with experimental observations.

UNCLASSIFIED

SECURITY CLASSIFICATION OF THIS PAGE (When Data Entered)



Rockwell International

MRDC41099.1FR

TABLE OF CONTENTS

	<u>Page</u>
1.0 INTRODUCTION.....	1
2.0 SUMMARY OF ACCOMPLISHMENTS.....	2
3.0 APPENDIX.....	3

Accession Per	
NTIS GRANT	<input checked="" type="checkbox"/>
FILE TAB	<input type="checkbox"/>
Revised	<input type="checkbox"/>
Classification	<input type="checkbox"/>
File No.	
Distribution	
Available Versions	
First	<input type="checkbox"/>
<i>[Signature]</i>	



i
C5570A/sn



Rockwell International

MRDC41099.1FR

1.0 INTRODUCTION

This is the final report for Contract No. N00014-76-C-1109 entitled, "Theoretical and Experimental Study of Heterojunction Bandmatching," which covered the period September 1976 to July 1983.

The energy-band discontinuities at an abrupt heterojunction interface are quantities of both practical and fundamental significance. The existence of these band discontinuities at an abrupt heterojunction provides the ability to selectively control transport properties of electrons and holes. The additional freedom in device design offered by heterojunctions permits new device concepts (for example, the high electron mobility transistor (HEMT)) to become feasible. Prior to initiation of this program, traditional methods of measuring band discontinuities yielded results with uncertainties of typically ± 0.1 eV. The ability to theoretically predict band offsets relied primarily on the electron affinity rule, which involves considerably larger uncertainties. Because device electrical characteristics are sensitive to potential variations on the order of the thermal energy, a clear need existed to improve the ability both to predict theoretically and to measure experimentally heterojunction band discontinuities.

The research program supported by Contract N00014-76-C-1109 developed an experimental technique based on the use of x-ray photoelectron spectroscopy (XPS) to measure band offsets with an absolute uncertainty of ± 0.04 eV and a relative uncertainty of ± 0.01 eV. In addition, the program contributed ideas to the development of a LCAO theory of heterojunctions by Prof. W.A. Harrison, which has substantially advanced the ability to predict band discontinuities. The accomplishments of this research program were reported in eleven publications.¹⁻¹¹ In Section 2.0 of this final report, the primary program accomplishments are briefly summarized. The Appendix (Section 3.0) reproduces the publications which were supported by this contract.



Rockwell International

MRDC41099.1FR

2.0 SUMMARY OF ACCOMPLISHMENTS

When this research program was initiated, a major objective was to determine heterojunction band discontinuities and factors which influence or control heterojunction band alignment; the program had both theoretical and experimental aspects. On the theoretical side, the problem was to predict accurately the magnitude of the conduction-and valence-band discontinuities at a heterojunction interface. It was proposed to do this by performing band structure calculations for lattice matched heterojunction pairs on an absolute energy scale so that valence-band discontinuities could be determined simply by subtracting tabulated energies of valence-band maxima. The problem was how to set up an absolute energy scale. Several discussions concerning this problem were held with Prof. W.A. Harrison (Department of Applied Physics, Stanford University). He suggested an energy scale based on Herman-Skillman ionization energies for free atoms corrected by a bonding energy which varies as the inverse square of bond length. This bonding correction takes into account the difference in ionization energies for a p-electron in a free atom, and a p-electron on an atom residing in a crystal lattice. Harrison published his LCAO theory (W.A. Harrison, J. Vac. Sci. Technol. 14, 1016 (1977)) and acknowledged our role in its development.

On the experimental side, the challenge was to develop an XPS method for measuring band discontinuities with an uncertainty on the order of the room temperature thermal energy. This new approach for measuring heterojunction band discontinuities was first described² in 1978 with refinements discussed in subsequent publications.^{5,8} The key factor required to apply XPS for heterojunction band discontinuity measurements is an accurate knowledge of core-level to valence-band maximum (VBM) binding-energy differences for the bulk semiconductors which form the abrupt heterojunction. The difficult part of this binding-energy difference measurement is the precise determination of the VBM in XPS data. A new approach for this determination was developed⁵ which involves least squares fitting of XPS data in the energy region around the VBM, with a function obtained by folding a theoretically calculated



MRDC41099.1FR

valence-band density of states with an experimentally determined instrumental response function. Detailed analysis¹⁰ of Ge and GaAs XPS data indicated that the uncertainty in determining the VBM position was < 0.019 eV, and that core level to VBM binding-energy differences for these materials could be determined with uncertainties < 0.026 eV. This uncertainty makes it possible to measure absolute heterojunction band discontinuities to \pm 0.04 eV, and in this program absolute band discontinuity measurements were carried out for Ge-GaAs,¹¹ GaAs-AlAs,⁶ ZnSe-GaAs⁷ and ZnSe-Ge⁷ heterojunctions.

Early in the program, it was found possible to measure changes in band discontinuities (relative values) with very high precision (\pm 0.01 eV) simply by monitoring changes in core-level binding-energy differences between atoms located on opposite sides of an abrupt heterojunction interface.¹ This excellent sensitivity led to the discovery that microscopic dipoles present at abrupt heterojunction interfaces can substantially affect observed band discontinuities. Variations in heterojunction band discontinuities were observed as functions of crystallographic orientation,^{1,11} growth sequence^{6,7} and growth conditions.^{6,7} It was also demonstrated by direct experimental test that heterojunction band discontinuities are nontransitive;⁴ this result established that band discontinuities depend on microscopic properties of the interface and cannot be predicted from individual semiconductor properties alone. The crystallographic orientation variation in band discontinuity for Ge-GaAs heterojunctions was examined in some detail theoretically.³ From electrostatic considerations, it was shown that polar interfaces cannot be atomically abrupt, but require at least two interfacial transition planes to be consistent with the experimental observations. The Fermi-level positions and band discontinuities were determined for Ge-GaAs (110) heterojunctions as a function of GaAs dopant type;⁹ these studies found no evidence for the presence of a dipole layer associated with interface defect levels.



Rockwell International

MRDC41099.1FR

3.0 APPENDIX

This appendix reproduces publications supported by Contract No. N00014-76-C-1109 in chronological order. These publications (which are referenced in this final report) are:

1. "Observation of the Orientation Dependence of Interface Dipole Energies in Ge-GaAs," R.W. Grant, J.R. Waldrop and E.A. Kraut, Phys. Rev. Lett. 40, 656 (1978).
2. "XPS Measurements of Abrupt Ge-GaAs Heterojunction Interfaces," R.W. Grant, J.R. Waldrop and E.A. Kraut, J. Vac. Sci. Technol. 15, 1451 (1978).
3. "Polar Heterojunction Interfaces," W.A. Harrison, E.A. Kraut, J.R. Waldrop and R.W. Grant, Phys. Rev. B 18, 4402 (1978).
4. "Semiconductor Heterojunction Interfaces: Nontransitivity of Energy-Band Discontinuities," J.R. Waldrop and R.W. Grant, Phys. Rev. Lett. 43, 1686 (1979).
5. "Precise Determination of the Valence-Band Edge in X-Ray Photoemission Spectra: Application to Measurement of Semiconductor Interface Potentials," E.A. Kraut, R.W. Grant, J.R. Waldrop and S.P. Kowalczyk, Phys. Rev. Lett. 44, 1520 (1980).
6. "XPS Measurement of GaAs-AlAs Heterojunction Band Discontinuities: Growth Sequence Dependence," J.R. Waldrop, S.P. Kowalczyk, R.W. Grant, E.A. Kraut and D.L. Miller, J. Vac. Sci. Technol. 19, 573 (1981).
7. "Measurement of ZnSe-GaAs (110) and ZnSe-Ge (110) Heterojunction Band Discontinuities by X-Ray Photoelectron Spectroscopy (XPS)," S.P. Kowalczyk, E.A. Kraut, J.R. Waldrop and R.W. Grant, J. Vac. Sci. Technol. 21, 482 (1982).
8. "Measurement of Potential at Semiconductor Interfaces by Electron Spectroscopy," R.W. Grant, E.A. Kraut, S.P. Kowalczyk and J.R. Waldrop, J. Vac. Sci. Technol. B 1, 320 (1983).
9. "Band Discontinuities and Interface Fermi-Level Positions in Ge-GaAs (110) Heterojunctions," S.P. Kowalczyk, R.W. Grant, J.R. Waldrop and E.A. Kraut, J. Vac. Sci. Technol. B 1, 684 (1983).



Rockwell International

MRDC41099.1FR

10. "Semiconductor Core-Level to Valence-Band Maximum Binding-Energy Differences: Precise Determination by X-Ray Photoelectron Spectroscopy," E.A. Kraut, R.W. Grant, J.R. Waldrop and S.P. Kowalczyk, Phys. Rev. B 28, 1965 (1983).
11. "Valence-Band Discontinuities for Abrupt (110), (100) and (111) Oriented Ge-GaAs Heterojunctions," J.R. Waldrop, E.A. Kraut, S.P. Kowalczyk and R.W. Grant, Surf. Sci. 132, 513 (1983).

Observation of the Orientation Dependence of Interface Dipole Energies in Ge-GaAs

R. W. Grant, J. R. Waldrop, and E. A. Kraut

Science Center, Rockwell International, Thousand Oaks, California 91360

(Received 19 December 1977)

The interfaces between a thin ($\sim 20\text{-}\text{\AA}$) abrupt epitaxial layer of Ge grown on substrates of (111), (110), and (100) GaAs have been investigated with x-ray photoelectron spectroscopy. Observed changes in core-level binding energies have been directly related to the crystallographic orientation dependence of interface dipoles and variations of band-gap discontinuities. The orientation variation of the band-gap discontinuities is found to be a significant fraction ($\approx \frac{1}{3}$) of the total band-gap discontinuity.

There has been considerable theoretical interest in the properties of ideal abrupt interfaces between different semiconductors, stimulated in part by the recent progress in molecular beam epitaxy (MBE) whereby truly abrupt interfaces can now be achieved. A basic property of the abrupt semiconductor interface is the relative alignment of the energy bands of the two semiconductors; i.e., how the energy difference in the band gaps (ΔE_g) is distributed between the valence- and conduction-band discontinuities (ΔE_v and ΔE_c) such that $\Delta E_g = \Delta E_v + \Delta E_c$.

The first and most widely used model for estimating ΔE_c (or ΔE_v) is based on electron affinity differences.¹ Critical evaluations^{2,3} have been made of this model. Alternative models for predicting ΔE_c have appeared,^{4,5} and two self-consistent calculations of the Ge/GaAs-interface electronic structure have been completed.^{6,7} Although it has long been recognized that interface dipoles could produce energy-band discontinuities which depend on crystallographic orientation of the interface plane, such effects have generally been ignored. Transport measurements⁸ on vapor-grown Ge/GaAs heterojunctions suggested that

there could be substantial (a few tenths of an eV) changes in valence- and conduction-band discontinuities, $\delta(\Delta E_v)$ and $\delta(\Delta E_c)$, dependent on crystallographic orientation. Unfortunately, it is relatively difficult to determine these dopant-level-independent quantities from transport measurements and the scatter in these data is as large as the measured effect.

To investigate the interface dipole orientation dependence, we have developed a contactless x-ray photoemission spectroscopy (XPS) technique which allows a direct probe of interface potential variations. Herein, we report the observation of sizable and systematic variations in ΔE_c for the Ge/GaAs interface as a function of crystallographic orientation. Figure 1 is a schematic energy-band diagram of an ideal abrupt Ge/GaAs interface. The relative positions of the average bulk crystal potential within the two semiconductors determine ΔE_v and ΔE_c .^{8,9} An orientationally dependent change in the interface dipole magnitude may shift the relative positions of the valence and conduction bands in the two semiconductors as shown schematically by dashed lines in Fig. 1. Figure 1 also shows the position of a

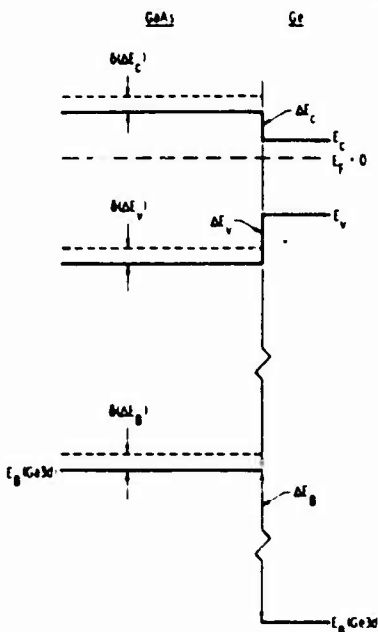


FIG. 1. Schematic energy-band diagram. The dashed lines illustrate a decreased value of ΔE_c , associated with an interface dipole layer that accelerates photoelectrons from a GaAs substrate relative to Ge 3d photoelectrons which do not cross the interface.

core level in Ge and in GaAs. As the average bulk crystal potential changes to adjust to the dipole variation, the relative binding energies of all levels on both sides of an abrupt interface (measured relative to the common Fermi level, E_F) must also vary by the change in dipole energy with orientation; i.e., $|\delta(\Delta E_c)| = |\delta(\Delta E_c')| = |\delta(\Delta E_c'')|$ also indicated by dashed lines in Fig. 1. For the Ge/GaAs interface, we will specifically consider the energy separation, ΔE_s , between the Ga 3d and Ge 3d core electron levels. A measurement of $\delta(\Delta E_s)$ by XPS thus provides a direct measure of $\delta(\Delta E_s)$. The dashed lines in Fig. 1 illustrate a change in the interface dipole which would increase the splitting between the Ga 3d and Ge 3d core levels to equal the decrease in ΔE_s .

Our experiment used Al $K\alpha$ ($\hbar\nu = 1486.6$ eV) radiation in conjunction with an extensively modified Hewlett-Packard model 5950A ESCA (electron spectroscopy for chemical analysis) spectrometer to excite photoelectrons from Ge/GaAs interfaces for which the Ge was an ≈ 20 -Å-thick layer on a thick (≈ 0.5 mm) GaAs substrate. The escape depth for the Ge 3d and Ga 3d photoelectrons is ≈ 20 Å. Thus, photoelectrons from both sides of the Ge/GaAs interface are observed simulta-

neously in the same XPS spectrum. Electrons which originate on the GaAs side of an abrupt interface pass through any dipole layer at the interface in order to be emitted from the free surface and detected, while electrons originating in the Ge do not. For example, an electron passing through a dipole layer in a direction from higher to lower electron density will experience an acceleration and, consequently, a relative increase in kinetic energy proportional to the dipole moment per unit area, τ , at the interface.⁹ A kinetic-energy increase will appear as an apparent binding-energy decrease in the XPS spectrum. In terms of the average charge density $\bar{\rho}(z)$ over planes parallel to the interface, the dipole moment per unit area is

$$\tau = \int z \bar{\rho}(z) dz.$$

The self-consistent calculations of Baraff, Appelbaum, and Hamann⁶ and Pickett, Louie, and Cohen⁷ have shown that the potential variations near an interface are localized to within 1 or 2 atomic layers, a length considerably less than the Ge 3d and Ga 3d photoelectron escape depths.

Interface states and bulk doping differences which cause band bending can complicate the ability to determine ΔE_s from transport measurements. In the XPS techniques described here, however, because the photoelectron escape depth is much smaller than typical band-bending lengths L ($L > 10^3$ Å for moderate dopant levels), the effect of interface states is to shift the potential within the sampled region on both sides of an interface by the same constant value. Therefore, since ΔE_s is the difference in core-level binding energy for photoelectrons which originate from each side of the interface, any potential shift due to interface states or other sources of band bending cancel. It is assumed that the two semiconductors are nondegenerately doped and that the dimensions perpendicular to the interface sampled by XPS are small compared to L .

The very thin (~ 20 -Å) epitaxial layers of Ge used for these interface studies were grown within the XPS apparatus on heated ($\approx 425^\circ\text{C}$) GaAs substrates by evaporative MBE techniques similar to those previously described,¹⁰ but at low flux rates. GaAs substrates with (100), (111), (III), and (110) faces were cut from a single boule of undoped GaAs (n -type carrier concentration 10^{16} cm^{-3}).¹¹ Laue back-reflection photography showed that the substrates were oriented to better than 1° . Each substrate was etched in 3:1:1 $\text{H}_2\text{SO}_4:\text{H}_2\text{O}_2:\text{H}_2\text{O}$ prior to insertion into the

XPS vacuum system. Substrate surfaces were cleaned by Ar⁺-ion sputtering (750 eV) followed by annealing at $\approx 575^\circ\text{C}$ to remove sputter damage (vacuum-system base pressure was low 10^{-10} Torr). Room-temperature low-energy electron-diffraction (LEED) patterns characteristic of (110) (1×1), (111)Ga (2×2), (III)As (1×1), and (100)Ga c(8×2) were obtained. In addition, a (100)As surface was also studied which was either c(2×8) or (2×4). Additional LEED measurements confirmed the epitaxy of the Ge overlayers. Following the XPS measurements, a metal point contact was made to the semiconductor surface to ensure reasonable diode characteristics.

Figure 2 shows an XPS spectrum from a sample of epitaxial Ge grown on a (110) (1×1) GaAs substrate. To determine ΔE_b , a background function which is proportional to the integrated photoelectron area was subtracted from the data to correct for the effect of inelastic photoelectron scattering. ΔE_b was measured between the centers of the peak widths at half of the peak heights. This procedure made it unnecessary to resolve the spin-orbit splitting of the Ge 3d and Ga 3d lev-

els (≈ 0.5 eV) to obtain high-precision peak positions.

Measurement results of eight different interfaces are given in Table I. In general, several (three to five) independent determinations were made on each interface. In all cases, measurement reproducibility was < 0.01 eV and was usually < 0.005 eV; calibration uncertainties increase the error limits to 0.1 eV. The measurements on the two samples of (110) (1×1) and (III)As (1×1) reproduce very well. We believe the discrepancy in the two values shown for (111)Ga (2×2) is real and represents a subtle difference in the interface properties grown on this surface.

If we arbitrarily reference all $\delta(\Delta E_b)$ values to the (110) charge-neutral surface such that $\delta(\Delta E_b)_{110} = 0$, we obtain the values of $\delta(\Delta E_b)$ shown in Table I. It is interesting that the (III)As and (111)Ga and the (100)As and (100)Ga differences are nearly symmetrically distributed around the (110) value. However, the known complexity of these surfaces¹² makes a simple interpretation of the variations in valence-band discontinuity difficult.

In summary, a technique has been developed to observe directly variations in band-gap discontinuities at abrupt semiconductor interfaces, and systematic changes in ΔE_b as a function of interface crystallographic orientation have been observed for Ge/GaAs. The maximum variation in ΔE_b between the (111) and (III) interfaces is ≈ 0.2 eV, which is a significant fraction ($\approx \frac{1}{4}$) of ΔE_b (0.75 eV). This result suggests that accurate future models used to predict ΔE_b and ΔE_c need to account for dipole orientation dependence.

We acknowledge helpful discussions with Profes-

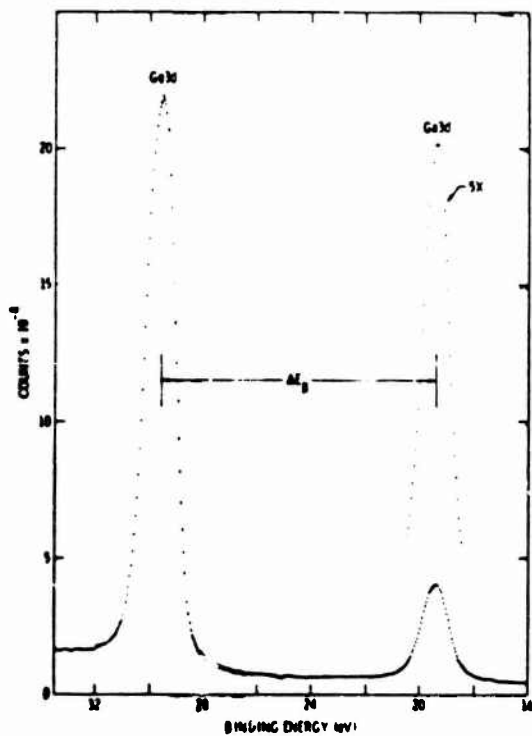


FIG. 2. XPS spectrum in the energy region of the Ga 3d and Ge 3d core levels obtained from a (110) Ge/GaAs interface. The thickness of the epitaxial Ge overlayer was ≈ 20 Å.

TABLE I. Ge-3d-Ga-3d binding-energy differences and corresponding variations in valence-band discontinuity for various Ge/GaAs interfaces.

Substrate surface	ΔE_b (eV)	$\delta(\Delta E_b)$ (eV)
(111)Ga (2×2)	10.27 ± 0.01	≈ -0.085
(100)Ga c(8×2)	10.31 ± 0.01	
(110) (1×1)	10.22 ± 0.01	-0.015
(100)As ...	10.20 ± 0.01	0
(100)As c(2×8)	10.21 ± 0.01	$+0.035$
(III)As (1×1)	10.17 ± 0.01	
(III)As (2×2)	10.11 ± 0.01	-0.10
(110) (1×1)	10.10 ± 0.01	

sor W. A. Harrison and appreciate the x-ray analysis performed by Dr. M. D. Lind. This work was supported by the U. S. Office of Naval Research, Contract No. N00014-76-C-1109.

⁶G. A. Baraff, J. A. Appelbaum, and D. R. Hamann, Phys. Rev. Lett. 38, 237 (1977), and J. Vac. Sci. Technol. 14, 999 (1977).

⁷W. E. Pickett, S. G. Louie, and M. L. Cohen, Phys. Rev. Lett. 39, 109 (1977), and to be published.

⁸F. F. Fang and W. E. Howard, J. Appl. Phys. 35, 612 (1964).

⁹J. A. Stratton, *Electromagnetic Theory* (McGraw-Hill, New York, 1941), p. 190.

¹⁰R. F. Lever and E. J. Huminski, J. Appl. Phys. 37, 3638 (1966).

¹¹Obtained from Morgan Semiconductor, Inc.

¹²See, e.g., W. Ranke and K. Jacobi, Surf. Sci. 63, 33 (1977); A. Y. Cho, J. Appl. Phys. 47, 2841 (1976); J. R. Arthur, Surf. Sci. 43, 449 (1974); L. L. Chang, L. Esaki, W. E. Howard, R. Ludeke, and G. Schul, J. Vac. Sci. Technol. 10, 655 (1973); several references to earlier work are contained in these papers.

¹R. L. Anderson, Solid-State Electronic. 5, 341 (1962).

²H. Kroemer, CRC Crit. Rev. Solid State Sci. 5, 555 (1975).

³J. L. Shay, S. Wagner, and J. C. Phillips, Appl. Phys. Lett. 28, 31 (1976).

⁴W. A. Harrison, J. Vac. Sci. Technol. 14, 1016 (1977).

⁵W. R. Frensley and H. Kroemer, Phys. Rev. 16, 2642 (1977).

XPS measurements of abrupt Ge-GaAs heterojunction interfaces

R. W. Grant, J. R. Waldrop, and E. A. Kraut

Rockwell International Science Center, Thousand Oaks, California 91360

(Received 24 January 1978; accepted 17 April 1978)

A method has been developed to grow thin epitaxial layers of Ge on GaAs substrates within an XPS system by an evaporative MBE technique. Abrupt heterojunctions with Ge layer thicknesses of $\approx 20 \text{ \AA}$ have been grown on (111), (110), and (100) GaAs crystal faces. By using XPS data obtained on these heterojunctions, variations in band gap discontinuities related to the crystallographic orientation dependence of interface dipoles have been observed directly. The data are also used to make an initial estimate of the valence band discontinuity for the abrupt Ge-GaAs heterojunction and with refinement of the technique, accurate values for this quantity should be obtainable.

PACS numbers: 73.40.Lq, 79.60.-i

I. INTRODUCTION

The use of heterojunctions in semiconductor devices can provide selective control over carrier transport properties which is unobtainable with single semiconductor devices. This effect arises from the energy band discontinuities which occur at a heterojunction; the total energy band gap discontinuity is ΔE_g and is equal to the difference in energy band gaps of the semiconductor pair. The distribution of ΔE_g between the valence and conduction bands, ΔE_v and ΔE_c , respectively, has fundamental interest as well as importance to semiconductor device design and understanding of device characteristics (clearly, $\Delta E_g = \Delta E_v + \Delta E_c$). The relative positions of the average bulk crystal potential determines ΔE_v and ΔE_c .¹⁻⁴ An orientationally dependent change in the interface dipole magnitude may shift the relative positions of the valence and conduction bands in the two semiconductors. If variations in band edge discontinuities are sizable, e.g., with respect to the thermal energy, they may also be important considerations for carrier transport within semiconductor devices.

Previous experimental investigations of heterojunction band discontinuities and the dependence of these discontinuities on crystallographic orientation have involved analysis of transport measurements to extract the information.⁵ Unfortunately, it is relatively difficult to determine with precision these dopant level independent quantities from transport measurements and the scatter in reported results is frequently large. In this paper, we will describe a new technique which employs x-ray photoelectron spectroscopy (XPS) in conjunction with abrupt heterojunctions grown by molecular-beam epitaxy (MBE) to study heterojunction band discontinuities. The method is a contactless potential probe of the junction which does not involve transport measurements. We have investigated abrupt Ge/GaAs interfaces with particular emphasis on the variation of ΔE_v with crystallographic orientation.

II. EXPERIMENT RATIONALE

The recent progress⁶ in MBE whereby truly abrupt het-

erojunctions can now be fabricated has at least in part stimulated considerable theoretical interest in the properties of ideal abrupt interfaces. Two self-consistent calculations of the Ge-GaAs interface electronic structure have been completed.^{2,4} Both of these calculations have shown that potential variations near the abrupt junction are localized to within 1 or 2 atomic layers normal to the interface.

The escape depth for energetic electrons excited within a solid by some form of incident radiation increases monotonically from ≈ 5 to $\approx 25 \text{ \AA}$ as the electron kinetic energy increases from about 100 to 1500 eV.⁷ Thus, the unscattered photoelectrons observed in a particular XPS peak which have kinetic energies $\gtrsim 1000 \text{ eV}$ sample over a distance which is large compared to the distance over which potential variations occur near an abrupt interface. If one can prepare a large area abrupt heterojunction sample which consists of a very thin top layer of one semiconductor ($\approx 20 \text{ \AA}$ thickness) grown onto a different semiconductor, it is possible to observe directly photoelectrons which originate from both sides of the junction in the same XPS spectrum. As we describe below, such an experimental arrangement can be used to study directly the band discontinuities at an abrupt heterojunction. A large photoelectron escape depth of several atomic layers will avoid unnecessary complications caused by any potential variation spread over 1 or 2 atomic layers at the abrupt interface. However, from another viewpoint, complications due to band bending in the two semiconductors must be considered. Typical band bending lengths for moderately doped semiconductors are 500–1000 \AA . The potential variation due to band bending in the interface region sampled by XPS should be small relative to the accuracy with which one is attempting to measure the band discontinuities. Thus, a sampling depth of $\approx 20 \text{ \AA}$ seems most suitable for the experiment described here.

Most XPS studies of core levels capitalize on variations in binding energies caused by chemical bonding effects which affect inner shell screening. However, it has long been recognized⁸ that the potential variations produced by changes in the Fermi level position in the surface region of semiconductor and insulator samples can also be observed as binding

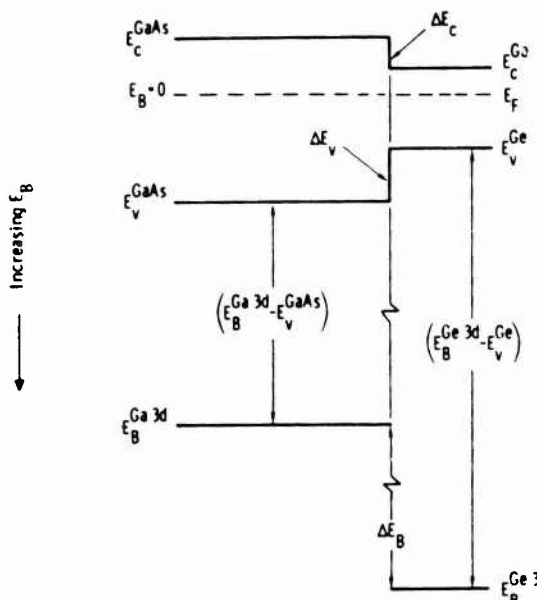


FIG. 1 Schematic energy band diagram for an abrupt Ge-GaAs heterojunction. The dimensions perpendicular to the interface are assumed to be small compared to the band bending length and thus band bending is neglected. Various quantities indicated in the figure are defined in the text.

energy variations in XPS spectra. We will use the latter effect, namely, the use of XPS as a potential probe, to study heterojunction discontinuities. Auger electron spectroscopy has previously been used for potential probing a semiconductor *p-n* junction.⁹

To illustrate the use of XPS for studying heterojunction band discontinuities, we show in Fig. 1 a schematic band diagram of an ideal abrupt heterojunction. Although an abrupt Ge/GaAs heterojunction is illustrated, as this is the interface reported on here, the technique is completely general for any abrupt heterojunction. With appropriate change of algebraic signs the expression given below for ΔE_0 at Ge-GaAs is easily generalized to other heterojunction pairs. For samples with electrical contact between sample and spectrometer, the XPS binding energies E_B are usually referenced to a common Fermi energy, E_F . Although we will use this concept in the following discussion (i.e., $E_B = 0$ at E_F), the choice of a reference energy can be arbitrary. A potential variation caused by the presence of an abrupt interface, or free surface or interface states, causes the energy positions of all bands, including the very narrow core level bands, to shift in energy. Within each individual semiconductor all bands will shift by an equal energy. If the band bending lengths are considerably greater than the XPS sampling depth (as we have assumed in Fig. 1), then the presence of surface or interface states will shift all energy levels measured by XPS in both semiconductors which form an abrupt heterojunction by the same amount. By referring to Fig. 1, a very simple expression is obtained for ΔE_0 , namely

$$\Delta E_0 = (E_B^{Ge\ 3d} - E_B^{Ge}) - (E_B^{Ga\ 3d} - E_B^{GaAs}) - \Delta E_B \quad (1)$$

where $E_B^{Ge\ 3d}$ and E_B^{Ge} are the binding energies of the Ge 3d core level and valence-band edge, respectively, in bulk Ge; $E_B^{Ga\ 3d}$ and E_B^{GaAs} are the binding energies of the Ga 3d core level and valence-band edge, respectively, in bulk GaAs. ΔE_B

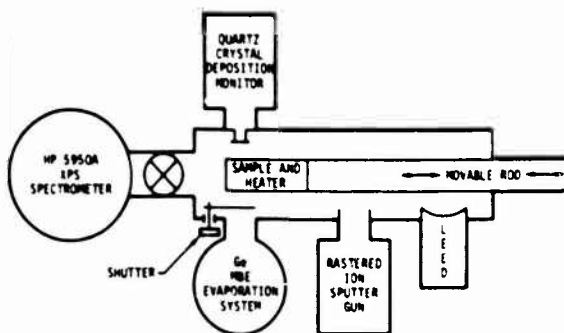
is the energy difference between the Ge 3d and Ga 3d levels measured with a Ge-GaAs heterojunction sample. Thus, we see from Eq. (1) that if the bulk core level binding energy relative to the valence band edge is known for both semiconductors which form a heterojunction, an XPS measurement of ΔE_B at an abrupt interface with the sample geometry described above will provide a direct measure of ΔE_0 .

At least two approaches might be tried to obtain the required very thin MBE-grown epitaxial layers. One might grow a layer somewhat thicker than necessary in a dedicated MBE apparatus, transfer the sample to the XPS apparatus and use a combination of sputtering and annealing (to remove sputter damage) to reduce the epitaxial layer to the desired thickness. Alternatively, the very thin epitaxial layer could be grown in place within the ultrahigh vacuum XPS system, as we chose to do. This latter approach avoids any use of sputtering to remove surface contamination or thin the epitaxial overlayer.

The semiconductor pair Ge/GaAs was chosen for study because of the nearly perfect lattice matching of this pair. In addition, by growing Ge on GaAs substrates, a very simple "single-cell" MBE system could be used. Considerable experience with both evaporative¹⁰ and vapor growth¹¹ of Ge on GaAs has been reported. The Ge/GaAs heterojunction has interesting device applications and as we will discuss in some detail below, it is the one system where a strong systematic variation in ΔE_V (or ΔE_C) with crystallographic orientation has been reported.¹²

III. EXPERIMENTAL

A schematic diagram of the experimental apparatus is shown in Fig. 2. A HP 5950A ESCA spectrometer with a completely redesigned sample preparation chamber was used. This spectrometer employed monochromatic AlK_α radiation ($h\nu = 1486.6$ eV) as the source of photoelectric excitation. A long high-vacuum bellows is used in conjunction with the movable sample rod. The base pressure in the bakeable sample preparation chamber was in the low 10^{-10} Torr range. The essential instrumentation on the sample preparation chamber included a LEED system, a rastered ion sputter gun, a Ge evaporation system with a shutter to interrupt the beam, and a quartz crystal film thickness deposition monitor. The sample holder incorporates a heater and thermocouple arrangement.



SCHEMATIC DIAGRAM OF EXPERIMENTAL APPARATUS

FIG. 2 Schematic diagram illustrating essential components of experimental apparatus.

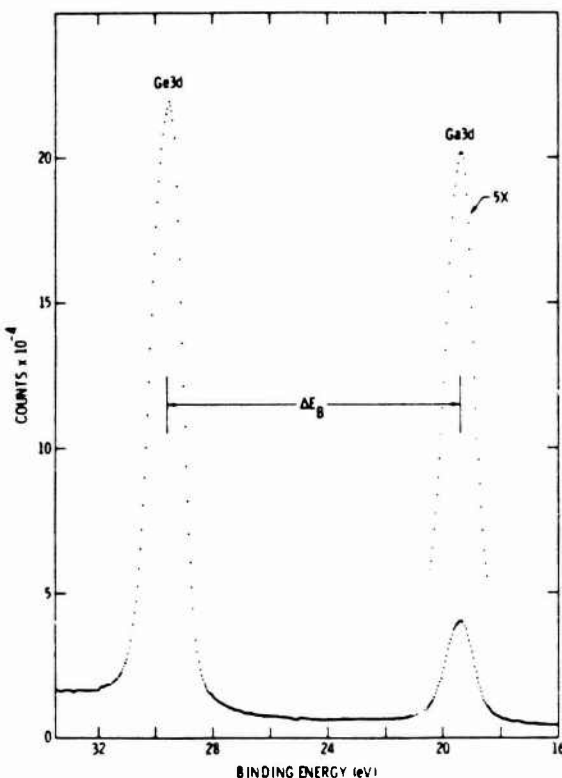


FIG. 3. Representative XPS spectrum in the region of the Ga 3d and Ge 3d core levels obtained from a (110) Ge-GaAs interface.

A temperature controller is used to hold the sample temperature between room temperature and $\approx 1000^{\circ}\text{C}$. The GaAs substrate material was attached to a Mo metal holder with In.

All the GaAs substrates were cut from a single boule of GaAs.¹³ Substrate crystal faces with (111), $\overline{(111)}$, (100), and (110) orientations were investigated. The orientation of the substrate materials was confirmed with Laue back-reflection x-ray photography and found to be better than 1° . Following chemical lapping, each substrate was etched in 3:1:1 $\text{H}_2\text{SO}_4:\text{H}_2\text{O}_2:\text{H}_2\text{O}$ prior to insertion into the XPS vacuum system.

After insertion into the sample preparation chamber, GaAs substrates were cleaned by sputtering with 750-eV Ar^+ ions. The GaAs was held at 575°C during sputtering and was subsequently annealed at this temperature for ≈ 10 min to remove sputter damage. Ti sublimation pumping was employed during sputtering to minimize any reactive background gases. After annealing, the surface cleanliness was assessed by XPS and the removal of sputter damage was confirmed by LEED.

The Ge evaporation source consisted of a simple resistively heated W wire-wound basket filled with undoped n-type ($\approx 10^{14} \text{ cm}^{-3}$) Ge. After stabilizing the evaporation rate to $\sim 1 \text{ \AA/s}$ as measured by the quartz deposition monitor, a $\sim 20\text{-\AA}$ layer of Ge was grown on the GaAs substrate. The Ge source to substrate distance was ≈ 12 in. and a mechanical shutter was used to initiate and terminate growth. During Ge growth the GaAs substrate was held at 425°C . After growth the sample was cooled to room temperature and LEED was used to confirm the epitaxy of the Ge overlayer.

Room-temperature LEED patterns of the GaAs substrates characteristic of (110) (1 \times 1), $\overline{(111)}\text{Ga}$ (2 \times 2), $\overline{(111)}\text{As}$ (1 \times 1) and (100)Ga c(8 \times 2) were obtained. In addition, a (100)As surface was also studied which was either c(2 \times 8) or (2 \times 4). Following the XPS measurement, a metal point-contact was made to the semiconductor surface to ensure reasonable diode characteristics.

IV. RESULTS

A. Measurement of ΔE_B

In Fig. 3, we show an XPS spectrum obtained from a sample consisting of a thin epitaxial layer of Ge grown on a GaAs (110) (1 \times 1) substrate. A background function which is proportional to the integrated photoelectron peak area was subtracted from the data to correct for the effect of inelastic photoelectron scattering. The quantity ΔE_B is measured between the centers of the peak widths at half of the peak heights. This procedure made it unnecessary to resolve the spin-orbit splitting of the Ge 3d and Ga 3d levels (≈ 0.5 eV) to obtain high precision peak positions.

In all, 33 independent measurements were made on eight different heterojunctions. In Fig. 4 we show representative background-subtracted XPS spectra obtained from samples having each of the crystallographic faces studied. Each peak has been normalized to an equal height for easy comparison

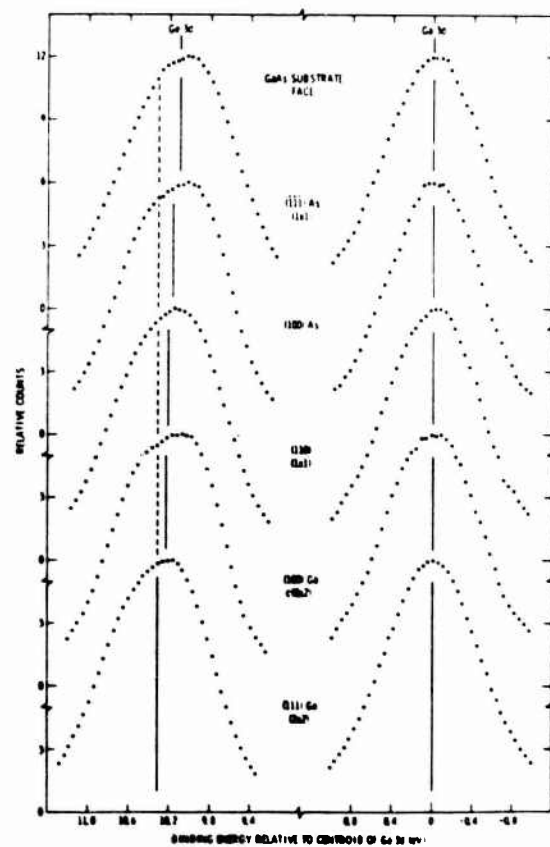


FIG. 4. XPS spectra in the region of the Ga 3d and Ge 3d core levels obtained for five different Ge-GaAs interfaces. The GaAs substrate faces on which the thin epitaxial Ge overlayers were grown are indicated in the figure. The vertical lines indicate the centroids of the various peaks as discussed in the text.

TABLE I. Ge 3d - Ga 3d binding energy differences, linewidths, Ge epitaxial layer thicknesses and variation in valence-band discontinuities for various Ge-GaAs interfaces.

Substrate surface	ΔE_B (eV)	$\Gamma(\text{Ga } 3d)$ (eV)	$\Gamma(\text{Ge } 3d)$ (eV)	Ge Layer Thickness (Å)	$\delta(\Delta E_v)$ (eV)
(111)Ga	10.27 ± .01	1.17 ± .02	1.25 ± .01	13	~ -0.085
(2 × 2)					
(111)Ga	10.31 ± .01	1.22 ± .02	1.26 ± .01	20	~ -0.085
(2 × 2)					
(100)Ga	10.22 ± .01	1.19 ± .02	1.25 ± .01	22	-0.015
c(8 × 2)					
(110)	10.20 ± .01	1.13 ± .01	1.29 ± .01	14	0
(1 × 1)					
(110)	10.21 ± .01	1.16 ± .01	1.27 ± .01	17	0
(1 × 1)(100)As	10.17 ± .01	1.15 ± .02	1.25 ± .01	14	+0.035
—					
(111)As	10.11 ± .01	1.21 ± .01	1.32 ± .01	13	+0.10
(1 × 1)					
(111)As	10.10 ± .01	1.22 ± .01	1.28 ± .01	18	+0.10
(1 × 1)					

in the figure and the centroid (which we define as the center of the peak width at half peak height) of each peak is indicated by a vertical solid line in the figure. The centroids of the five Ga 3d peaks have been aligned in the figure. The dashed vertical reference line which runs through the Ge 3d peaks is the centroid of the Ge 3d peak observed from the heterojunction which was grown on the GaAs (111)Ga (2 × 2) substrate. In Fig. 4 it is clearly observed that ΔE_B is dependent on the crystallographic orientation of the interface; we will return to a discussion of this observation below.

Measurement results on the eight different interfaces are given in Table I. In general, three to five independent measurements were made on each interface and the averaged values are presented in the table. In all cases, measurement reproducibility for ΔE_B was $< \pm 0.01$ eV and in most cases it was $< \pm 0.005$ eV. Calibration uncertainties increase the total error limits for ΔE_B to ± 0.01 eV. In the table, we also list values for the average linewidths Γ of the Ge 3d and Ga 3d levels which were measured at half of the peak height. If a sizable potential variation occurred either within the heterojunction area sampled by XPS or within the photoelectron escape depth, one would expect this variation to affect Γ . Although the values of Γ scatter somewhat there is little significant systematic variation with crystallographic orientation (the Γ 's observed on the (111)As faces seem to be slightly larger than on the other faces). We also list the Ge epitaxial layer thicknesses in the Table. This thickness was calculated from the relative Ge 3d to Ga 3d line intensities by assuming an escape depth of 20 Å and equal photoelectric cross sections for the two lines.

B. ΔE_v Considerations

By using the ΔE_B values given in Table I, in conjunction with Eq. (1), we could now calculate ΔE_v if accurate values of $(E_B^{\text{Ge } 3d} - E_c^{\text{Ge}})$ and $(E_B^{\text{Ge } 3d} - E_c^{\text{GaAs}})$ were known. Several determinations of $(E_B^{\text{Ge } 3d} - E_c^{\text{GaAs}})$ have been reported for bulk

GeAs; these are 18.9 ± 0.1 eV,¹⁴ 18.82 ± 0.15 eV,¹⁵ 18.9 ± 0.1 eV,¹⁶ and 18.8 ± 0.1 eV.¹⁷ Our own estimate is 19.0 eV. For $(E_B^{\text{Ge } 3d} - E_c^{\text{Ge}})$ in bulk Ge, values of 29.0 ± 0.1 eV¹⁶ and 29.3 ± 0.1 eV¹⁷ are reported; our own estimate is 29.5 eV. At present, the uncertainty of our own estimates is $\approx \pm 0.2$ eV. By using values from Refs 16 and 17, we obtain $\Delta E_v = -0.10 \pm 0.14$ eV and $\Delta E_v = +0.30 \pm 0.14$ eV, respectively; our own estimates give $\Delta E_v = +0.3 \pm 0.3$ eV for the (110) Ge-GaAs interface. Clearly, it will be necessary to obtain more accurate values of $(E_B^{\text{Ge } 3d} - E_c^{\text{Ge}})$ and $(E_B^{\text{Ge } 3d} - E_c^{\text{GaAs}})$ before meaningful comparisons with theory can be made; we expect to report refined values in a later publication.

C. Measurement of $\delta(\Delta E_v)$

The main difficulty in determining accurate values for $(E_B^{\text{Ge } 3d} - E_c^{\text{Ge}})$ and $(E_B^{\text{Ge } 3d} - E_c^{\text{GaAs}})$ in bulk Ge and GaAs, respectively, lies with the accuracy to which E_c^{Ge} or E_c^{GaAs} can be determined from the XPS data.

However the change in ΔE_v with crystallographic orientation, which we will define as $\delta(\Delta E_v)$, can be determined to the same accuracy as which the Ge 3d and Ga 3d line centroid positions are determined. If we set $(E_B^{\text{Ge } 3d} - E_c^{\text{Ge}}) - (E_B^{\text{Ge } 3d} - E_c^{\text{GaAs}}) = C$, where C is a materials constant, then Eq. (1) becomes $\Delta E_v = C - \Delta E_B$. If we now denote the values of ΔE_v observed on two different crystallographically oriented interfaces by subscripts 1 and 2, $\delta(\Delta E_v)$ becomes

$$\delta(\Delta E_v) = (\Delta E_v)_1 - (\Delta E_v)_2 = (\Delta E_B)_2 - (\Delta E_B)_1 \quad (2)$$

and the poorly known value of C is eliminated. In Table I, we tabulate values of $\delta(\Delta E_v)$ which have arbitrarily been referenced to the (110) charge neutral surface such that $\delta(\Delta E_v)_{110} = 0$; the values of ΔE_B used to calculate $\delta(\Delta E_v)$ are also given in Table I.

The measurements on the two samples of (110) (1 × 1) and (111)As (1 × 1) reproduce very well. The discrepancy in the two values shown for (111)Ga (2 × 2) seems to be real and most likely represents a subtle difference in the properties of these two interfaces.

V. DISCUSSION

The first and most widely used model for estimating ΔE_v (or ΔE_c) is based on electron affinity differences.¹⁸ Critical evaluations^{1,19} have been made of this model and alternative models for predicting ΔE_v have appeared.^{2-4,20} Although it has been recognized that interface dipoles could produce energy band discontinuities which depend on crystallographic orientation of the interface plane, such effects have generally been ignored. The experiment described herein provides a sensitive method to probe variations in the interface dipoles as can be seen from Eq. (2).

Specifically, considering the interface formed by a thin Ge epitaxial overlayer grown on a GaAs substrate, photoelectrons which originate on the GaAs side of the abrupt interface must pass through any dipole layer at the interface before being emitted from the free surface to be detected; photoelectrons originating in the Ge do not. An electron which passes through the dipole layer in a direction from higher to lower electron density will experience an acceleration and consequently a

relative increase in kinetic energy proportional to the dipole moment per unit area at the interface.²¹ This kinetic energy increase will appear as an apparent binding energy decrease in the XPS spectrum. The dipole associated with $\delta(\Delta E_v)$ relative to the (110) interface points from the GaAs into the Ge for Ga terminated faces.

Fang and Howard¹² have carried out the only other systematic investigation of interface dipole dependence on crystallographic orientation for Ge-GaAs. Their results imply that ΔE_v (111)Ga < ΔE_v (111)As < ΔE_v (110). The magnitude of the variations in ΔE_v which they observe are consistent with the values reported here. However, while we also find ΔE_v (111)Ga < ΔE_v (111)As, our results contradict the earlier results in that we observe ΔE_v (110) < ΔE_v (111)As. We suspect that the difference in the nature of interface states found on different crystal faces and the difference in heterojunction preparation techniques may account for this discrepancy.

It is interesting to note from Table I that the (111)As and (111)Ga and the smaller (100)As and (100)Ga $\delta(\Delta E_v)$ values are nearly symmetrically distributed around the (110) value. The smaller $|\delta(\Delta E_v)|$ values for (100) interfaces relative to (111) suggest the possibility that the magnitude of the dipole may depend on the bond angle at the interface. Despite the known complexity of the GaAs reconstructed free surfaces²² (e.g., the (111)As (1 × 1) surface is thought to be a Ga-terminated surface), related heterojunction interfaces formed for example on the (111)Ga and (111)As crystal faces of GaAs, may readjust to form identical geometries with the Ga and As atoms interchanged.

ACKNOWLEDGMENTS

We thank Professor W. A. Harrison for helpful discussions and acknowledge Dr. F. J. Szalkowski for designing the sample preparation chamber used in this work. We also appreciate the x-ray analysis performed by Dr. M. D. Lind. Work was supported by the Office of Naval Research, Contract No. N00014-76-C-1109.

- ¹H. Kroemer, CRC Crit. Rev. Solid State Sci. **5**, 555 (1975).
- ²W. E. Pickett, S. G. Louie, and M. L. Cohen, Phys. Rev. Lett. **39**, 109 (1977), to be published.
- ³W. R. Frenley and H. Kroemer, Phys. Rev. B **16**, 2642 (1977).
- ⁴G. A. Baraff, J. A. Applebaum, and D. R. Hamann, Phys. Rev. Lett. **38**, 237 (1977); J. Vac. Sci. Technol. **14**, 999 (1977).
- ⁵A. G. Milnes and D. L. Feucht, *Heterojunctions and Metal-Semiconductor Junctions*, (Academic, New York, 1972), Chaps. 2 and 4 and Refs. therein.
- ⁶See, for example, A. Y. Cho and J. R. Arthur, *Progress in Solid-State Chemistry*, edited by J. McCaldin and G. Somorjai (Pergamon, New York, 1975), Vol. 10, p. 157; L. L. Chang, L. Esaki, W. E. Howard, and R. Ludeke, J. Vac. Sci. Technol. **10**, 11 (1973).
- ⁷See, for example, I. Lindau and W. E. Spicer, J. Electron Spectrosc. **3**, 409 (1974).
- ⁸J. Auleynter and O. Hornfeldt, Arkiv Fysik **23**, 165 (1963).
- ⁹J. R. Waldrop and J. S. Harris, J. Appl. Phys. **46**, 5214 (1975).
- ¹⁰See, e.g., R. F. Lever and E. J. Huminski, J. Appl. Phys. **37**, 3638 (1966); I. Ryu and K. Takahashi, J. Appl. Phys. **4**, 850 (1955); J. E. Davey, Appl. Phys. Lett. **8**, 164 (1966).
- ¹¹See, e.g., A. R. Riben, D. L. Feucht, and W. G. Oldham, J. Electrochem. Soc. **113**, 245 (1966); J. C. Marinace, IBM J. **280** (1960).
- ¹²F. F. Fang and W. E. Howard, J. Appl. Phys. **35**, 612 (1964).
- ¹³Obtained from Morgan Semiconductor, Inc., our own Hall measurements subsequent to our initial report [Phys. Rev. Lett. **40**, 656 (1978)] indicate that the material is p-type, $\approx 10^{15} \text{ cm}^{-3}$. Experimental results and conclusions are independent of doping type.
- ¹⁴C. C. Chang, P. H. Citrin, and B. Schwartz, J. Vac. Sci. Technol. **14**, 943 (1977).
- ¹⁵L. Ley, R. A. Pollak, F. R. McFeely, S. P. Kowalczyk, and D. A. Shirley, Phys. Rev. B **9**, 600 (1974).
- ¹⁶M. Cardona, C. M. Penchina, N. J. Shevchik, and J. Tejeda, Solid State Commun. **11**, 1655 (1972).
- ¹⁷D. E. Eastman and J. L. Freeouf, Phys. Rev. Lett. **33**, 1601 (1974).
- ¹⁸R. L. Anderson, Solid State Electron. **5**, 341 (1962).
- ¹⁹J. L. Shay, S. Wagner, and J. C. Phillips, Appl. Phys. Lett. **28**, 31 (1976).
- ²⁰W. A. Harrison, J. Vac. Sci. Technol. **14**, 1016 (1977).
- ²¹J. A. Stratton, *Electromagnetic Theory* (McGraw-Hill, New York, 1941), p. 190.
- ²²See, e.g., W. Ranke, and K. Jacobi, Surf. Sci. **63**, 33 (1977); A. Y. Cho, J. Appl. Phys. **47**, 2841 (1976); J. R. Arthur, Surf. Sci. **43**, 449 (1974); L. L. Chang, L. Esaki, W. E. Howard, R. Ludeke, and G. Schul, J. Vac. Sci. Technol. **10**, 655 (1973); several references to earlier work are contained in these papers.

Polar heterojunction interfaces

W. A. Harrison,* E. A. Kraut, J. R. Waldrop, and R. W. Grant

Science Center, Rockwell International, Thousand Oaks, California 91360

(Received 9 June 1978)

A study of heterojunction interface geometry based on our measured differences in 3d core-state binding energies for germanium and gallium at Ge-GaAs heterojunctions of different crystallographic orientations is reported. For the interfaces which have been studied, i.e., (110), (100) Ga, (100) As, (111) Ga, and (111) As, orientation-dependent variations in dipole contributions to valence-band discontinuities of about 0.2 eV have been observed. From electrostatic considerations we deduce the simplest interface geometries consistent with the facts that the differences are small and no large charge accumulations can occur at the junction. An abrupt planar junction is allowed for the (110) interface, but the polar interfaces require at least two transition planes of atoms with compositions which are deduced from the two conditions above. The electrostatic calculations were based upon the differences in nuclear charge and are unaffected by the resulting polarization of the bonds if that polarization is described in an "electronegativity" approximation. In this approximation there would in fact be no dipole shift for the ideal geometries proposed. An improved treatment of the bond polarization based upon the bond-orbital model gives residual dipole shifts somewhat smaller than those observed, and in poor agreement with our measurements. Inclusion of lattice-distortion effects at the interface also fails to account for the observed dipole shifts. We conclude that the experimentally prepared junctions must contain deviations from the ideal atom arrangements. The number of these deviations required to account for the observed shifts is on the order of one for every fifteen interface atoms.

I. INTRODUCTION

It has been possible to understand the essential properties of heterojunctions without concern for the possibility of electrostatic dipole shifts at the interface. Band-edge discontinuities could be predicted from differences in experimental electron affinities¹ or theoretically from differences in bulk energy bands.² A direct estimate of the dipole for a Si-Ge junction,³ a detailed treatment of the Ge-GaAs nonpolar (110) junction by Pickett, Louie, and Cohen,⁴ and general considerations of junctions by Frenscley and Kroemer⁵ all suggested that indeed the dipole effects should be small, at most on the scale of a few tenths of an eV.

If, however, there were no electrostatic dipole shifts at the interface, the band-edge discontinuities would necessarily be identical for any pair of materials, independent of the crystal orientation of the interface separating them. Thus a measure of differences for different crystal faces can give unambiguous evidence for dipole shifts and experimental distinction of dipole shifts from intrinsic band-energy differences associated with electron affinities. We analyze here a direct measurement of the differences in dipole shifts on different interfaces for Ge-GaAs heterojunctions,⁶ and thus the first direct evidence of electrostatic dipole shifts.

To see what these measurements can tell us

about the junction, we need a formulation of the electrostatic properties of the different junctions. This leads immediately to the fact that properties such as dipole shifts are extremely sensitive to the detailed geometry of the interface. Because details are not known experimentally, we use the experimental findings, with the electrostatic formulation, to learn about the geometry. We find that the analysis places rather stringent conditions on the geometries which must exist in the experimental systems.

In Sec. II, the experimental results concerning the measurement of the relative dipole shifts are briefly summarized. In Sec. III, we make a careful formulation of the electrostatics for (110), (100), and (111) interfaces, and include bond dipoles in a simple approximation, finding that the ideal planar geometry is not allowed for the polar interfaces. We then proceed to find the simplest geometry which is consistent with the experimental findings of only small shifts. Geometries are in fact found which give no shift at all and the problem becomes that of understanding the observed small shifts. Improvements in the calculation of electron redistribution, discussed in Sec. IV, do not account for them, nor do lattice distortions suggested by covalent radii, and discussed in Sec. V. In Sec. VI, we conclude that the experimentally prepared junctions must contain deviations from the proposed ideal-atom arrangements.

II. SUMMARY OF EXPERIMENTAL RESULTS FOR Ge-GaAs HETEROJUNCTIONS

For convenience, in this section we briefly summarize our experimental findings on the relative dipole shifts for Ge-GaAs heterojunctions with different crystallographic orientations. These results which employ x-ray photoelectron spectroscopy (XPS) as the primary measurement technique have now been reported.⁵

Substrates of GaAs with (100), (111), and (110) faces were cleaned within the XPS vacuum system by Ar⁺-ion sputtering (750 eV) followed by annealing at about 575°C to remove sputter damage. After annealing the surface, cleanliness was confirmed by XPS and the removal of sputter damage was assessed by low-energy electron diffraction (LEED). Very thin ($\approx 20 \text{ \AA}$) epitaxial layers of Ge were grown within the XPS apparatus on heated ($\approx 425^\circ\text{C}$) GaAs substrates by evaporative molecular beam epitaxy (MBE) techniques. Additional LEED measurements confirmed the epitaxy of the Ge overlayers. XPS was used to measure the differences in Ge-3d and Ga-3d core-level binding energies at Ge-GaAs heterojunctions with different crystallographic orientations. As discussed in Ref. 5, observed changes in core-level binding energies provide a direct measure of the crystallographic orientation dependence of interface dipoles and variations of band-gap discontinuities.

Measurements were carried out on eight different interfaces. In Table I we summarize the results. Additional experimental details may be found in Ref. 5.

III. THEORY OF THE DIPOLE SHIFT

We are concerned here with potentials arising from infinite arrays of charges, a type of problem known to be very tricky and even to lead to conditionally convergent answers in some cases. It is therefore absolutely essential to proceed with care and to be certain that we include the essential physical effects correctly. A model of the system may not be adequate; we must treat the system itself.

To do this we start with a plane (to become the

TABLE I. Ge 3d-Ga 3d binding energy differences ΔE_B for various Ge-GaAs heterojunctions. All error limits are $\pm 0.01 \text{ eV}$.

Substrate	surface	(111) Ga	(100) Ga	(110)	(100) As	(111) As
ΔE_B (eV)		10.27	10.22	10.20	10.17	10.11
		10.31		10.21		10.10

junction plane) through a germanium crystal, with germanium atoms extending indefinitely on both sides. We imagine having solved for the electronic states in this system which by definition has no dipole shift across the junction. We will then "freeze" the electronic structure and imagine transferring protons between nuclei to the right of the junction such as to convert half of the nuclei to gallium (atomic number one less than germanium) and half to arsenic (atomic number one greater than germanium). This shift of protons (theoretical alchemy⁶) will of course produce an exactly calculable change in electrostatic potential and may produce an accumulation of nuclear charge at the interface or a dipole layer at the interface. [In fact, both occur at polar interfaces, (100) and (111).] We then allow the electronic system to relax, which if done sufficiently accurately would lead to a precise description of the true Ge-GaAs heterojunction with this particular set of germanium, gallium, and arsenic atom positions. The change in electronic structure can, of course, only be done approximately but the most important qualitative features can be obtained rigorously.

We begin with a discussion of the (110) interface, which provides a reference for the other interfaces. Shown in Fig. 1 is a Ge-GaAs (110) interface resulting from the transfer of protons,

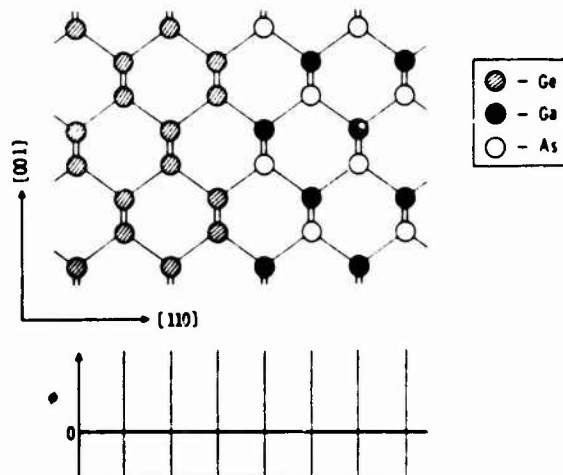


FIG. 1. A (110) heterojunction between Ge and GaAs. The crystal is viewed along the [110] direction with the [001] direction vertical. Note that every plane of atoms parallel to the junction is on the average neutral corresponding to a nonpolar junction. The symbols used to identify specific atoms are defined in this figure and are the same in all figures. All atoms are tetrahedrally bonded; the "double" bonds schematically illustrated in the figures are two tetrahedral bonds separated by the usual 109° tetrahedral bond angle and projected on to the plane of the figure.

with the electronic structure still frozen as in germanium. It is apparent from the figure that each plane of atoms parallel to the interface is still neutral on average. This corresponds to the transfer of protons parallel to the surface, perhaps downward in the figure. This also corresponds to no charge accumulation at the interface nor any electrostatic dipole layer. There are, of course, fluctuations in electrostatic potential along the interface, but the potential averaged over a plane parallel to the interface (which is equivalent to the potential at one point due to charges averaged over planes parallel to the surface) is unchanged. At a heterojunction interface, the terms dipole shift and charge accumulation are defined as a discontinuity in average potential and average potential slope, respectively. The average potential is defined as the potential averaged over a plane midway between adjacent atomic planes. We will return later to the relaxation of the electronic structure and see that its effect should be very small.

We turn next to a (100) interface shown in Fig. 2. Again, think of the electronic structure as frozen to be the same as in germanium. In this case each plane of atoms parallel to the interface is charged; this corresponds to proton transfer perpendicular to the interface. The consequences of this transfer may not be immediately obvious, but we may again understand them by averaging the charge distribution over planes parallel to the interface. We may readily integrate Poisson's equation from the germanium on the left, where we take the potential to be constant and zero through the junction. The result is illustrated at the bottom of Fig. 2. Upon crossing the first plane of negatively charged atoms the potential gradient becomes positive and constant, and then becomes zero again after crossing the first plane of positively charged atoms. Thus the potential in the GaAs contains an average gradient in addition to a fluctuating component; the average gradient may be thought of as coming from charge accumulation at the interface due to proton transfer, and therefore polarization density, perpendicular to the interface, and terminating at the interface. In any case, it is real and unambiguous and results in a potential which cannot be sustained in the real system because it leads to potential differences over a few atom distances which are greater than the band gap; spontaneous generation of carriers would immediately occur.

Let us turn to the redistribution of the electrons due to the redistribution of protons. We look first at the response to the fluctuating component of the potential, with the average potential gradient subtracted. This becomes just the fluctuating po-

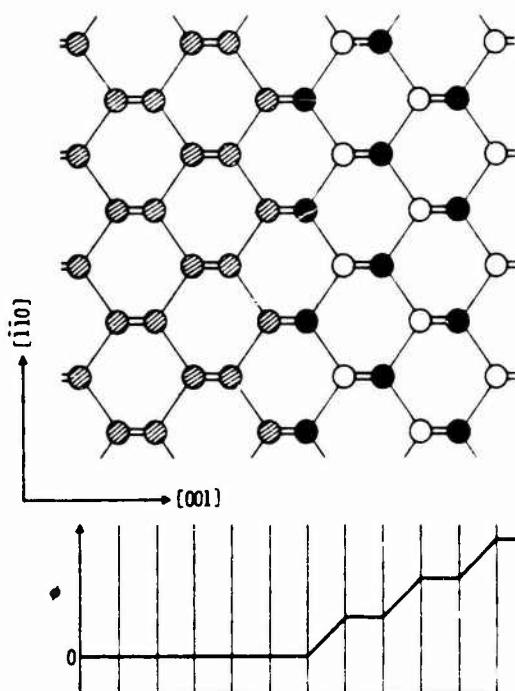


FIG. 2. A (001) heterojunction between Ge and GaAs, again viewed along the $\langle\bar{1}\bar{1}0\rangle$ direction with the $\langle\bar{1}\bar{1}0\rangle$ direction now vertical. Note that the first atomic plane to the right of the junction is entirely Ga [it is therefore called a (001) Ga junction] which, without bond polarization, is negatively charged. The potential averaged over planes parallel to the junction, is obtained by integrating Poisson's equation from left to right. A nonzero average electric field has arisen to the right of the junction due to charge accumulation. It is not eliminated by bond polarization although this will change the sign of the effective charge on the Ga (see Sec. IV).

tential which would arise in a bulk crystal from converting the germanium nuclei to gallium and arsenic nuclei [for example, by transferring protons parallel to the surface of a slab with $\langle\bar{1}\bar{1}0\rangle$ surfaces]. The charge redistribution could be calculated rather reliably in a linear combination of atomic orbitals (LCAO) context and in the bond-orbital model⁷ in particular, but the essential features are more easily understood in terms of an electronegativity approximation. In that approximation we assert that the added proton lowers the energy of the atomic states on the arsenic atom, the removed proton raises the energy on the gallium atom, and this effect polarizes the intervening bonds towards the arsenic. This will produce a dipole in the bond but *no net change in the charge of two in the bond*. Whatever charge is added to the arsenic is removed from the neighboring gallium atoms. This would follow from any nearest-neighbor (or higher-order neighbor) LCAO or Wannier-function calculation. It follows

that charge redistribution in the bonds at the interface cannot remove the charge accumulation which arose from the proton transfers.

We turn next to the average potential gradient, which has not been eliminated by the bond distortions. (In our construction this occurred in the GaAs, but it could as well have been in the Ge; it is the *difference* in gradients which is guaranteed by the electrostatic calculation.) This gradient will cause an additional polarization of each bond extending indefinitely to the right and therefore can cause a charge accumulation. This is just the dielectric polarization of GaAs and reduces the average field by a factor of the dielectric constant ϵ . We are left with an average potential gradient which may be readily calculated. The charge density in each plane is $2e/a^2$, where a is the cube edge, 5.65 Å for GaAs. The change in the potential gradient ($\nabla^2\phi = -4\pi\rho$) is 4π times this. To obtain the average gradient we divide by 2 and by the dielectric constant $\epsilon = 10.9$ for GaAs and multiply by e to obtain a change in electrostatic potential energy of

$$\delta E = 4\pi e^2/\epsilon a = 2.9 \text{ eV} \quad (1)$$

for each distance a . This corresponds to a huge field and, as we indicated earlier, would raise the valence band maximum at one point above the conduction-band minimum a few atom distances away, thus producing instantaneous carriers (in this case, one electron per area a^2) and reducing the net charge at the interface to zero. This is exactly the result which Baraff, Appelbaum, and Hamann⁸ obtained by detailed treatment of just this junction geometry. As Baraff⁸ has emphasized, it is guaranteed by this geometry of the junction.

There is, however, no experimental evidence for such a huge free-carrier density or such a large qualitative difference in junctions prepared upon (100) faces rather than (110) faces. Indeed, it is almost inconceivable that a junction could be prepared with one electron per surface atom in an antibonding (conduction-band) state. We therefore postulate that the planar geometry must be modified to eliminate the excess charge; the planar geometry shown in Fig. 2 is not expected to occur in a real junction. We proceed to seek the simplest modification which is acceptable.

The geometry of Fig. 2 produced fields which corresponded to a deficit of one proton for every two surface atoms at the junction. In terms of our theoretical alchemy one proton must be added for every two surface atoms. Note that this could be done by adding a proton to half of the gallium atoms in the first gallium plane to the right of the junction in Fig. 2, converting them to germanium

atoms, or it could be done by adding one to half of the last plane of germanium atoms to the left of the junction, converting them to arsenic atoms. There are innumerable other ways to add the protons, but these two are the simplest; the first is illustrated in Fig. 3.

We may again average the charges over atom planes, leaving the electrons frozen in the germanium electronic structure, and integrate Poisson's equation through the junction as indicated below in Fig. 3. The added protons have eliminated the average potential gradient in the GaAs and therefore produce an allowed geometry in this regard. However, this geometry has produced a shift in the average potential in the GaAs of $\delta = \pi e^2/2a\epsilon = 0.37$ eV. One way of seeing that there is a dipole shift here is to construct to the right of the GaAs shown in Fig. 3 the analogous junction with an extra half-plane of gallium atoms (so the entire system is neutral) and with germanium to the right; that is, to construct a GaAs slab surrounded by germanium. We then see that the potential in the germanium to the right is shifted with respect to that on the left by twice the value given above. This large dipole did not occur on the (110) junction illustrated in Fig. 1 and is not consistent with the much smaller differences

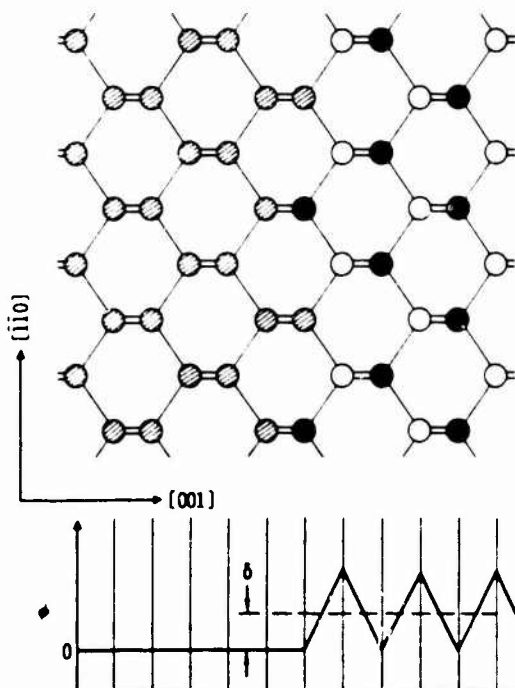


FIG. 3. A (001) heterojunction as in Fig. 2, but with $\frac{1}{2}$ of the Ga atoms in the junction plane replaced by Ge atoms. The average electric field in the GaAs has been eliminated but there is still a dipole shift δ much larger than is experimentally observed. The dipole shift is not eliminated by bond polarization.

in dipole shifts on different surfaces which are observed (Sec. II). We conclude that this geometry also is not correct; however, the redistribution of electronic charge must first be considered.

We approximated the redistribution in terms of an increased electronegativity on each arsenic atom which polarized neighboring bonds in proportion to the electronegativity difference with the neighboring atoms. We may do this atom by atom near the junction and see immediately that the dipoles induced to the right of each atom are just equal and opposite to those on the left; *no net dipole layer is introduced* and the shift in average potential remains. Thus the geometry of Fig. 3 must be modified.

It is interesting that this same result was obtained by Frensel and Kroemer⁴ who modeled the total charge distribution at a polar interface by just such an electronegativity model. They found no charge accumulation and no dipole shifts for geometries such as those of Figs. 2 and 3. We note that this model omits the very important difference in nuclear charges which is an essential feature of real junctions.

The conclusion of no net dipole layer would be modified slightly by a more realistic LCAO calculation. We will see in Sec. V that in the bond-orbital approximation,⁷ the excess electronic charge on the arsenic is not extracted equally from the neighbors on the two sides. This does not modify our earlier conclusion concerning total-charge accumulations, but it does introduce dipole shifts of the order of a few hundredths of an eV for the geometries we have discussed. These are not large enough to cancel the 0.37 eV shift found above; thus we conclude that the (100) geometry, consisting of a single transition layer (the half-gallium layer of Fig. 3) does not occur.

The simplest modification which eliminates the dipole shift requires two transition layers, a $\frac{1}{4}$ -gallium layer and a $\frac{1}{4}$ -arsenic layer as schematically illustrated in Fig. 4. It seems appropriate to think of this as a modification of a geometry with the last GaAs layer being gallium and we therefore refer to this as a (100) $\frac{1}{4}$ -Ga surface. The integration of Poisson's equation, shown below, indicates that there is no dipole shift nor charge accumulation. The second alternative is a $\frac{1}{4}$ -arsenic and $\frac{1}{4}$ -gallium layer; it can be constructed by interchanging gallium and arsenic atoms in Fig. 4. We refer to it as the (100) $\frac{1}{4}$ -As junction. Either type of junction can be grown on a given (100) surface of GaAs, which we will see is in contrast to the (111) surface. All other allowed alternatives involve more than two transition planes and will not be considered. It would be difficult to guess the precise pattern

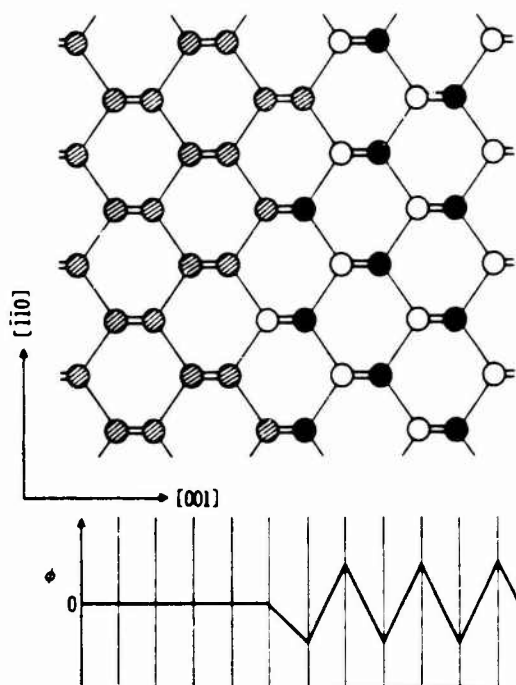


FIG. 4. A (001) heterojunction as in Figs. 2 and 3, but with two transition planes. The first is $\frac{1}{4}$ As, the second $\frac{3}{4}$ Ga with the remaining atoms Ge; it is appropriate to refer to it as a (100) $\frac{1}{4}$ -Ga junction. This is the simplest junction geometry which eliminates both charge accumulation and dipole shift.

which occurs in a real junction although electrostatic energies are usually lowered by high-symmetry patterns. The geometries shown in Figs. 3-6 are only intended to illustrate the average composition of atom planes without specifying a two-dimensional symmetry pattern. The highest symmetry allowed for the (100) interface would be 1×4 , but it is possible that a 2×4 pattern would have lower electrostatic energy.

It is fair to ask how such a pattern would arise experimentally. If it were possible to construct a planar junction, as in Fig. 2, with its sheet of compensating carriers, the chemical force derivable from the excess energy of electrons in anti-bonding states would cause diffusion of gallium atoms out of the junction or arsenic atoms in until there was no excess nuclear charge at the junction and no free carriers. In fact, a residual dipole would favor diffusion in such a way as to eliminate the dipole. It seems more likely, however, that the growth process itself produces a nonplanar junction such as that shown in Fig. 4 directly, as an interface of lowest energy.

We have applied this same analysis to the (111) junctions, requiring that in the electronegativity

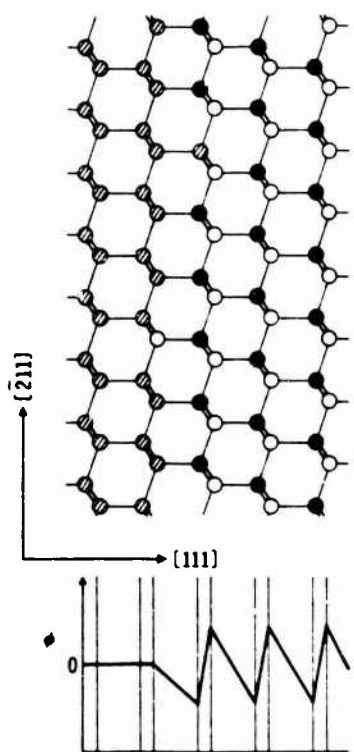


FIG. 5. A (111) heterojunction, viewed along the $[01\bar{1}]$ direction, constructed on the (111) Ga face of GaAs. It is a two-transition-plane junction with the first plane $\frac{1}{3}$ As and the second plane $\frac{2}{3}$ Ga. We call it a (111) $\frac{2}{3}$ -Ga junction. This is one of the two-plane geometries giving no charge accumulation nor dipole shift, as seen in the potential plot below. The other is shown in Fig. 6.

approximation there be no charge accumulation nor dipole shift at the junctions. In Fig. 5 we show a (111) interface. Note that along the $[111]$ direction atomic planes are alternately connected by bonds parallel to the $[111]$ direction and bonds (three times as many) inclined to that direction. Thus there are two distinct $[111]$ directions and two crystallographically distinct (111) junctions; Fig. 5 illustrates the orientation with gallium atoms at the end of the parallel bonds away from the germanium. This is usually called the (111) Ga face since it is assumed that the crystal will terminate with the minimum number of bonds broken leading in this case to a Ga terminating plane. We find that for this crystallographic arrangement there are two kinds of interfaces with two transition planes which give no charge accumulation and no dipole shift in the electronegativity approximation. The interface shown in Fig. 5 terminates in a Ga plane, with $\frac{1}{3}$ of the gallium atoms replaced by germanium; the first germanium plane has $\frac{1}{3}$ of the Ge atoms replaced by As. We call it the (111) $\frac{2}{3}$ -Ga geometry. The second

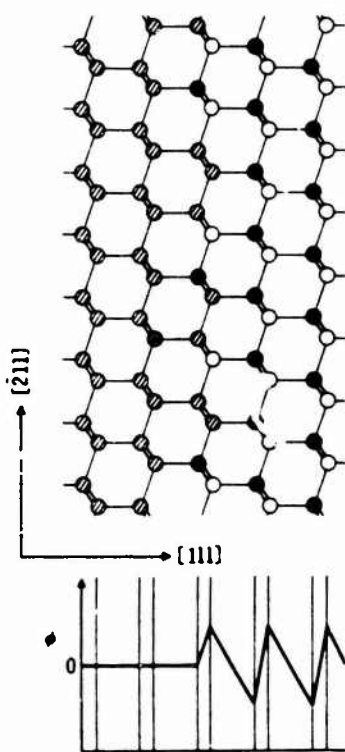


FIG. 6. The second two-transition-plane geometry for a heterojunction, on a (111) Ga face, such as that shown in Fig. 5; it gives no charge accumulation and no dipole shift. The first plane is $\frac{2}{3}$ Ga; the second is $\frac{1}{3}$ As. We call it a (111) $\frac{1}{3}$ -Ga junction. The corresponding two allowed geometries on the (111) As face of GaAs are obtained by interchanging empty and full circles on Fig. 5 and here.

alternative (with two transition planes) terminates the GaAs in a Ga plane with $\frac{1}{3}$ of the Ga atoms replaced by Ge with $\frac{1}{3}$ of the As atoms in the next GaAs plane replaced by Ge; it is shown in Fig. 6. Both Figs. 5 and 6 give allowed geometries for a heterojunction on the crystallographic (111) Ga face of the GaAs. The allowed geometry for a heterojunction on a (111) As face can be constructed by interchanging Ga and As atoms in Figs. 5 and 6.

This completes the specification of the simplest allowed interface geometries on the different crystallographic interfaces. They have been chosen to give no charge accumulation at the interface and, in the electronegativity approximation, no dipole shift.

IV. CORRECTIONS TO THE ELECTRONEGATIVITY APPROXIMATION

We have used only the smallness of the dipole shifts, not the actual values, to learn about the interface geometry. We wish also to see what can

be learned from the shifts themselves. The ideal geometries proposed in Figs. 1 and 4-6, and the electronegativity model or the bond polarization have led to no dipole shift at all. Small dipole shifts may be expected to arise from corrections to the electronegativity model, from distortions of the lattice at the interface, and from deviations from the ideal arrangements of atoms we have proposed. These are discussed here and in Secs. V and VI.

We first improve on the electronegativity model by using the bond-orbital model.⁷ Each bond is treated individually by using known parameters⁶ to obtain the effective charge on each plane; Poisson's equation is then integrated over these effective charges, just as was done with the frozen-electron charges in Sec. III. It is interesting that bond polarization actually changes the sign of most effective charges but as we have seen this has only a small effect on the net dipole shift. The calculation is rather intricate because with two transition planes the effective charges on four planes are modified. We have carried the analysis through and will give here only the final resulting dipole contribution to ΔE_s . Enough details will be given in Sec. V to see exactly how the calculation was performed.

For the (110) interface shown in Fig. 1 a contribution of +0.02 eV is obtained. For the (100) $\frac{1}{4}$ -Ga junction shown in Fig. 4 we also obtain +0.02 eV but for the (100) $\frac{1}{4}$ -As interface obtained by interchanging Ga and As atoms in Fig. 4 we obtain 0.00 eV. Both the (111) $\frac{1}{4}$ -Ga interface shown in Fig. 5 and the (111) $\frac{1}{4}$ -As interface shown in Fig. 6 yield a contribution of -0.01 eV. The corresponding (111) $\frac{1}{4}$ -As and (111) $\frac{1}{4}$ -As interfaces yield 0.05 eV. By subtracting shifts from that for the (110) interface we may make a direct comparison with the experimental shifts. We find that the magnitudes of the relative shifts are about half of those observed but for both (111) faces they are just the opposite sign as those observed. It is not clear which of the two (100) geometries is to be associated with the gallium-rich and arsenic-rich surfaces.

V. EFFECT OF LATTICE DISTORTIONS

It is to be expected that the ideal germanium geometry will not continue through the junction. A table of covalent radii for tetrahedral systems¹⁰ gives a value of 1.22 Å for Ge, a value of 1.26 Å for Ga, and a value of 1.18 Å for As. We see by summing radii that the GaAs bond length equals the Ge-Ge bond length, in accord with the good match in lattice constant but a Ge-Ga bond should be about 2% longer and the Ge-As bond 2% shorter.

The effect of these distortions is included next.

For this aspect of the problem the electronegativity approximation is not adequate. It would imply that the effective charges on the atoms remain constant as the lattice is distorted while it is well known^{6,7,11} that charge redistribution gives effects as large as the displacement of static charge. We therefore use the bond-orbital model,^{6,7} discussed in Sec. IV, which is known to give a good account of both effects.¹¹

The dipole associated with each bond has a contribution from the electron-charge distribution and from the difference in nuclear charge at the two ends of the bond. (A quarter of each nucleus is associated with each bond.) For a Ge-Ga bond, for example, the dipole is given by^{6,7,11}

$$\vec{p} = \frac{1}{2}(\alpha_p - \frac{1}{4})ed\vec{d}, \quad (2)$$

where \vec{d} is the vector distance from the Ge to the Ga nucleus. (We have dropped a scale factor, $= 1.4$ used in the earliest treatments.¹¹) α_p is the polarity given by $V_p/(V_2^2 + V_3^2)^{1/2}$ based upon a polar energy^{6,7}

$$V_p = \frac{1}{2}(\epsilon_p^{G\alpha} - \epsilon_p^{G\beta}) \quad (3)$$

(with values 0.73 eV for Ge-Ga, 0.78 eV for As-Ge, and 1.51 eV for As-Ga) and a covalent energy given by

$$V_2 = 2.16\pi^2/md^2 \quad (4)$$

(equal to 2.76 for all bonds if d is taken to be 2.44 Å for all). It is these dipoles, or more particularly effective atomic charges obtained by summing the dipoles from the four bonds directed at each atom, which were used in the calculation of the dipole shifts listed in Sec. IV. They were used to determine charge densities averaged over atomic planes. We then integrated Poisson's equation through the junction. The results included a reduction by a factor of the dielectric constant, as did the potential shifts in Eq. (1). This approximates the self-consistent response of the intervening bonds to the charge redistribution.

We are interested here in the change due to distortion. The change in magnitude of the dipole due to a change in bond length d is

$$\delta p = \frac{1}{2}ed\delta\alpha_p + \frac{1}{2}e(\alpha_p - \frac{1}{4})\delta d. \quad (5)$$

From Eq. (5) we see that

$$\delta\alpha_p = \frac{-V_2 V_3 \delta V_3}{(V_2^2 + V_3^2)^{3/2}} = 2\alpha_p(1 - \alpha_p^2) \frac{\delta d}{d} \quad (6)$$

and thus

$$\delta p = (-2\alpha_p^2 + 3\alpha_p - \frac{1}{4})e\delta d/2. \quad (7)$$

We will approximate the effect of distortion by

this change in dipole for any Ge-Ga or Ge-As bond due to a change in bond length d computed from the covalent radii given above; i.e., +0.04 and -0.04 Å, respectively, for the Ge-Ga and Ge-As bonds. By using the expressions given above (with an appropriate V , for the Ge-As bond) we obtain a magnitude of δp of $0.24e\delta d$ for the Ge-Ga bond and $0.26e\delta d$ for the Ge-As bond.

In both cases the effect of the distortion is to transfer electrons to the germanium atom. Physically the reason for the same sign is that the increase of bond length for the Ge-Ga bond makes it more polar, increasing the difference in electronic charges, while the decrease of the Ge-As bond length makes it less polar, decreasing the difference in electronic charges. Since the Ge has excess charge in the first case and a deficit in the second, in both cases the transfer of electrons is to the germanium. The fact that the sign is the same, along with an almost equal magnitude, leads directly to the result that lattice distortions have little effect on our observed variation in dipole shifts for different crystallographic orientations.

We note first that if the difference between the $0.24e\delta d$ and $0.26e\delta d$ for the two bond types is neglected, any dipole shift arising from bond distortion will not be changed by interchanging gallium and arsenic atoms. Thus bond distortion in the (100) interface shown in Fig. 4 will lead to the same dipole shift as in the corresponding interface obtained with Ga and As atoms interchanged. Furthermore, a shift of the electrostatic energy in the germanium relative to that in the GaAs will be proportional to the number of Ge-Ga and Ge-As bonds per unit area of interface and this is the same in the allowed geometry of Fig. 4 as in the abrupt geometry of Fig. 2. (One fourth of the bonds to the right from the last full Ge layer are Ge-As bonds, $\frac{1}{2}$ from the next layer are Ge-Ga bonds, and $\frac{1}{4}$ from the next layer are Ge-As bonds. This is equivalent to having all Ge-Ga or Ge-As bonds in one layer.) The dipole shift is in fact independent of interface geometry. We obtain its magnitude by considering the abrupt geometry, multiplying the average change in bond dipole, $\delta p = 0.25e\delta d$, by the cosine of the angle it makes with the surface ($3^{-1/2}$), multiplying by 4π from Poisson's equation, multiplying by the bond density ($4/a^2$), and dividing by the dielectric constant to obtain

$$\delta E = 0.25(\delta d/d)4\pi e^2/\epsilon a = 0.012 \text{ eV}, \quad (8)$$

with the electron potential energy higher in the germanium than in the GaAs. In fact, the product of the bond-angle cosine and bond density is identical for the (110) and (111) surfaces so this model predicts the same dipole shift for all interfaces considered and therefore no contribution to the measured differences.

This model is rather crude but should give the principal effect of bond distortion. Since the shift obtained is small compared to the observed differences, and corrections to the model would be smaller, bond distortions cannot alone account for the observed differences in dipole shift.

VI. CONCLUSIONS

We conclude that the smallness of the differences in dipole shift on the different crystallographic faces is inconsistent with a structure containing less than two transition layers. With two or more layers a structure can be selected which in the simplest (electronegativity model) approximation gives no dipole differences at all. We found further that the leading corrections to this model for the ideal structure gave smaller dipole shifts than those observed and that their signs were not consistent with those of the experimental shifts. Finally, we considered the expected distortions of the lattice at the interface and found that the effects were small and independent of crystal orientation.

We therefore conclude that an explanation of the experimentally observed dipole shifts must be a deviation from the structures proposed in Figs. 4-6. The simplest kind of deviation would be an interchange of atom pairs. This shift of a single proton between adjacent planes, separated by $\frac{1}{4}a$, introduces a dipole of $\frac{1}{4}ea$. If the number of such displacements was a fraction x of the two interface atoms per area a^2 , the dipole shift would be $4\pi e^2(a/4)(2x/a^2)/\epsilon = 2\pi e^2 x/\epsilon a$. To obtain a dipole shift of 0.1 eV, a value of $x = 0.07$ is required. We see no inconsistency of such a compositional mixing with our experimental results.

ACKNOWLEDGMENT

This work was partially supported by the U. S. ONR under Contract No. N00014-76-C-1109.

- *Permanent address: Applied Physics Dept., Stanford University, Stanford, Calif. 94305.
- ¹R. L. Anderson, in *Proceedings of the International Conference on Semiconductors, Prague, 1960* (Czechoslovakian Academy of Science, Prague, 1960), p. 563.
- ²W. A. Harrison, *J. Vac. Sci. Technol.* 14, 1016 (1977).
- ³W. E. Pickett, S. G. Louie, and M. L. Cohen, *Phys. Rev. Lett.* 39, 109 (1977).
- ⁴W. R. Frensley and H. Kroemer, *Phys. Rev. B* 16, 2642 (1977).
- ⁵An initial account of these experimental findings has been reported: R. W. Grant, J. R. Waldrop, and E. A. Kraut, *Phys. Rev. Lett.* 40, 656 (1978); also, a more detailed discussion of the experimental approach has been prepared for publication, *J. Vac. Sci. Technol.* (to be published).
- ⁶W. A. Harrison, "The Physics of Solid State Chemistry," in *Festkörperprobleme*, edited by J. Treusch (Vieweg, Braunschweig, 1977).
- ⁷W. A. Harrison, *Phys. Rev. B* 8, 4487 (1973); the full development will appear in W. A. Harrison, *The Physics of the Chemical Bond* (Freeman, San Francisco, to be published).
- ⁸G. A. Baraff, J. A. Appelbaum, and D. R. Hamann, *Phys. Rev. Lett.* 38, 237 (1977); *J. Vac. Sci. Technol.* 14, 999 (1977).
- ⁹G. A. Baraff (private communication).
- ¹⁰C. Kittel, *Introduction to Solid State Physics*, 3rd ed. (Wiley, New York, 1967), p. 105.
- ¹¹W. A. Harrison, *Phys. Rev. B* 10, 767 (1974).

Precise Determination of the Valence-Band Edge in X-Ray Photoemission Spectra: Application to Measurement of Semiconductor Interface Potentials

E. A. Kraut, R. W. Grant, J. R. Waldrop, and S. P. Kowalczyk

Rockwell International Electronics Research Center, Thousand Oaks, California 91360

(Received 26 December 1979)

A highly precise method for locating the valence-band edge in x-ray photoemission spectra is reported. The application to measuring semiconductor interface potentials is discussed. X-ray photoemission-spectroscopy experiments on Ge and GaAs(110) crystals have given Ge 3d, Ga 3d, and As 3d core level to valence-band edge binding-energy differences of 29.55, 18.81, and 40.73 eV to a precision of ± 0.02 eV. For illustration, the valence-band discontinuity at an abrupt Ge/GaAs(110) heterojunction is determined to be 0.53 ± 0.03 eV.

PACS numbers: 73.40.Lq, 73.40.Ns, 73.40.Qv, 79.60.Eq

We report a method for markedly increasing the precision in locating the valence-band edge in spectra observed by XPS (x-ray photoemission spectroscopy). It is shown, by use of this method, how the binding-energy difference between a semiconductor core level and the valence-band edge can be precisely determined and how the result enters into the measurement of heterojunction band discontinuities, Schottky-barrier heights, and interface band bending. Accurate XPS determination of the above quantities requires that experimental values of core level to valence-band-edge energies be known with a precision better than the ± 0.1 eV uncertainty typically quoted in the literature. A procedure for obtaining a better precision has not been previously discussed. A determination of the valence-band discontinuity for the Ge/GaAs(110) heterojunction precise to ± 0.03 eV will be given. A precision of this order is needed to critically test models that predict heterojunction band discontinuities.

The disruption of a perfect crystal lattice produced by the presence of either a metal, semiconductor, or vacuum interface is generally accompanied by a deviation of the charge distribution near the interface from that deeper in the bulk semiconductor. Consequently, Poisson's equation predicts a spatially varying electrostatic potential V_{BS}^X which bends all of the bands or energy levels by the same amount as a function of distance away from the interface. For semiconductor X in Fig. 1(a), the energy of a core level E_{CL}^X , the valence-band maximum E_v^X , and the conduction-band minimum E_c^X , are shown in the bulk (b) and at an interface (i) with either a metal, semiconductor Y , insulator, or vacuum. Binding energy E_B is measured with respect to the Fermi level E_F ($E_F = 0$). The band gap E_g ,

position of the Fermi level in the bulk relative to the valence-band edge δ^X , band-bending potential potential V_{BS}^X , and depletion-layer width W are also shown in Fig. 1(a).

Given an XPS measurement of the position of the core level $E_{CL}^X(i)$ at the interface and the binding-energy difference $(E_{CL}^X - E_v^X)$ between core level E_{CL}^X and the valence-band maximum E_v^X , it follows from Fig. 1(a) that the position of the conduction-band minimum at the interface is given by

$$E_c^X(i) = (E_{CL}^X - E_v^X) + E_c^X - E_{CL}^X(i), \quad (1)$$

the position of the valence-band maximum at the interface is given by

$$E_v^X(i) = E_{CL}^X(i) - (E_{CL}^X - E_v^X), \quad (2)$$

and the band-bending potential V_{BS}^X at a surface or interface is given by

$$qV_{BS}^X = (E_{CL}^X - E_v^X) + \delta^X - E_{CL}^X(i). \quad (3)$$

The experimental determinations of E_{CL}^X and E_v^X for Ge and GaAs were carried out with a UHV modified Hewlett-Packard model-5950A XPS spectrometer which has a monochromatized Al $K\alpha$ ($h\nu = 1486.6$ eV) x-ray source; this system has been described previously.¹ Each XPS spectrum was collected by repeatedly (> 100 scans) sweeping a 50-eV energy interval. The energy interval contained both the core level(s) of interest and the valence-band region. The spectrometer energy scale was calibrated to 0.02%. The (110) specimens of Ge and GaAs were prepared by etching in dilute HF and 4:1:1 ($H_2SO_4:H_2O_2:H_2O$) acid solutions, respectively. This was followed by *in situ* sputter and anneal cycles until the 1×1 low-energy electron diffraction pattern characteristic of GaAs(110) (Ref. 2) and a complex pattern which resembles the reported³ c(8

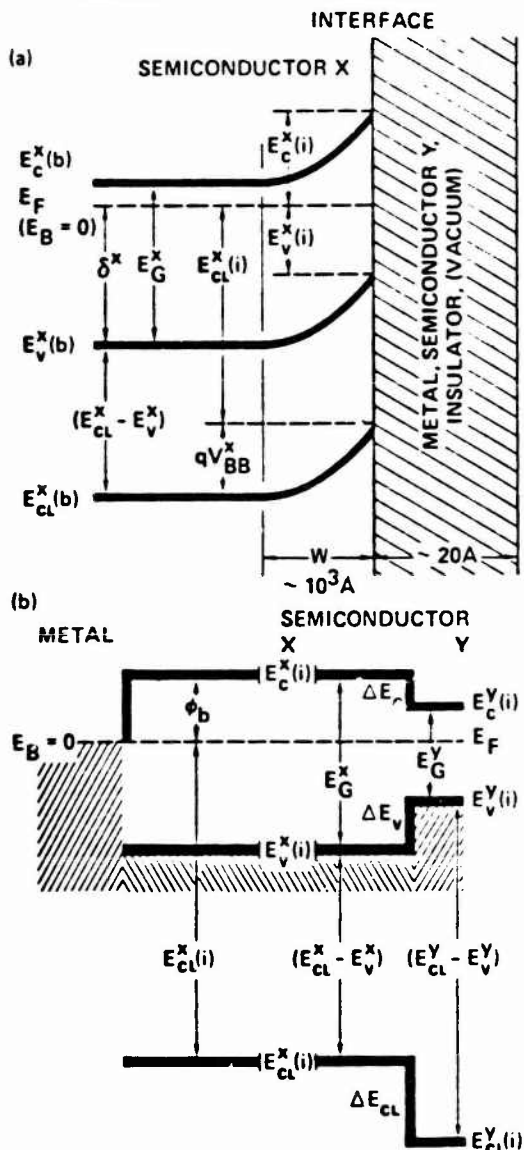


FIG. 1. (a) Generalized energy-band diagram at an abrupt interface between a semiconductor and vacuum, metal, insulator, or a different semiconductor; (b) schematic flat-band diagram at a metal-semiconductor (left) or heterojunction (right) interface.

$\times 10$) pattern characteristic of room-temperature Ge(110) were obtained. A background function which is proportional to the integrated photoelectron peak area was subtracted from the data to correct for the effect of inelastic photoelectron scattering. The core-level energy position was defined to be the center of the peak width at half of the peak height. This procedure made it unnecessary to resolve the spin-orbit splitting of the relatively narrow Ga, Ge, and As 3d levels to obtain high-precision peak positions. The es-

cape depth of the photoelectrons in the experiment here is $\sim 20 \text{ \AA}$. This escape depth (several atomic layers) minimizes any complications caused by potential variation spread over 1 or 2 atomic layers at an abrupt interface and also is insensitive to band bending at the interface which occurs over a typical width of $\sim 1000 \text{ \AA}$.⁴

The energy levels defined in Fig. 1(a) as measured within the $\sim 20 \text{ \AA}$ XPS sampling depth are shown in Fig. 1(b) for a heterojunction interface and for a metal-semiconductor interface. The Schottky-barrier height $\phi_b = E_c^X(i)$ at the metal-semiconductor interface is given by Eq. (1) and the valence-band discontinuity ΔE_v at the heterojunction interface is given by

$$\Delta E_v = (E_{cl}^Y - E_v^Y) - (E_{cl}^X - E_v^X) - \Delta E_{cl}, \quad (4)$$

where $\Delta E_{cl} = E_{cl}^Y(i) - E_{cl}^X(i)$. The effect of interface states is to shift the potential within the sampled region on both sides of an interface by the same constant value. Thus, any potential shift due to interface states or other sources of band bending cancel.

The determination of $(E_{cl} - E_v)$ depends on locating the position of the valence-band maximum E_v in the XPS data with greater accuracy than has been generally attempted previously. The required accuracy is achieved by fitting the XPS valence-band data in a limited region around the estimated position of E_v with an instrumentally broadened valence-band density of states (VBDOS) $N_v(E)$ chosen so that

$$N_v(E) = \int_0^\infty n_v(E') g(E - E') dE'. \quad (5)$$

The recent Chelikowsky-Cohen⁵ nonlocal pseudo-potential VBDOS has been used for $n_v(E')$ in Eq. (5) to analyze the Ge and GaAs data shown in Fig. 2. The instrumental resolution function $g(E)$ is separately determined by observing Au 4f core-level line shapes in metallic gold. These lines have an inherent linewidth ($\sim 0.29 \text{ eV}$),⁶ narrower than $g(E)$, and narrower than most photoelectron lines of other solids. Typical experimentally observed Au 4f line shapes $W_{4f}^{Au}(E)$ have full widths at half maximum (FWHM) of 0.86 eV and are related to $g(E)$ by

$$W_{4f}^{Au}(E) = \int_{-\infty}^{\infty} g(E - E') L(E') dE', \quad (6)$$

where $L(E')$ is a Lorentzian line shape (FWHM = 0.29 eV) and represents the inherent lifetime broadening of the Au 4f levels. Both $W_{4f}^{Au}(E)$ and $g(E)$ in (6) are analytically representable as the fold of Gaussian and Lorentzian line shapes

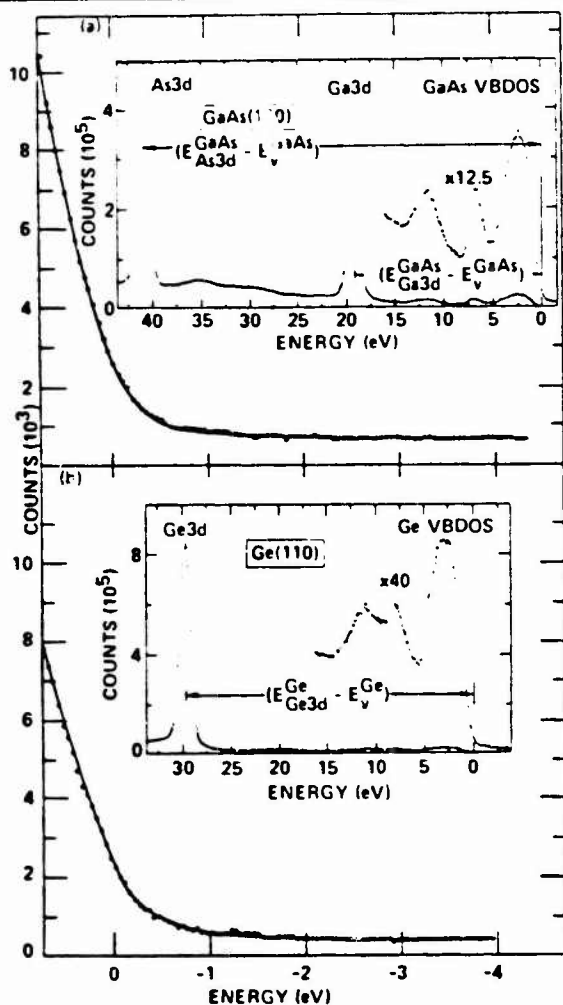


FIG. 2. Least-square fit of instrumentally broadened theoretical VBDOS (solid curve) to XPS data (points) in the region of the valence-band edge for (a) GaAs and (b) Ge. Insets show the XPS spectra which contain the VBDOS and the outermost core levels. The energy scale is zero at the valence-band edge.

(Voigt functions).⁷ Instrumental resolution functions $g(E)$ determined from Eq. (6) and used to analyze the data in Fig. 2 have typical FWHM = 0.81 eV and are the result of folding a Gaussian with a Lorentzian which has a half width equal to 20% of the Gaussian half width.⁸

Our procedure for precisely determining the valence-band edge employs the method of least squares. The position of the valence-band maximum E_v is determined by fitting the leading edge of the experimental XPS spectrum $J(E)$ to $N_v(E)$ with

$$J(E) = S N_v(E - E_v) + B, \quad (7)$$

TABLE I. Core level to valence-band maximum binding-energy difference (eV) for Ge and GaAs.

$E_{Ge3d}^{Ge} - E_v^{Ge}$	$= 29.55 \pm 0.02$ eV
$E_{Ga3d}^{GaAs} - E_v^{GaAs}$	$= 18.81 \pm 0.02$ eV
$E_{Al3d}^{GaAs} - E_v^{GaAs}$	$= 40.73 \pm 0.02$ eV

where S is a scale factor and B is a constant random-noise background. The fits obtained for Ge and GaAs are shown by solid curves in Fig. 2. As only the leading edge of the XPS valence-band spectrum is fitted, where the orbital symmetry is essentially p in character, matrix-element effects enter only through the constant scale factor S in Eq. (7).

By using the technique discussed above, $(E_{Ge3d}^{Ge} - E_v^{Ge})$, $(E_{Ga3d}^{GaAs} - E_v^{GaAs})$, and $(E_{Al3d}^{GaAs} - E_v^{GaAs})$ have been obtained from measurements of (110) oriented single crystals of Ge and GaAs. The results obtained from analysis of the data shown in Fig. 2 are presented in Table I.

The valence-band discontinuity ΔE_v for an abrupt Ge/GaAs(110) heterojunction can now be obtained by using the previously reported value of $\Delta E_{CL} = (E_{Ge3d}^{Ge} - E_{Ga3d}^{GaAs}) = 10.21 \pm 0.01$ eV and the results from Table I in Eq. (4). This leads to

$$\Delta E_v = 0.53 \pm 0.03 \text{ eV}$$

for the valence-band discontinuity at an abrupt Ge/GaAs(110) heterojunction interface. Our experimental evidence¹ indicates that this value of ΔE_v is intrinsic to an abrupt Ge/GaAs(110) interface. The precision of the method presented here can provide a sensitive test for the effect of interface nonideality on the magnitude of ΔE_v .

In summary, the method reported here for precisely determining core-level to valence-band-edge binding-energy differences makes possible the use of XPS for high-accuracy measurements of heterojunction band discontinuities, Schottky-barrier heights, and interface band-bending potentials.

This work was supported in part by the U. S. Office of Naval Research Contract No. N00014-76-C1109.

¹R. W. Grant, J. R. Waldrop, and E. A. Kraut, Phys. Rev. Lett. **40**, 656 (1978), and J. Vac. Sci. Technol. **15**, 1451 (1978).

²F. Jona, IBM J. Res. Dev. **9**, 375 (1965).

³B. Z. Olsanetsky, S. M. Repinsky, and A. A.

Shklyaev, *Surf. Sci.* **64**, 224 (1977).

⁴For a heavily doped semiconductor with a depletion width $< 10^3 \text{ \AA}$, a small correction to E_{CL}^X and E_v^X may be required due to the potential variation within the photoelectron sampling depth. For the moderate doping levels of our samples ($< 10^{17} \text{ cm}^{-3}$), this correction was $< 0.01 \text{ eV}$.

⁵J. R. Chelikowsky and M. L. Cohen, *Phys. Rev. B* **14**, 556 (1976).

⁶P. Pianetta and I. Lindau, *J. Electron Spectrosc.*

Relat. Phenom. **11**, 13 (1977).

⁷G. K. Wertheim, M. A. Butler, K. W. West, and D. N. E. Buchanan, *Rev. Sci. Instrum.* **45**, 1369 (1974).

⁸Phonon broadening of the Au 4f lines used to determine $g(E)$ was calculated following P. H. Citrin *et al.* [Phys. Rev. B **16**, 4256 (1977)] and was found to affect the $g(E)$ width by $< 0.01 \text{ eV}$; a similar result was found by P. H. Citrin *et al.* [Phys. Rev. Lett. **41**, 1425 (1978)]. This contribution to $g(E)$ affects the position of the derived value of E_v by $< 0.01 \text{ eV}$.

Pressure Dependence of Superconducting Transition Temperature of High-Pressure Metallic Te

F. P. Bundy and K. J. Dunn

General Electric Company, Corporate Research and Development, Schenectady, New York 12301

(Received 19 December 1979)

Existing data at high pressures of Berman, Binzarov, and Kurkin show that the various metallic forms of Te have considerable variation of their superconduction temperatures, T_c , depending upon the phase and the pressure; the observed T_c 's ranged from 2.5 to 4.3°K over the pressure span of 40 to 150 kbar. The present experiments, with use of a diamond-tipped apparatus with a cryogenic arrangement, have extended the pressure range to over 300 kbar. The results indicate that a new metallic phase develops in the 150–180-kbar region, which has a higher T_c of about 6.5°K.

PACS numbers: 74.10.+v, 62.50.+p

Many covalently bonded crystalline materials such as Si, Ge, Te, Se, etc., which are insulators or semiconductors in their usual low-pressure forms, transform to metallic phases under sufficient pressure,^{1–4} some of these "high-pressure metals" exhibit superconductivity at low temperatures.^{5–8} In 1973, Berman, Binzarov, and Kurkin⁹ (BBK) published their results for an extensive series of high-pressure cryogenic experiments with Te in which they explored the T_c of the metallic forms of Te over the pressure range of about 38–260 kbar (which corresponds to about 38–150 kbar on the modern pressure scale).^{10,11} Their findings are shown here in Fig. 1, in which T_c is plotted against P (modern scale). They concluded that in this range there are three different metallic phases: the first (38–60 kbar) having an unusually large positive dT_c/dP ; the second (60–75 kbar) with a nearly zero dT_c/dP ; and the third (75 kbar and up) with a strong negative dT_c/dP .

With our new apparatus¹² one of the early runs (to test the apparatus and procedure) was made with a specimen of Te because it was known to be superconducting. The run was made at about 220 kbar. This specimen exhibited an excellent superconducting transition as shown in Fig. 2, but at

a much higher temperature than observed by BBK. This discrepancy indicated that Te may have a different metallic phase at the higher pressure.

This report gives the results of a recent series of experiments done with our apparatus¹³ in which a specimen was compressed at room temperature in eight successive steps from 50 to 305 kbar and was tested at each step for superconductivity by cooling it to about 2.7°K. At the lower pressures our results agree moderately well with those of BBK, and at higher pressures a new metallic phase with the higher T_c does indeed develop, as was suggested by our earlier experiment.

The series of tests spanned a period of 44 days, as each warmup took a few days of time. After warming through the T_c zone, measurements were taken of the resistance of the "normal-state" metal on up to room temperature to provide information for determining the Grüneisen "characteristic temperature" of electrical conductivity, Θ .¹⁴

The room-temperature resistance behavior during the eight stepwise loadings is shown in Fig. 3(a). The room-temperature electrode resistance of about 0.18Ω needs to be subtracted from the values shown in order to get the specimen resistance. Note that during the first cryogenic temperature cycle, at 7.2 tons loading, the room-

Semiconductor Heterojunction Interfaces: Nontransitivity of Energy-band Discontinuities

J. R. Waldrop and R. W. Grant

Electronics Research Center, Rockwell International, Thousand Oaks, California 91360

(Received 18 September 1979)

A direct experimental test has revealed that heterojunction energy-band discontinuities are nontransitive. This result was obtained by an x-ray photoemission-spectroscopy investigation of abrupt (110) interfaces in the heterojunction series Ge/CuBr, CuBr/GaAs, and GaAs/Ge. The sum of the valence-band discontinuities for these interfaces is 0.64 ± 0.05 eV, a large deviation from the zero sum expected by transitivity.

A fundamental feature of an abrupt semiconductor heterojunction is the discontinuity in the valence band and conduction band, ΔE_v and ΔE_c , that arises from the bandgap change ΔE_g across the interface. Theoretical models¹⁻³ have been proposed to predict ΔE_v (or ΔE_c); these models have as a common feature a transitive relationship for the band discontinuities. In general, such models express a band discontinuity as the difference in an energy associated with each individual semiconductor. The widely used electron-affinity rule,⁴ whereby $\Delta E_v(A/B) = |x^A - x^B|$, is an example of a transitive model; x is the respective electron affinity of semiconductors A and B which form the junction A/B . Transitivity, if true, is appealing for the relative simplicity

brought to the resulting models; implied is that interface properties *per se* need not be investigated to predict ΔE_v and ΔE_c .

A transitive model has the property that if $\Delta E_v(A/B)$, $\Delta E_v(B/C)$, and $\Delta E_v(C/A)$ are the valence-band discontinuities associated with heterojunction interfaces from semiconductors A , B , and C , the relationship

$$\Delta E_v(A/B) + \Delta E_v(B/C) + \Delta E_v(C/A) = 0 \quad (1)$$

must be valid. Since $\Delta E_v + \Delta E_c = \Delta E_g$, any conclusions drawn for ΔE_v can always be expressed in terms of ΔE_c . An experimental test of Eq. (1) is thus a test of transitivity.

The electronic properties of relatively few abrupt heterojunctions have been studied experi-

mentally. As a result, data are not available to determine whether heterojunction band-edge discontinuities are transitive. Semiconductors in row four of the periodic table, Ge, GaAs, ZnSe, and CuBr, are all lattice matched, have tetrahedral crystal structures, and range from covalent to highly ionic. Thus, if these semiconductors can be grown epitaxially to form abrupt heterojunctions, characterization of at least three appropriate interfaces would test transitivity.

We report the first experimental results which demonstrate that no general transitive relationship exists for heterojunction band discontinuities. Specifically, by using x-ray photoemission spectroscopy (XPS) the (110) nonpolar abrupt interfaces in the series Ge/CuBr, CuBr/GaAs, and GaAs/Ge have been found to exhibit a large deviation from transitivity. To study this series of junctions, CuBr epitaxial layers were grown on Ge and GaAs; this to our knowledge is the first reported characterization of a heterojunction involving a I-VII compound.

A generalized band diagram is given in Fig. 1 for a heterojunction interface between semiconductors *A* and *B*. Shown are the valence- and conduction-band edges E_v^A and E_c^A , $\Delta E_v(A/B) = E_v^B - E_v^A$, $\Delta E_c(A/B) = E_c^B - E_c^A$, and the binding-energy separation, $\Delta E_b(A/B) = \Delta E_b^B - \Delta E_b^A$, between arbitrary core levels *b* which have binding energy E_b^A and E_b^B in semiconductors *A* and *B*, respectively. By inspection of the figure, $\Delta E_v(A/B)$ can be expressed as

$$\begin{aligned} \Delta E_v(A/B) &= \Delta E_b(A/B) + (E_b^A - E_v^A) \\ &\quad - (E_b^B - E_v^B). \end{aligned} \quad (2)$$

Since *A/B* is any heterojunction, similar expressions can be written for $\Delta E_b(B/C)$ and $\Delta E_b(C/A)$. Upon substitution of these expressions into Eq. (1), terms of the form $(E_v^A - E_v^A)$ cancel to yield

$$\Delta E_b(A/B) + \Delta E_b(B/C) + \Delta E_b(C/A) = 0. \quad (3)$$

These ΔE_b quantities can be measured with high accuracy at appropriate heterojunctions by XPS; thus, Eq. (3) provides a sensitive and direct experimental test of Eq. (1). In our experiment, *A* = Ge, *B* = CuBr, and *C* = GaAs. Although the binding energies in Fig. 1 and in XPS measurements are referenced to the Fermi energy E_F such that $E_b = 0 = E_F$, Eqs. (1)-(3) involve only energy differences. Thus, knowledge of the actual position of the Fermi level is not required and bulk doping differences or interface states resulting in band

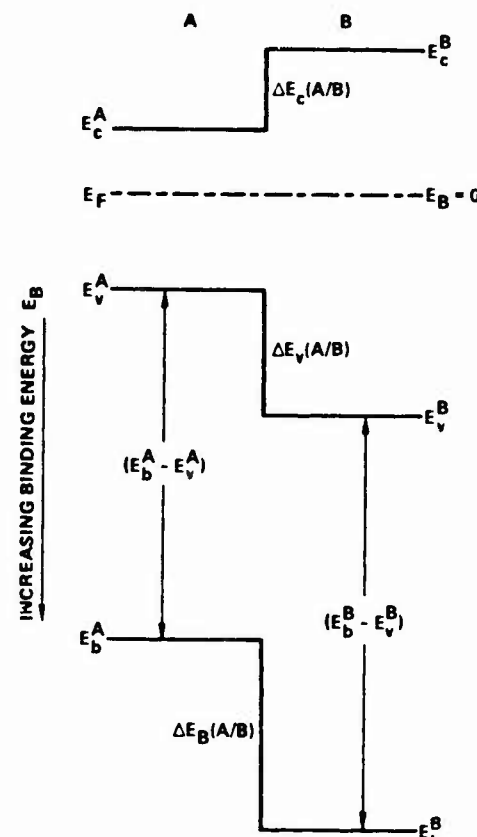


FIG. 1. Generalized energy-band diagram for a thin abrupt *A/B* heterojunction interface.

bending do not affect the analysis or the XPS measurement.

The experimental apparatus consists of a Hewlett-Packard 5950A XPS spectrometer combined with an ultrahigh-vacuum sample preparation chamber. This system also includes LEED (low-energy electron diffraction), a rastered sputter ion gun, a sample heater, and a CuBr sublimation source. System base pressure is $\sim 2 \times 10^{-10}$ Torr. The XPS x-ray source is Al $K\alpha$ ($\lambda = 1486.6$ eV) radiation.

Epitaxial CuBr films were grown on (110)GaAs and (110)Ge substrates by vacuum sublimation of CuBr. Sublimation has frequently been used to prepare polycrystalline films of CuBr with zinc-blende structure.⁴

The GaAs substrate was etched in 4:1:1 $H_2SO_4 : H_2O_2 : H_2O$ solution and was cleaned under vacuum by heating ($\sim 620^\circ C$) until no O or C was detectable by XPS. At room temperature this surface exhibited the (1×1) LEED pattern which is observed on the cleaved, stoichiometric (110) surface. The Ge substrate was etched in a dilute HF solution

and then cleaned under vacuum by ~ 1 -keV Ar^+ ion sputtering and 550°C annealing cycles until no O or C was detectable and a LEED pattern was obtained. The room-temperature (110)Ge LEED pattern was complex and strongly resembled the reported $c(8 \times 10)$ pattern.⁵

The CuBr film growth proceeded at a deposition rate of $\sim 3 \text{ \AA/sec}$ on room-temperature substrates; growth was stopped at a layer thickness of $25-30 \text{ \AA}$. Chamber vacuum during deposition was 2×10^{-9} Torr. No O or C was detectable in the XPS spectra of the CuBr films.

Examination by LEED was used to confirm the epitaxy of the CuBr films. The CuBr overlayer on GaAs exhibited a sharp LEED pattern that appeared to contain only integral-order spots and have lattice vectors parallel to the corresponding substrate vectors. Only the electron energy maximizing the pattern spot intensities distinguished the overlayer and clean substrate patterns; this suggests a (1×1) surface structure for the CuBr on (110)GaAs. Deposition of CuBr on room-temperature (110)Ge did not result in a LEED pattern; however, slow incremental heating of the sample to $\sim 150^\circ\text{C}$ caused a pattern to appear. No evidence of higher-order spots was observed in the CuBr LEED pattern and, as with GaAs, the lattice vectors were parallel to the corresponding substrate vectors. This suggests that CuBr epitaxially grown on (110)Ge also forms a (1×1) surface structure.

For heterojunction samples consisting of a thin (on the order of the $25\text{-}\text{\AA}$ XPS sampling depth)

overlayer of one semiconductor on a thick substrate of another, photoelectrons originating from each side of the interface can be observed in the same XPS spectrum. The upper half of Fig. 2 shows the core-level XPS binding-energy spectrum in the vicinity of the As 3d and Br 3d core-level peaks for the (110)CuBr/GaAs junction; similarly, the lower half of Fig. 2 shows a spectrum that includes the Ge 3d and Br 3d peaks for the (110)Ge/CuBr junction. For both junctions, a core-level peak originating from each side of the interface is evident. The ΔE_s indicated in the figure is that needed to test Eq. (3). To accurately determine ΔE_s , a background function which is proportional to the integrated peak area was subtracted from the data to correct for the effect of inelastic scattering. Core-level energies were consistently measured at the center of the peak width at half-height; this eliminated the necessity of resolving spin-orbit splitting to obtain high-precision peak positions.

Interface abruptness was assessed by comparing core-level peaks from pure samples of Ge, GaAs, and CuBr with the corresponding core-level peaks from the thin heterojunction samples. No evidence of interfacial chemical reactions was found (interfacial chemical effects would produce XPS peak broadening or splitting). In addition, the reduction of substrate core-level peak intensities with coverage and the accompanying appearance of the overlayer LEED pattern was consistent with uniform film growth and abrupt junction formation.

Table I gives the ΔE_s values measured for Ge/CuBr, CuBr/GaAs, and GaAs/Ge. The core level used in Ge, GaAs, and CuBr was Ge 3d, As 3d, and Br 3d, respectively. The ΔE_s value for the GaAs/Ge heterojunction was obtained from previously reported (110)Ge/GaAs data⁶ which used the Ga 3d core level in GaAs. In an independent measurement on clean (110)GaAs [surfaces which exhibited (1×1) LEED patterns] the energy separation, determined as described above, of

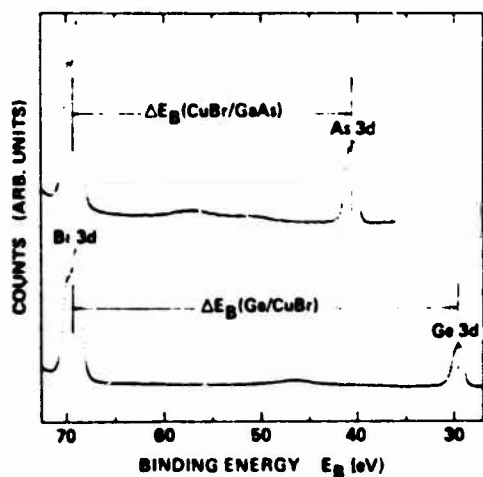


FIG. 2. XPS core-level spectra in the binding-energy region of the Br 3d, As 3d, and Ge 3d levels obtained from thin, abrupt (110)CuBr/GaAs and (110)Ge/CuBr heterojunctions.

TABLE I. XPS core-level binding-energy difference ΔE_s for abrupt interfaces which involve Ge, GaAs, and CuBr.

Interface	ΔE_s (eV)
(110)Ge/CuBr	39.85 ± 0.03
(110)CuBr/GaAs	-28.77 ± 0.03
(110)GaAs/Ge	-11.72 ± 0.02

the Ga 3d and As 3d core levels was found to be 21.92 ± 0.01 eV.⁷ This value was used to compute the ΔE_s (GaAs/Ge) quoted in Table I.

Substitution of the ΔE_s values in Table I into Eq. (3) shows that the sum is nonzero and that Eq. (3), and therefore Eq. (1), is clearly not satisfied: $\Delta E_s(\text{Ge/CuBr}) + \Delta E_s(\text{CuBr/GaAs}) + \Delta E_s(\text{GaAs/Ge}) = -0.64 \pm 0.05$ eV. This result provides the first direct experimental proof that semiconductor-heterojunction band discontinuities are nontransitive quantities.

For perspective, this transitivity deviation can be compared to the magnitude of the ΔE_s 's involved. By use of valence-band XPS data from pure samples of Ge, GaAs, and CuBr, and approximate value of the parameter $E_v - E_c$ for each material was estimated by inspection. From Eq. (2) the ΔE_s 's of Ge/CuBr, CuBr/GaAs, and GaAs/Ge are found to be in the range: $0.4 \leq \Delta E_s \leq 0.9$ eV. Thus, the 0.64-eV transitivity deviation is comparable in magnitude to the individual ΔE_s values.

An interesting consequence of nontransitivity would appear in a repeating slab structure of, for example, Ge/CuBr/GaAs/Ge, etc. If the bulk semiconductor doping is chosen so that a flat-band condition is expected, the electrostatic potential would have to change by 0.64 eV for each repeat of three interfaces. Therefore, the potential across a repeating structure would become arbitrarily large. As this is unreasonable, nontransitivity of energy-band discontinuities implies that charge accumulation and/or space-charge formation must occur at one or more of the interfaces in each three-junction sequence to result in band bending that cancels the potential change.

A primary objective for a theoretical model of semiconductor heterojunctions should be a quantitative prediction of the interface band discontinuities. Models¹⁻³ which have been developed for this purpose have a transitive relationship for the band discontinuities. The widely used electron-affinity rule¹ depends on the difference in a sur-

face property of semiconductor materials (this approach has been reviewed in detail⁸). Models developed in Refs. 2, 3 express band discontinuities in terms of bulk-material properties. The explicit calculation of interface electronic structure has been used to obtain energy-band discontinuities for a few selected heterojunctions.^{9,10} The self-consistent pseudopotential calculations¹⁰ for (110) interfaces of Ge/GaAs, GaAs/ZnSe, and ZnSe/Ge suggest that these band discontinuities may be nontransitive; however, the reported error limits do not allow an unambiguous conclusion. The large deviation from transitive behavior for semiconductor-heterojunction energy-band discontinuities that we report suggests that heterojunction models need to explicitly treat true interface properties associated with reconstruction and charge redistribution and should not be inherently transitive if ΔE_s and ΔE_c are to be accurately predicted.

The authors acknowledge helpful discussions with Dr. E. A. Kraut and Dr. S. P. Kowalczyk. This work was supported by the U. S. Office of Naval Research, Contract No. N00014-76-C-1109.

¹R. L. Anderson, Solid-State Electron. **5**, 341 (1962).

²W. A. Harrison, J. Vac. Sci. Technol. **14**, 1016 (1977).

³W. R. Frensel and H. Kroemer, Phys. Rev. B **16**, 2642 (1977).

⁴See, for example, S. F. Lin, W. E. Spicer, and R. S. Bauer, Phys. Rev. B **14**, 4551 (1976).

⁵B. Z. Olshanetsky, S. M. Repinsky, and H. A. Shklyarev, Surf. Sci. **64**, 224 (1977).

⁶R. W. Grant, J. R. Waldrop, and E. A. Kraut, Phys. Rev. Lett. **40**, 656 (1978).

⁷R. W. Grant, J. R. Waldrop, S. P. Kowalczyk, and E. A. Kraut, unpublished data.

⁸H. Kroemer, Crit. Rev. Solid State Sci. **5**, 555 (1975).

⁹G. A. Baraff, J. A. Appelbaum, and D. R. Hamann, Phys. Rev. Lett. **38**, 237 (1977).

¹⁰W. E. Pickett, S. G. Louie, and M. L. Cohen, Phys. Rev. Lett. **39**, 109 (1977); W. E. Pickett and M. L. Cohen, Phys. Rev. B **18**, 939 (1978); J. Ihm and M. L. Cohen, Phys. Rev. B **20**, 729 (1979).

XPS measurement of GaAs-AlAs heterojunction band discontinuities: Growth sequence dependence

J. R. Waldrop, S. P. Kowalczyk, R. W. Grant, E. A. Kraut, and D. L. Miller

Rockwell International Microelectronics Research & Development Center, Thousand Oaks, California 91360

(Received 17 February 1981; accepted 24 April 1981)

We report the direct measurement, by x-ray photoemission spectroscopy, of the valence-band discontinuity, ΔE_v , for two types of abrupt GaAs-AlAs (110) heterojunctions grown by molecular beam epitaxy: (i) those formed by growth of GaAs on AlAs, and (ii) those grown in the reverse sequence, AlAs on GaAs. The ΔE_v at GaAs-AlAs interfaces is, on average, 0.25 eV larger than at AlAs-GaAs interfaces. The ΔE_v for GaAs-AlAs heterojunctions was found to average 0.4 eV; the corresponding ΔE_v for AlAs-GaAs heterojunctions averaged 0.15 eV. The 0.25 eV difference in average ΔE_v value that we observe for the two types of interface demonstrates that the energy-band discontinuities depend on growth sequence in the GaAs-AlAs heterojunction system.

PACS numbers: 73.40.Lq, 68.55.+b, 33.60.Fy, 81.10.-h

I. INTRODUCTION

Heterojunctions involving the GaAs-Al_xGa_{1-x}As system have attracted considerable recent experimental and theoretical interest. A wide range of devices and applications for this heterojunction system have been either developed or envisioned; including, lasers, superlattices, modulation-doped structures, transistors, CCDs, and solar cells. A fundamental feature of the electronic structure of heterojunctions is the discontinuity in the valence band and conduction band, ΔE_v and ΔE_c , owing to the band gap difference ΔE_g across the interface. Since the electrical properties of heterojunctions can strongly depend on ΔE_v and ΔE_c , knowledge of their magnitude in the important GaAs-Al_xGa_{1-x}As system is essential.

We report the direct measurement, by x-ray photoemission spectroscopy (XPS), of the valence-band discontinuity for two types of GaAs-AlAs (110) abrupt heterojunctions: (i) those formed by growth of GaAs on AlAs (designated GaAs-AlAs), and by the reverse growth sequence, (ii) AlAs grown on GaAs (AlAs-GaAs). These heterojunctions were grown under similar conditions by molecular beam epitaxy (MBE). The ΔE_v for the GaAs-AlAs interfaces ranged from 0.32 to 0.50 eV with a 0.4 eV average value. The ΔE_v for AlAs-GaAs interfaces ranged from 0.12 to 0.19 eV with a 0.15 eV average value. This 0.25 eV difference in average ΔE_v value that we observe for the two types of interface demonstrates that heterojunction band discontinuities in the GaAs-AlAs system depend on the MBE growth sequence in which the interface is formed (noncommutativity effect).

II. EXPERIMENTAL PROCEDURE

The schematic energy-band diagram given in Fig. 1 for an abrupt GaAs-AlAs (or AlAs-GaAs) heterojunction interface depicts the energy values we measure by XPS to ascertain ΔE_v .

(additional details of XPS heterojunction measurements may be found elsewhere^{1,2}). Shown are the valence and conduction band edges, E_v and E_c , $\Delta E_v \equiv (E_v^{AlAs} - E_v^{GaAs})$, $\Delta E_c \equiv (E_c^{GaAs} - E_c^{AlAs})$, and the binding-energy difference $\Delta E_B = (E_{Al2p}^{AlAs} - E_{Ga3d}^{GaAs})$ across the interface between the Al 2p core level from the AlAs side of the junction and the Ga 3d core level from the GaAs side. Thus by inspection, ΔE_v is

$$\Delta E_v = \Delta E_B + (E_{Ga3d}^{GaAs} - E_v^{GaAs}) - (E_{Al2p}^{AlAs} - E_c^{AlAs}) \quad (1)$$

The core-level to valence-band binding-energy difference terms in Eq. (1) are material constants which are separately measured on samples of pure GaAs and AlAs³; thus Eq. (1) is of the form $\Delta E_v = \Delta E_B + \text{constant}$. It follows that any change in ΔE_B value measured in a series of heterojunctions by XPS directly corresponds to the same change in ΔE_v . Note that a measurement of ΔE_v also measures ΔE_c through the relationship $\Delta E_v + \Delta E_c = \Delta E_g$.

For an appropriate GaAs-AlAs (or AlAs-GaAs) heterojunction sample, ΔE_B can be measured with high accuracy by XPS to provide a direct measure of ΔE_v . Moreover, although the binding-energy scale in Fig. 1 is referenced to the Fermi level, Eq. (1) for ΔE_v involves solely energy differences. Thus it is not necessary to know the actual Fermi-level position; any bulk doping difference or interface states that result in band bending do not affect the analysis or the XPS measurement.

The experimental apparatus is a Hewlett-Packard 5950A XPS spectrometer combined with an ultrahigh vacuum (UHV) sample preparation chamber. This system includes LEED (low energy electron diffraction) and a sample heater. System base vacuum pressure is $\sim 1 \times 10^{-10}$ Torr (1.3×10^{-8} Pa). The XPS x-ray source is monochromatic Al K α ($h\nu = 1486.6$ eV) radiation.

The two types of abrupt heterojunction samples were grown by MBE in a system designed and constructed at our laboratory. For each type of sample the substrate is (110) oriented

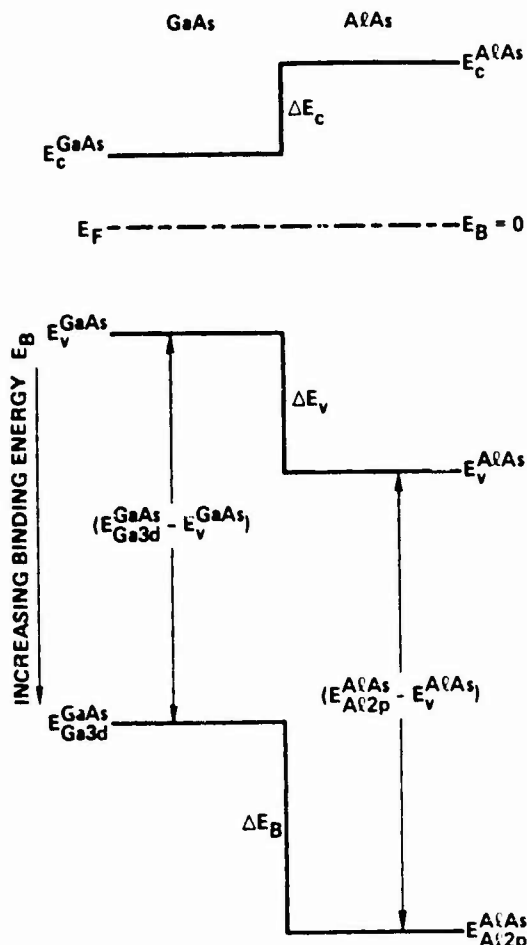


FIG. 1. Schematic energy-band diagram for an abrupt GaAs-AlAs (AlAs-GaAs) interface.

n-type GaAs ($N_D \sim 5 \times 10^{16} \text{ cm}^{-3}$) upon which is first grown an $\sim 5000 \text{ \AA}$ GaAs buffer layer. To form an AlAs-GaAs junction suitable for XPS investigation, a $\sim 20 \text{ \AA}$ thick layer of AlAs is grown onto this buffer layer. For the GaAs-AlAs junction this AlAs layer is continued to a thickness of $\sim 1000 \text{ \AA}$ then followed by the growth of an $\sim 20 \text{ \AA}$ thick GaAs top layer. In each sample the junction studied is that between the 20 \AA top layer and layer directly underneath. The 20 \AA top layer thickness is adequate to ensure that the heterojunction interface properties are bulk-like.⁴ All the layers were grown at a temperature of 580°C . Careful control was exercised over substrate temperature and the fluxes from the Ga, Al, and As sources to keep sample-to-sample growth conditions as similar as possible. Interfaces in the AlAs-GaAs heterojunction system formed by MBE are well known to be abrupt on the order of atomic dimensions.⁵

The samples were protected from contamination, particularly oxidation, during their removal from the MBE growth system to the XPS apparatus by using a novel transfer technique (which will be described in detail elsewhere). In brief, after growth of the epitaxial layers a finished sample is cooled to $<20^\circ\text{C}$ and exposed to only the MBE As₄ source to condense a protective layer of elemental As onto the sample surface. After transfer in air to the XPS vacuum system, which takes $\sim 10 \text{ min}$, and following attainment of UHV, the sample is heated to $\sim 350^\circ\text{C}$ to evaporate the As overlayer. XPS and

LEED measurements show that this procedure leaves the underlying GaAs or AlAs surface atomically clean and crystalline.

For our heterojunction samples, in which a thin (on the order of the 25 \AA XPS sampling depth) surface layer of one semiconductor lies on a relatively thick ($>500 \text{ \AA}$) layer of another, photoelectrons that originate from each side of the interface are observed in the same XPS spectrum. For example, the upper spectrum in Fig. 2 is the XPS core-level spectra for a GaAs-AlAs sample over a binding-energy interval that includes the Al 2p, Ga 3d, and As 3d peaks; similarly, the lower spectrum is for an AlAs-GaAs sample. In each spectrum the photoelectrons in the Al 2p peak originate from the AlAs side of the interface and the photoelectrons contributing to the Ga 3d peak originate from the GaAs side. The ΔE_B shown in Fig. 2 indicates the Al 2p to Ga 3d energy separation in each spectrum that is needed to evaluate Eq. (1).

To accurately determine ΔE_B from the raw data, a background function which is proportional to the integrated peak area was subtracted from each core-level peak to correct for the effect of inelastic scattering. Core-level energies were consistently measured at the center of the peak-width at half-height.

III. RESULTS

Table I gives the ΔE_B values measured (at room temperature) for the Al 2p to Ga 3d core-level binding-energy difference for three GaAs-AlAs interfaces (a-c) and for three

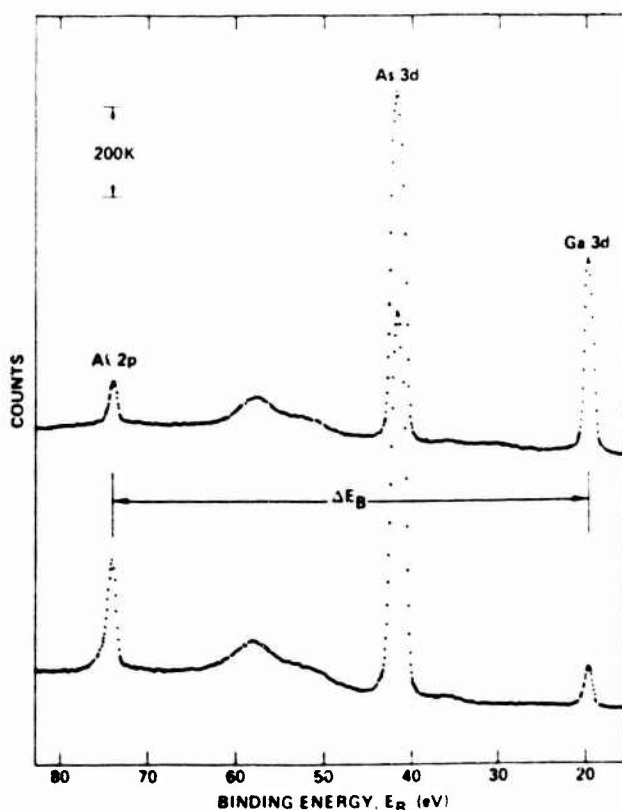


FIG. 2. XPS core-level spectra in the binding-energy region of the Al 2p and Ga 3d levels obtained from MBE-grown GaAs-AlAs (upper) and AlAs-GaAs (lower) (110) interfaces.

TABLE I. XPS core-level binding-energy difference ΔE_B (Al 2p to Ga 3d) and valence-band discontinuity ΔE_v for GaAs-AlAs and AlAs-GaAs interfaces.

Sample	Interface	ΔE_B (eV) ^{a)}	ΔE_v (eV)
a	GaAs-AlAs	54.60	0.50
b	GaAs-AlAs	54.42	0.32
c	GaAs-AlAs (~600°C)	54.48	Avg
d	AlAs-GaAs	54.29	0.19
e	AlAs-GaAs	54.22	0.12
f	AlAs-GaAs	54.24	Avg
g	(f heated to ~550°C)	54.27	0.17

^{a)} Error limit is ± 0.02 eV.

AlAs-GaAs interfaces (d-f). Samples a-d are Si-doped and are from different growth runs; samples e and f are undoped AlAs on Sn-doped GaAs and are from the same growth run. Samples c and g were heated momentarily to $\sim 600^\circ$ and $\sim 550^\circ$ C, respectively.

We have recently reported a value of 18.81 ± 0.02 eV for $(E_{\text{GaAs}}^{\text{GaAs}} - E_{\text{t}}^{\text{GaAs}})$ in GaAs.¹ By using the same procedure described for GaAs, we have measured $(E_{\text{Al2p}}^{\text{AlAs}} - E_{\text{t}}^{\text{AlAs}})$ for AlAs and have obtained a preliminary value of 72.9 eV. Substitution of these values into Eq. (1) gives $\Delta E_v = \Delta E_B - 54.1$ eV, which is used to obtain the ΔE_v values listed in Table I. The results of additional experiments which are in progress should provide a refined value for $(E_{\text{Al2p}}^{\text{AlAs}} - E_{\text{t}}^{\text{AlAs}})$ and thus refined values for ΔE_v .

For the GaAs-AlAs interface the average value of ΔE_v is 0.4 eV; the individual interface ΔE_v values are within ± 0.10 eV of the average. The AlAs-GaAs interface has an average value for ΔE_v of 0.15 eV; the individual interface ΔE_v values are within ± 0.04 eV of the average. No change in ΔE_v as a result of heating was apparent for either type of interface. As a group, the samples show a variation in ΔE_v of 0.38 eV, which is a large fraction of $\Delta E_g = 0.7$ eV (calculated by using the indirect, room temperature, AlAs band gap, $E_g = 2.15$ eV).

IV. DISCUSSION

The 0.25 eV difference in average ΔE_v value that we observe for the two types of interface (which follows directly from the ΔE_B values) is clear evidence that ΔE_v depends on MBE growth sequence in the GaAs-AlAs system. Such a noncommutativity effect for energy-band discontinuities indicates a large variation in magnitude of an interface electrostatic dipole. This dipole variation could arise if the AlAs-GaAs and GaAs-AlAs interfaces have different characteristic structures. The small variation in ΔE_v observed for AlAs-GaAs may indicate, for example, a more reproducible structure for this interface. The larger variation in ΔE_v for GaAs-AlAs is evidence for a less reproducible interface structure.

The interface effects which give rise to noncommutativity in the GaAs-AlAs system are likely to be the same which cause the nontransitivity² seen when comparing the energy-band discontinuities associated with three or more heterojunction pairs. Thus the noncommutativity effect is probably also present in other heterojunction systems.

Optical measurements of superlattices that consist of alternating layers of $\text{Al}_x\text{Ga}_{1-x}\text{As}$ and GaAs for $x = 0.2$ by Dingle *et al.*⁶ found that $\Delta E_v / \Delta E_g = 0.15$. In comparison, if we use the difference in direct gaps for $x = 1$, which is $\Delta E_g = 2.9 - 1.43 = 1.47$ eV, and our average value of 0.15 eV for AlAs-GaAs, then we find $\Delta E_v / \Delta E_g \sim 0.1$ for this interface. By using the average ΔE_v of 0.4 eV for the GaAs-AlAs interface we find $\Delta E_v / \Delta E_g \sim 0.3$. Thus our results suggest that growth sequence should be considered when assuming $\Delta E_v / \Delta E_g = \text{constant}$ for all values of x .

The noncommutativity of ΔE_v with respect to growth shows that the carrier-confinement potentials formed in superlattice $\text{Al}_x\text{Ga}_{1-x}\text{As}-\text{GaAs}$ quantum well structures may be more complex than present models suggest. Noncommutativity also has implications for modulation-doped heterojunction structures,⁷ as, for example, when ΔE_v is used to confine at the interface the electrons transferred from a heavily n-type $\text{Al}_x\text{Ga}_{1-x}\text{As}$ layer to an adjacent undoped GaAs layer. For GaAs-AlAs interfaces our results have shown that ΔE_v is significantly smaller than presently predicted and consequently will provide a less effective confinement barrier than expected. In fact, this may explain the recently reported observation that MBE grown modulation-doped $\text{Al}_x\text{Ga}_{1-x}\text{As}-\text{GaAs}$ interfaces show a mobility enhancement while GaAs-Al_xGa_{1-x}As interfaces do not.⁸

In summary, we have measured the energy-band discontinuities for MBE grown GaAs-AlAs and AlAs-GaAs interfaces and have found a significant difference in magnitude as a function of growth sequence (noncommutativity effect).

ACKNOWLEDGMENTS

The authors thank Peter Newman for the MBE sample growths. This work was supported by the U.S. Office of Naval Research, Contract No. N00014-76-C-1109.

¹E. A. Kraut, R. W. Grant, J. R. Waldrop, and S. P. Kowalczyk, Phys. Rev. Lett. 44, 1620 (1980).

²J. R. Waldrop and R. W. Grant, Phys. Rev. Lett. 43, 1686 (1979).

³If sizable chemical shifts were to occur with interface bond formation the core-level to valence-band terms could be affected. However, since in our experiment the escape depth for XPS photoelectrons is large compared to the interface dimension (by a factor of ~ 10), only $\sim 10\%$ of the photoelectrons contributing to an XPS spectrum originate from the atoms at an abrupt interface. Also, chemical shifts, if present should broaden the Ga 3d and Al 2p core-level peaks observed from heterojunction samples compared to those from pure GaAs and AlAs samples. No difference in Ga 3d or Al 2p core-level peak widths (to within ~ 0.03 eV) was observed in the spectra from heterojunctions and the respective pure materials, thus any chemical shifts associated with the interface are not expected to complicate the ΔE_v measurements.

⁴W. E. Pickett, S. G. Louie, and M. L. Cohen, Phys. Rev. B 17, 815 (1978).

⁵L. Esaki and L. L. Chang, CRC Crit. Rev. Solid State Sci. 6, 195 (1976); L. L. Chang, A. Segmüller, and L. Esaki, Appl. Phys. Lett. 28, 39 (1976).

⁶R. Dingle, W. Wiegmann, and C. H. Henry, Phys. Rev. Lett. 33, 827 (1974); R. Dingle, A. C. Gossard, and W. Wiegmann, Phys. Rev. Lett. 34, 1327 (1975).

⁷R. Dingle, H. L. Stormer, A. C. Gossard, and W. Wiegmann, Appl. Phys. Lett. 33, 665 (1978).

⁸H. Morkoc, L. C. Witkowski, T. J. Drummond, C. M. Stachak, A. Y. Cho, and B. G. Streetman, Electron. Lett. 16, 753 (1980).

Measurement of ZnSe-GaAs(110) and ZnSe-Ge(110) heterojunction band discontinuities by x-ray photoelectron spectroscopy (XPS)

Steven P. Kowalczyk, E. A. Kraut, J. R. Waldrop, and R. W. Grant

Rockwell International, Microelectronics Research and Development Center, Thousand Oaks, California 91360

(Received 27 January 1982; accepted 5 April 1982)

X-ray photoelectron spectroscopy was used to study the growth and energy-band alignment of ZnSe-GaAs(110) and ZnSe-Ge(110) heterojunctions. The ZnSe-GaAs heterojunctions were formed by growing ZnSe on GaAs(110). Growth temperatures were varied to produce both epitaxial and nonepitaxial interfaces. For ZnSe grown at $\sim 300^\circ\text{C}$ on GaAs(110), the valence-band discontinuity ΔE_v was 0.96 eV; for ZnSe deposited at room temperature and crystallized at $\sim 300^\circ\text{C}$, ΔE_v is 1.10 eV. The Ge-ZnSe(110) interfaces were formed by depositing Ge(ZnSe) on ZnSe(Ge)(110) at room temperature, followed by $\sim 300^\circ\text{C}$ crystallization. The corresponding ΔE_v 's were 1.52 and 1.29 eV, respectively. Our measured ΔE_v values for epitaxial heterojunctions are compared with the predictions of theoretical models. Our results demonstrate that substantial interface structure dependent contributions to ΔE_v can occur at Ge-ZnSe(110) and GaAs-ZnSe(110) heterojunctions.

PACS numbers: 73.40.Lq, 71.25.Tn, 79.60.Eq

I. INTRODUCTION

Semiconductor heterojunction structures are becoming an increasingly important element in the design of advanced solid-state electronic devices. Among the key parameters which characterize semiconductor-semiconductor contacts are the valence-band and conduction-band discontinuities, ΔE_v and ΔE_c , respectively, present at the interface between two semiconductors. In the past, these key quantities have been predicted by using simple phenomenological models; however, in recent years, more sophisticated quantum mechanical calculations of the electronic structure of heterojunctions have also become available.¹⁻⁷ These calculations either predict the band discontinuities, or use the band discontinuities as input parameters. Thus, there is a necessity for reliable measurements of these band discontinuities on a wide variety of heterojunctions. Photoemission techniques have been recently applied to the determination of ΔE_v .⁸⁻¹⁴ X-ray photoelectron spectroscopy has been shown to be particularly useful for the direct determination of ΔE_v .^{11,15-17} One of the principal results of these XPS studies was to demonstrate that interface properties can significantly influence ΔE_v . Thus, in the Ge-GaAs, GaAs-CuBr, Ge-CuBr series of heterojunctions, it was shown that ΔE_v is not a transitive property¹⁵; for GaAs-AlAs heterojunctions, ΔE_v was found to depend on the growth sequence.¹⁶

In this paper, we report the results of XPS measurements on heterojunctions of ZnSe with the isoelectronic, lattice-matched semiconductors Ge and GaAs. All the investigated heterojunctions were grown *in situ* under ultrahigh vacuum (UHV) conditions by \sim tens of molecular beam epitaxy (MBE). The goal of the present paper is to study the role of growth details on the magnitude of ΔE_v , and to compare these results with the available models used to predict ΔE_v .

II. XPS MEASUREMENTS

The XPS measurements were obtained with a Hewlett-Packard HP 5950A electron spectrometer system,¹⁸ modi-

fied for UHV ($< 10^{-10}$ Torr). Monochromatized AlK α ($h\nu = 1486.6$ eV) x rays were utilized as the excitation source. The sample substrates are mounted on Mo plates with In. The Mo plate is clamped to a sample heater capable of heating to $\sim 1000^\circ\text{C}$. The sample preparation chamber includes a low energy electron diffraction (LEED) system.

The schematic energy-band diagrams, Figs. 1(a) and 1(b), illustrate the XPS technique¹¹ for determining band discontinuities for the GaAs-ZnSe and Ge-ZnSe heterojunctions. It can be easily seen that three quantities are necessary to determine ΔE_v for a particular heterojunction, two of which are the core-level to valence-band maximum energy separation for each constituent of the heterojunction. For example, in the case of the GaAs-ZnSe heterojunction, one needs to obtain the quantities ($E_{\text{Ga}3d}^{\text{GaAs}} - E_{\text{Zn}3d}^{\text{GaAs}}$) and ($E_{\text{Zn}3d}^{\text{ZnSe}} - E_{\text{Zn}3d}^{\text{ZnSe}}$). The third quantity, obtained by measurement on the heterojunction itself (Fig. 2), is a core-level binding-energy difference ΔE_{Cl} for a core level on each side of the heterojunction. Thus, for the GaAs-ZnSe case, ΔE_{Cl} is ($E_{\text{Ga}3d}^{\text{GaAs}} - E_{\text{Zn}3d}^{\text{ZnSe}}$). For the materials of interest in this study, we have previously¹¹ obtained ($E_{\text{O}2s}^{\text{Oxid}} - E_{\text{O}2s}^{\text{Oxid}}$) = 18.81 ± 0.02 eV and ($E_{\text{O}2s}^{\text{Oxid}} - E_{\text{O}2s}^{\text{Oxid}}$) = 29.55 ± 0.02 eV. Therefore, the only quantities we need to obtain are ($E_{\text{Zn}3d}^{\text{ZnSe}} - E_{\text{Zn}3d}^{\text{ZnSe}}$) and the ΔE_{Cl} for the various heterojunctions grown under the desired conditions.

III. GROWTH DETAILS

The substrates for the growths were bulk grown GaAs which had been wafered and polished to give a (110) surface and 20 mil thickness (obtained from Crystal Specialties). Prior to mounting on the Mo plates, the substrates were chemically etched with a fresh 4:1:1 solution of $\text{H}_2\text{SO}_4:\text{H}_2\text{O}_2:\text{H}_2\text{O}$ for ~ 1 min to remove polishing damage. The substrates were loaded into the spectrometer vacuum within several minutes of etching. This surface preparation produced a several monolayer thick native oxide layer.¹⁹ The growth sur-

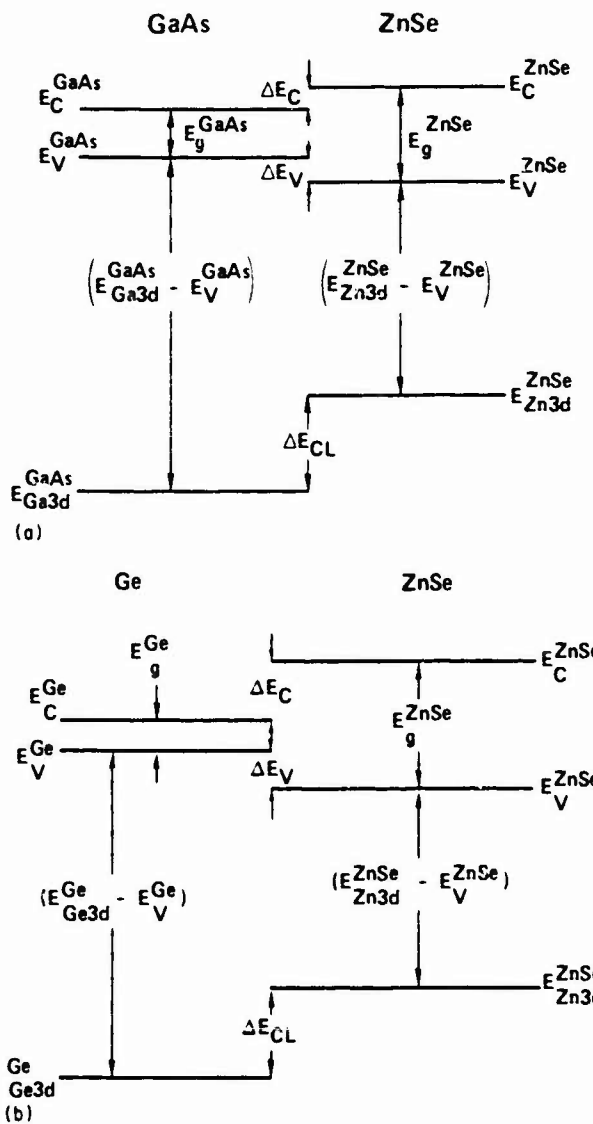


FIG. 1. Schematic energy-band diagram which shows the quantities necessary to determine ΔE_v and ΔE_c for a heterojunction. (a) GaAs-ZnSe; (b) Ge-ZnSe.

face is prepared by heating to $\sim 550^\circ\text{C}$ for ~ 30 s in the UHV of the sample preparation chamber. This treatment yields an atomically clean and ordered surface as determined by XPS spectra of contaminant spectral regions and LEED.¹⁹ The crystallinity of all substrates prior to overlayer deposition was confirmed in all cases by LEED measurements.

The ZnSe source is a single charge quartz oven filled with high purity (99.999%) ZnSe (from Cerac). ZnSe evaporates via congruent vaporization to produce a Zn and Se₂ flux. Similar single charged MBE sources have been successfully used for ZnSe by Smith and Pickhardt²⁰ and by Ludeke.²¹ XPS measurements of the relative Zn and Se core-level intensities and splittings were used to confirm that the surfaces prepared in this manner were atomically clean and stoichiometric. The ZnSe films were grown at rates of ~ 1 Å/min. Films deposited at room temperature could be crystallized by annealing to $\sim 300^\circ\text{C}$ for ~ 1 min, as determined by LEED measurements. Films were also grown epitaxially

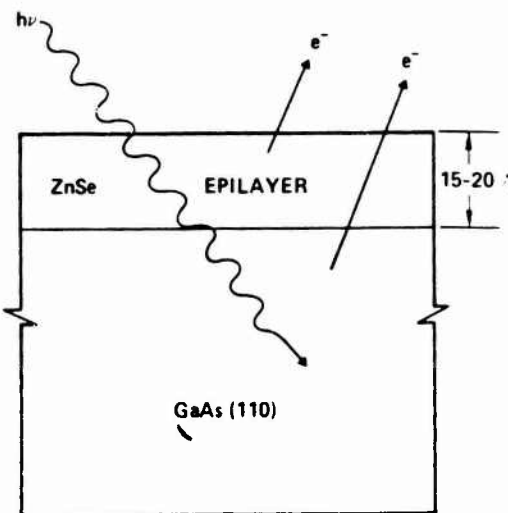


FIG. 2. Schematic of sample for XPS measurements of ZnSe-GaAs(110) heterojunction.

with substrate temperatures of $\sim 300^\circ\text{C}$. Samples deposited with substrate temperatures of $\sim 400^\circ\text{C}$ would not grow, due to re-evaporation from the surface. The Ge source was a resistively heated W basket, as used previously in studies of the Ge-GaAs(110) heterojunction.¹¹ The Ge deposition rates were generally ~ 1 Å/s. Ge films deposited at room temperature could be crystallized by annealing to $\sim 300^\circ\text{C}$, as determined by LEED.

IV. RESULTS

Figure 3 shows a XPS spectrum of the Zn3d core-level and valence-band region from a ZnSe(110) epilayer (~ 100 Å). To determine $(E_{Zn3d}^{ZnSe} - E_{Zn3d}^{ZnSe})$, the Chelikowsky-Cohen nonlocal pseudopotential valence-band density of states for ZnSe²² is broadened by the instrumental line shape (a Voigt function). The instrumental function is obtained from an analysis of the Au4f line shape as described in more detail in Ref. 11. The instrumentally broadened theoretical function is least squares fit to the experimental data in the region

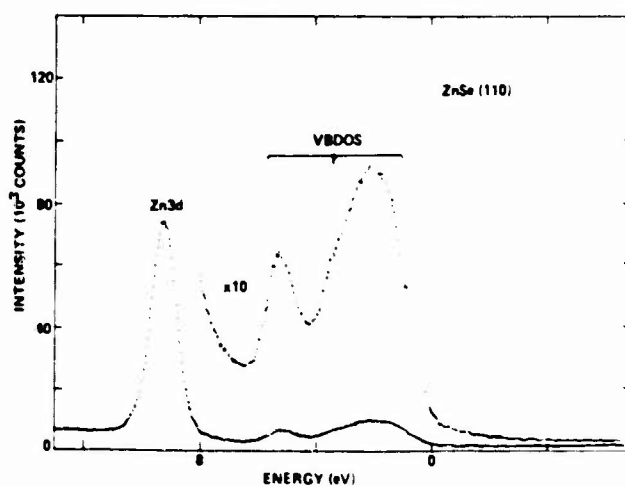


FIG. 3. XPS spectrum of the Zn3d core-level and valence-band region from a ZnSe(110) epilayer.

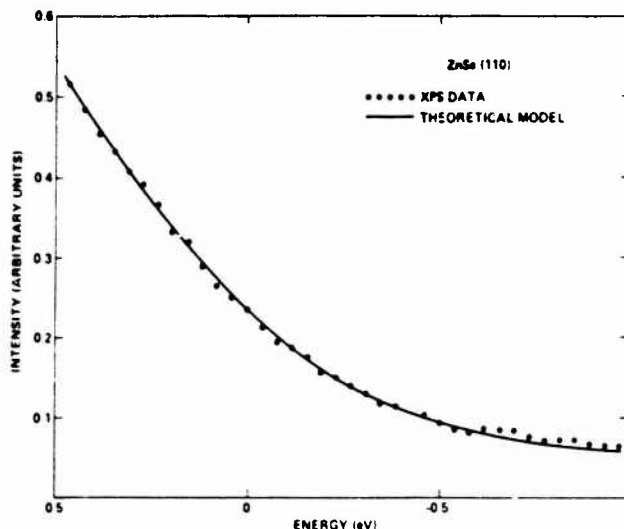


FIG. 4. Comparison of XPS data (...) with the fitted instrumentally broadened theoretical density of states (—) in the region of the valence-band maximum of ZnSe(110). The valence-band maximum is at zero energy.

around the valence-band maximum. The fit of the theoretical model to the XPS data for ZnSe(110) in the region of the valence-band maximum is shown in Fig. 4. This analysis gives $(E_{\text{Ge}3d}^{\text{ZnSe}} - E_{\text{Zn3d}}^{\text{ZnSe}})$ as 8.90 ± 0.02 eV. The Zn3d core-level data had a background function subtracted which is proportional to the integrated photoelectron peak area. The core-level energy position is defined as the center of the peak width at half-height. This definition makes resolution of the spin-orbit splitting of the Zn3d levels unnecessary. All the relevant core-level to valence-band maximum binding-energy differences are tabulated in Table I.

Figure 5 shows XPS spectra from three heterojunctions. Spectra such as these, after background subtraction of all core levels as described above, were used to obtain ΔE_{Cl} for a variety of heterojunctions. The ΔE_{Cl} for the heterojunctions prepared under several conditions are summarized in Table II.

V. DISCUSSION

Table III lists the measured ΔE_{v} 's for the epitaxial heterojunctions grown in this study. For the ZnSe-GaAs(110) system, there is more than a 0.1-eV difference in ΔE_{v} between samples where the ZnSe was deposited at room temperature and crystallized at ~ 300 °C and those which were grown epitaxially at ~ 300 °C. For the Ge-ZnSe(110) system, there was a ~ 0.2 -eV difference in ΔE_{v} , depending on the growth

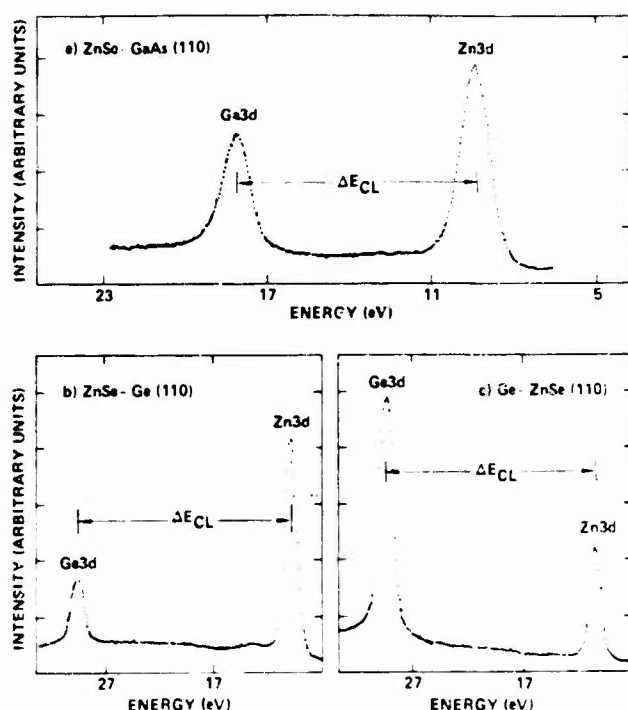


FIG. 5. XPS core-level spectra from three heterojunctions: (a) ZnSe-GaAs(110); (b) ZnSe-Ge(110); and (c) Ge-ZnSe(110).

sequence. Thus, the details of growth, which probably affect the detailed structure at the interface, can have a substantial effect on ΔE_{v} . None of the available heterojunction theories have as yet accounted for interface structure dependent contributions to ΔE_{v} .

To determine a ΔE_{v} for the nonepitaxial heterojunctions by using the ΔE_{Cl} values given in Table II, it is necessary to know the core-level to valence-band maximum binding-energy differences of the nonepitaxial overlayer material. Presumably, these values would depend on the amorphous nature or crystalline state of the overlayer. In either case, as these values are presently not known, we will only compare the observed ΔE_{Cl} 's presented in Table II. For the Ge-ZnSe(110) heterojunctions, there was a ~ 0.3 -eV difference in ΔE_{Cl} before and after the Ge layers were converted from amorphous to crystalline. For the ZnSe-Ge(110) heterostructure, there was no difference in ΔE_{v} between annealed

TABLE II. Core-level binding-energy differences ΔE_{Cl} (eV)* for several heterojunctions.

Heterojunction	Epitaxial	Nonepitaxial
Ge-ZnSe(110)	19.13 ± 0.02^b	18.81 ± 0.02^b
ZnSe-Ge(110)	19.36 ± 0.02^b	19.36 ± 0.02^b
ZnSe-GaAs(110)	$8.81 \pm 0.01^{a,c}$...
		$8.95 \pm 0.02^{a,d}$

* ΔE_{Cl} is either $(E_{\text{Ge}3d}^{\text{Ge}} - E_{\text{Zn3d}}^{\text{ZnSe}})$ or $(E_{\text{Ga3d}}^{\text{GaAs}} - E_{\text{Zn3d}}^{\text{ZnSe}})$.

^a Overlayer deposited on substrate at 23 °C and annealed at ~ 300 °C.

^b Overlayer deposited on substrate at 23 °C and not annealed.

^c Average of three samples.

^d Overlayer deposited on substrate at ~ 300 °C.

TABLE I. Core-level to valence-band maximum binding-energy differences (eV).

$(E_{\text{Ge}3d}^{\text{Ge}} - E_{\text{Zn3d}}^{\text{ZnSe}})$	$= 29.55 \pm 0.02^a$
$(E_{\text{Ga3d}}^{\text{GaAs}} - E_{\text{Zn3d}}^{\text{ZnSe}})$	$= 18.81 \pm 0.02^a$
$(E_{\text{Zn3d}}^{\text{ZnSe}} - E_{\text{Zn3d}}^{\text{ZnSe}})$	$= 8.90 \pm 0.02^a$

^a Reference 11.

^b This work.

TABLE III. Valence-band discontinuities for epitaxial heterojunctions.

Heterojunction	ΔE_v (eV)
Ge-ZnSe(110)	1.52 \pm 0.03 ^a
ZnSe-Ge(110)	1.29 \pm 0.03 ^a
ZnSe-GaAs(110)	1.10 \pm 0.03 ^{a,b}
	0.96 \pm 0.03 ^b

^aOverlayer deposited on substrate at 23 °C and annealed at ~300 °C.^bAverage of three samples.^cOverlayer deposited on substrate at ~300 °C.

and unannealed ZnSe layers. This may be due to the ZnSe being polycrystalline for room temperature deposition, while room temperature deposition of the Ge yields amorphous films.

In Table IV, the ΔE_v predictions of various models are given. An early, still frequently employed, model is the electron affinity rule (EAR) proposed by Anderson.²³ Other methods include the LCAO approach of Harrison²⁴ and a pseudopotential model of Frenzley and Koenemer (FK).²⁵ Self-consistent pseudopotential (SCPP) calculations have also recently become available.⁴⁻⁶ Table IV indicates that the LCAO approach gives closest agreement with the experimental values (Table III) for the epitaxial interfaces. Margaritondo *et al.*⁹ have previously noted that the LCAO model is in reasonable agreement with ΔE_v 's obtained by depositing amorphous Ge on several semiconductors. However, the significance of comparing data on nonlattice matched heterojunctions which involve amorphous layers with predictions of an LCAO model for crystalline interfaces requires further explanation.

TABLE IV. Predictions of ΔE_v (in eV) by several theories.

Heterojunction	LCAO ^a	FK ^b	EAR ^c	SCPP ^d
Ge-ZnSe(110)	1.46	1.84	1.97	2.00 ^e
ZnSe-GaAs(110)	1.05	1.21	1.22	2.00 ^f

^aReference 24.^bReference 25.^cA. G. Milnes and D. L. Feucht, *Heterojunctions and Metal-Semiconductor Junctions* (Academic, New York, 1972), p. 9.^dReference 5.^eReference 6.

In summary, ΔE_v values have been obtained for ZnSe-GaAs(110) and ZnSe-Ge(110) heterojunctions prepared under several different growth conditions. ΔE_v was shown to be significantly dependent on the growth parameters, i.e., the details of interface structure.

ACKNOWLEDGMENT

This work was supported by ONR Contract #N00014-76-C-1109.

- ¹M. L. Cohen, *Adv. Electron. Electron Phys.* **51**, 1 (1980).
- ²J. Pollman, *Festkörperprobleme* **20**, 117 (1980).
- ³M. Schlüter, *Festkörperprobleme* **18**, 155 (1978).
- ⁴W. E. Pickell, S. G. Louie, and M. L. Cohen, *Phys. Rev. B* **17**, 815 (1978).
- ⁵W. E. Pickell and M. L. Cohen, *Phys. Rev. B* **18**, 939 (1978).
- ⁶J. Ihm and M. L. Cohen, *Phys. Rev. B* **20**, 729 (1979).
- ⁷A. Madhukar and J. Delgado, *Solid State Commun.* **37**, 199 (1981).
- ⁸G. Margaritondo, N. G. Stoffel, A. D. Katani, H. S. Edelman, and C. M. Bertoni, *J. Vac. Sci. Technol.* **18**, 784 (1981).
- ⁹A. D. Katani, R. R. Daniels, Te-Xiu Zhao, and G. Margaritondo, *J. Vac. Sci. Technol.* **20**, 662 (1982); G. Margaritondo, *Bull. Am. Phys. Soc. Ser. II* **27**, 140 (1982).
- ¹⁰P. Perfetti, D. Denley, K. A. Mills, and D. A. Shirley, *Appl. Phys. Lett.* **33**, 667 (1978).
- ¹¹E. A. Kraut, R. W. Grant, J. R. Waldrop, and S. P. Kowalczyk, *Phys. Rev. Lett.* **44**, 1620 (1980).
- ¹²R. S. Bauer and J. C. McMenamin, *J. Vac. Sci. Technol.* **15**, 1444 (1978); R. S. Bauer, *ibid.* (submitted).
- ¹³R. W. Grant, J. R. Waldrop, and E. A. Kraut, *J. Vac. Sci. Technol.* **15**, 1451 (1978); *Phys. Rev. Lett.* **40**, 656 (1978).
- ¹⁴W. Mönch, R. S. Bauer, H. Gant, and R. Murschall, *J. Vac. Sci. Technol.* **21**, 498 (1982); W. Mönch, *Bull. Am. Phys. Soc. Ser. II* **27**, 141 (1982); W. Mönch and H. Gant, *J. Vac. Sci. Technol.* **17**, 1094 (1980).
- ¹⁵J. R. Waldrop and R. W. Grant, *Phys. Rev. Lett.* **43**, 1686 (1979).
- ¹⁶J. R. Waldrop, S. P. Kowalczyk, R. W. Grant, E. A. Kraut, and D. L. Miller, *J. Vac. Sci. Technol.* **19**, 573 (1981).
- ¹⁷S. P. Kowalczyk, W. J. Schaffer, E. A. Kraut, and R. W. Grant, *J. Vac. Sci. Technol.* **20**, 705 (1982).
- ¹⁸K. Seigbahn, D. Hammond, H. Feliner-Feldegg, and E. F. Barnett, *Science* **176**, 245 (1972).
- ¹⁹R. W. Grant, S. P. Kowalczyk, J. R. Waldrop, and W. A. Hill, in *The Physics of MOS Insulators*, edited by G. Lucovsky, S. T. Pantelides, and F. L. Galeener (Pergamon, New York, 1980), p. 202.
- ²⁰D. L. Smith and V. Y. Pickhardt, *J. Appl. Phys.* **46**, 2366 (1975).
- ²¹R. Ludeke, *Solid State Commun.* **24**, 725 (1977).
- ²²J. R. Chelikowsky and M. L. Cohen, *Phys. Rev. B* **14**, 556 (1976).
- ²³R. L. Anderson, *Solid State Electron.* **5**, 341 (1962).
- ²⁴W. A. Harrison, *Electronic Structure and the Properties of Solids* (Freeman, San Francisco, 1980), pp. 252-55.
- ²⁵W. R. Frenzley and H. Kroemer, *Phys. Rev. B* **16**, 2642 (1977).

Measurement of potential at semiconductor interfaces by electron spectroscopy

R. W. Grant, E. A. Kraut, S. P. Kowalczyk, and J. R. Waldrop

Rockwell International, Microelectronics Research and Development Center, Thousand Oaks, California 91360

(Received 10 January 1983; accepted 3 March 1983)

Electron spectroscopy performed in ultrahigh vacuum can be used to measure potential and heterojunction band discontinuities at abrupt semiconductor interfaces. The technique provides a direct contactless and nondestructive means to determine and correlate interface chemistry and potential. This article discusses some of the factors which affect applications of Auger electron spectroscopy, ultraviolet photoelectron spectroscopy, soft x-ray photoelectron spectroscopy, and x-ray photoelectron spectroscopy for semiconductor interface potential measurements.

PACS numbers: 73.40.Lq, 82.80.Pv

I. INTRODUCTION

The application of the frequently employed forms of electron spectroscopy, i.e., Auger electron spectroscopy (AES), ultraviolet photoelectron spectroscopy (UPS), soft x-ray photoelectron spectroscopy (SXPS), and x-ray photoelectron spectroscopy (XPS) to determine semiconductor interface elemental and chemical composition by analyzing emitted electron kinetic energies is well known. Several edited volumes and reviews (see, e.g., Refs. 1-8) as well as comparisons of relative merits (see, e.g., Refs. 9-11) have been published related to these techniques.

It is well established^{12,13} that the kinetic energy, E_K , of electrons emitted from a semiconductor depends on the position of the Fermi level (E_F) within the semiconductor band gap. This makes it possible to determine E_F relative to the semiconductor band edges in the region of the semiconductor from which the electrons originate. Electron spectroscopy can therefore measure semiconductor interface-potential-related quantities, i.e., band bending, Schottky-barrier height, and heterojunction band discontinuities, by a contactless nondestructive technique and provide a direct correlation of interface chemistry and potential. The majority of electron spectroscopic interface potential measurements have typically reported accuracies of ± 0.1 eV. Although many important results have been obtained with this level of accuracy, improvement would benefit several studies related to semiconductor device performance. This article discusses some of the principal factors which limit the application of electron spectroscopy for semiconductor interface-potential measurements and concludes that with refinement of currently existing experimental techniques it should be possible to improve substantially the measurement accuracy.

II. E_F MEASUREMENT AT SEMICONDUCTOR INTERFACES

The basic approach for utilizing electron spectroscopy to measure interface potentials is illustrated with the schematic energy-band diagram shown in Fig. 1. The quantities E_c^x , E_v^x , E_{cl}^x , δ^x , E_F^x , and V_{BB} defined in this figure are the conduction-band minimum, the valence-band maximum, the binding energy of an arbitrary core level, the position of E_F

in the semiconductor bulk relative to E_v^x , the energy gap, and the interface band-bending potential in semiconductor x respectively. The depletion layer width associated with V_{BB} is W and the binding-energy E_B scale (as discussed in Sec. II A) is referenced to E_F ($E_B = 0$ at E_F); E_B is defined both in the region of the bulk (b) semiconductor outside the depletion layer and at the interface (i). In order to use electron spectroscopy for potential measurements it is important to ensure that the sample has sufficient conductivity that it does not charge under the influence of the exciting beam (photons or electrons) and that the sample and spectrometer are in electrical contact.

An abrupt semiconductor interface which is suitable for electron spectroscopic investigation must have an overlayer (which may be a metal, semiconductor, insulator, or vacuum) thickness which is comparable to (or less than) the emitted electron escape depth, λ , and an interface width which is a fraction of λ . Several compilations of λ as a function of E_K have been published (see, e.g., Refs. 14 and 15). Although λ will depend somewhat on the materials involved, the nominal values of λ decrease from ≈ 20 to ≈ 5 Å for increasing E_K from ≈ 10 eV to ≈ 100 eV and increase to ≈ 25 Å at E_K of ≈ 1500 eV. The 10-1500 eV E_K range is typical for most electron spectroscopy measurements, thus the nominal

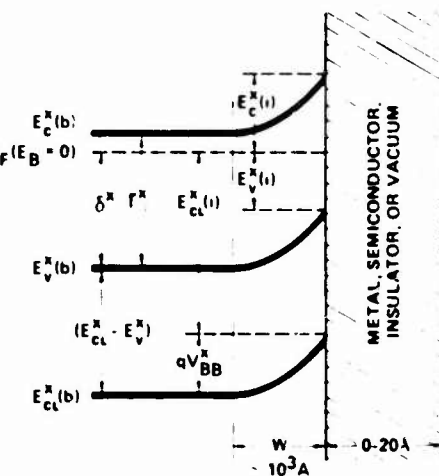


FIG. 1. Schematic energy-band diagram at an abrupt semiconductor interface.

overlayer thickness convenient for study is indicated as 0–20 Å in Fig. 1. Numerous studies have shown (see, e.g., Refs. 16–20) that the ultimate semiconductor interface E_F position is established after only a few monolayers or less of overlayer are deposited so that interface potential properties of these very thin samples can be expected to be retained for the much thicker (~10³ Å) overlayers of direct interest for semiconductor device applications.

By inspection of Fig. 1, it follows that if $E_{CL}^x(i)$ is measured by electron spectroscopy at an interface between semiconductor x and an overlayer, the position of $E_c^x(i)$, which is the Schottky-barrier height for an n -type semiconductor, is

$$E_c^x(i) = (E_{CL}^x - E_v^x) + E_g^x - E_{CL}^x(i). \quad (1)$$

The position of $E_v^x(i)$, which is the Schottky-barrier height for a p -type semiconductor, is

$$E_v^x(i) = E_{CL}^x(i) - (E_{CL}^x - E_v^x). \quad (2)$$

The interface band-bending potential is given by

$$qV_{BB} = (E_{CL}^x - E_v^x) + \delta^x - E_{CL}^x(i), \quad (3)$$

where q is the electronic charge. Assuming that δ^x and E_g^x are known, the only quantity required to determine interface potential and barrier heights in addition to the $E_{CL}^x(i)$ measurement is thus the material constant ($E_{CL}^x - E_v^x$).

Figure 1 is drawn specifically for photoelectron spectroscopic studies in which a core level associated with semiconductor x is being studied. This situation is most appropriate for SXPS and XPS studies. Although in some UPS studies a low binding-energy core level is observable, frequently a prominent feature of the semiconductor valence-band spectrum is studied rather than a core level. In this case, the quantity ($E_{CL}^x - E_v^x$) in Eqs. (1)–(3) is replaced by the binding-energy difference between the valence-band feature, E_{VBF}^x , and E_v^x . AES can also be used to determine semiconductor interface potentials; an effective binding energy E_{AES}^x can be defined for a particular Auger transition energy, E_T , and $E_{CL}^x - E_v^x$ in Eqs. (1)–(3) can be replaced by $E_{AES}^x - E_v^x$.

The measurement of semiconductor interface potential as illustrated schematically in Fig. 1 is simplified in at least two important ways. The first simplification which follows from Poisson's equation, assumes a specified and equal variation of all bands or energy levels up to an interface of infinitesimal width. Even for an atomically abrupt interface, the local density of states for the atom layer at the interface is known to differ from the bulk density of states (see, e.g., Refs. 21–24). It is also well established that chemical reactions and interdiffusion on a monolayer scale or more can occur at semiconductor interfaces even when they are formed at room temperature (see, e.g., Refs. 25–29). The effects may alter the potential distribution due to the formation of an interfacial dipole layer of finite width in the immediate vicinity of the interface. In addition, interfacial chemical bonding can produce interface chemical shifts³⁰ which, if not experimentally resolved, can alter the apparent value of $E_{CL}^x(i)$. The second simplification implied in Fig. 1 is the existence of a unique value of $E_{CL}^x(i)$ within the electron sampling depth.

Even without the microscopic interfacial effects mentioned above, the potential variation away from the interface region will follow Poisson's equation. For a flat-band condition, W will be zero and $E_{CL}^x(i) = E_{CL}^x(b)$ independent of the semiconductor doping level. However, in the more general case where $E_{CL}^x(i) \neq E_{CL}^x(b)$, the potential will vary with distance from the interface and a range of $E_{CL}^x(i)$ values will be observed within the electron escape depth. For a fixed interface E_F position, W for a specific semiconductor increases for decreasing doping density.

The above considerations suggest that in order to measure semiconductor interface potential by electron spectroscopy there is an advantage to collecting the electron signal primarily in a region near, but not precisely at, an abrupt interface. The best situation would be to have sufficient energy resolution to resolve electron signals originating in the interface region from those originating in the bulk semiconductor very near to the interface. As a rough generality, the energy resolution of electron spectroscopies increases for decreasing E_K analysis. However, for low E_K electrons which originate from low E_B core levels, the fraction of the total electron signal which originates in the bulk semiconductor very near to the interface may be small due to the small λ . Thus in some cases it may be advantageous to sacrifice energy resolution in order to gain a fairly large λ and thus minimize the fraction of electron signal originating from the monolayer or two interfacial region. A large λ , however, will cause electrons to be collected at different potentials within the depletion layer. Thus it may also be desirable to use moderately or lightly doped semiconductors for study so the W can be made very large relative to λ . A typical W for a moderately doped (10¹⁷ cm⁻³) semiconductor with E_F near midgap is ~10³ Å as shown in Fig. 1. Poisson's equation can be used to calculate the potential variation for a given doping density and V_{BB} and to estimate the measurement error from this origin for a given λ . In most cases a measurement error of ≤0.01 eV can be expected for ≤10¹⁷ cm⁻³ doping density even for $\lambda \approx 25$ Å.

The accuracy with which electron spectroscopy can be used for interface-potential measurements depends on how well the E_F position of the spectrometer can be calibrated and the accuracy with which $E_{CL}^x - E_v^x$ or equivalent quantities involving E_{VBF}^x and E_{AES}^x for UPS and AES can be determined. These factors are discussed below.

A. Spectrometer energy scale

To determine semiconductor interface-potential parameters by electron spectroscopy, Eqs. (1)–(3), $E_{CL}^x(i)$ must be measured [for UPS and AES the equivalent parameters $E_{VBF}^x(i)$ and $E_{AES}^x(i)$ can be measured]. This involves measurement of E_K as described schematically in Fig. 2. For photoemission the electron kinetic energy immediately outside the surface of the semiconductor x interface (1) sample is

$$E_K^x(1) = h\nu - E_{CL}^x(1) - \phi^x(1) \quad (4)$$

[for AES, $E_K^x(1) = E_T - E_{AES}^x(i) - \phi^x(1)$], where $\phi^x(1)$ is the work function of the interface (1) sample. As the photoelectron passes into the spectrometer, E_K becomes

$$E_K^{SP}(1) = h\nu - E_{CL}^x(1) - \phi^{SP}. \quad (5)$$

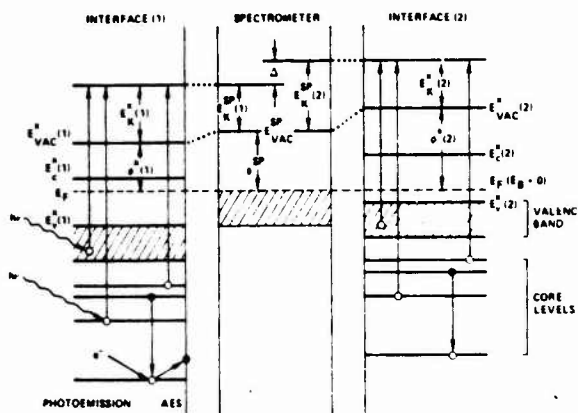


FIG. 2. Schematic energy-level diagram which illustrates the measurement by electron spectroscopy of interface potential for two samples of semiconductor x in electrical contact with the electron spectrometer.

The right-hand side of Fig. 2 illustrates an equivalent situation for a different interface (2) formed on semiconductor x . In this case E_K immediately outside the surface of semiconductor interface (2) is

$$E_K^{(2)} = h\nu - E_{CL}^{(2)} - \phi^{(2)}, \quad (6)$$

which in the spectrometer becomes

$$E_{SP}^{(2)} = h\nu - E_{CL}^{(2)} - \phi^{SP}. \quad (7)$$

Subtracting Eq. (7) from Eq. (5) points out that

$$\Delta = E_{K}^{SP}(1) - E_{K}^{SP}(2) = E_{CL}^{(2)} - E_{CL}^{(1)} \quad (8)$$

and thus a change in $E_{CL}^{(i)}$ between two samples appears as a change in E_{K}^{SP} regardless what values $\phi^{(1)}$ and $\phi^{(2)}$ may have.

To be useful for semiconductor interface-potential measurements, $E_{CL}^{(i)}$ must be determined relative to the electron spectrometer E_F position. Various approaches have been used to calibrate the E_F position for electron spectrometers. For UPS and SXPS where the electron analyzer resolution is in general extremely good, it is common to measure the energy position of E_F for a convenient metallic reference sample (see, e.g., Refs. 31-33). The binding energies of core levels for metallic reference samples³⁴ can be conveniently used in XPS experiments. Thermionic and field emission sources^{35,36} are also being used for calibration purposes. No attempt will be made here to document all possible spectrometer calibration techniques. However, it must be remembered that absolute measurement of semiconductor interface potentials by electron spectroscopy is directly related to the accuracy with which the spectrometer E_F position can be determined. This determination is of equal importance to the accuracy with which the ($E_{CL}^{(i)} - E_K^{(i)}$) parameters in Eqs. (1)-(3) can be determined.

B. Some comparisons of electron spectroscopies

Any attempt to compare merits of related experimental techniques will be subjective and applications to specific material systems will provide exceptions to any generalities. With these reservations in mind, this section briefly compares some of the characteristics of AES, UPS, SXPS, and XPS for semiconductor interface-potential measurements.

I. AES

A major limitation of AES for potential measurement application is the energy width of most Auger transitions. The lifetimes of the initial and final electronic states involved in the Auger transition contribute to line broadening. In addition, if valence-band transitions are involved, band dispersions will broaden the energy width. Thus, in general, most AES energies are only quoted to ± 1 eV although recent efforts³⁷ are in progress to improve substantially this accuracy for selected metallic reference samples. As mentioned above, there are some advantages to utilizing large λ for potential measurements which can be done for AES by employing high E_K transitions.

AES has the advantage over other electron spectroscopies of having good spatial resolution. This is especially true when AES is performed in a scanning electron microscope (SEM) by using the SEM electron beam for excitation. By using a SEM, submicron spatial resolution AES can be performed. This unique advantage of AES over photoemission has made it possible to study potential variations in electrically active devices as was first demonstrated³⁸ by studying the potential variation across a reverse-biased abrupt $p^+ - n$ junction in GaAs. The technique has also subsequently been used to study potential variations in the vicinity of grain boundaries in Si (Ref. 39) and GaAs.⁴⁰

2. UPS

UPS has been employed for many semiconductor interface potential measurements (see, e.g., Refs. 41 and 42). The energy resolution for the low E_K photoelectrons studied is usually excellent which minimizes the difficulty to determine E_b in UPS spectra with good accuracy. A primary difficulty is that features of the valence-band spectrum which are generally studied have quite broad energy widths. As overlayers are deposited onto the semiconductor surface, the overlayer valence-band spectrum will overlap the semiconductor valence-band spectrum; in addition, the secondary electron background may change. These considerations can make it difficult to determine $E_{VB}^*(i)$ with good accuracy. Thus, in general, the accuracy of UPS for semiconductor interface-potential measurements is limited to about ± 0.1 eV.⁴² One can obtain large λ for UPS studies by analyzing low-binding-energy valence-band spectrum features excited by low-energy photons.

3. SXPS

SXPS that is based on synchrotron radiation has the advantage of a variable energy photon source for semiconductor interface studies. With suitable monochromators this source can span the energy range from ≈ 10 eV to several keV. Practical considerations regarding currently available monochromators have restricted most photoemission studies to photon energies between ≈ 10 and ≈ 300 eV. In this energy range, SXPS provides an extremely surface-sensitive probe with excellent energy resolution that allows studies of both valence-band spectral features and low E_b core levels. The usefulness of this technique for interface chemistry and interdiffusion studies is well established.¹¹ However, as men-

tioned above, extreme surface sensitivity (λ may be as small as $\approx 5 \text{ \AA}$) may actually complicate the measurement of potential near a semiconductor interface. Larger λ can of course be achieved by using higher-energy radiation but at present decreased resolution and intensity considerations do not appear to make this an attractive alternative.

4. XPS

The XPS technique, which employs monochromatized radiation, has the ability to study narrow well resolved core levels in an E_K range where $\lambda \approx 25 \text{ \AA}$. The primary disadvantage with most current XPS instruments is the modest ($\approx 0.5 \text{ eV}$) energy resolution available. This limited energy resolution can decrease the sensitivity of the technique for interface chemistry studies. An advantage of XPS for semiconductor interface-potential measurements is that the typical large values of λ make it possible to maximize the fraction of electron signal collected in the region of the bulk semiconductor which is near but not precisely at an interface. Because well-resolved and sharp core-level spectra can be studied for almost all semiconductors, in general the presence of overlayers does not cause substantial spectral interference to complicate the measurement of E_{CL}^x (i). The limited energy resolution causes some difficulty in determining the position of E_v^x in XPS spectra. This determination is needed to obtain the $(E_{CL}^x - E_v^x)$ parameter in Eqs. (1)-(3). A method to overcome this difficulty will be outlined in Sec. IV.

III. HETEROJUNCTION BAND DISCONTINUITY MEASUREMENTS BY PHOTOEMISSION

In addition to measuring the position of E_F at semiconductor interfaces, electron spectroscopy can be used to determine heterojunction band discontinuities (see, e.g., Refs. 43 and 44). This determination is illustrated schematically in Fig. 3. As in Fig. 1, this figure is drawn specifically for photoelectron studies which involve core levels, and it is assumed that the overlayer thickness of semiconductor y is comparable to λ . Prominent UPS valence-band spectral features of the two semiconductors could also be used if the energy positions of such features could be well resolved and AES could be used for the measurement if $E_{AES}^x - E_v^x$ parameters for the semiconductors were known with sufficient accuracy. In Fig. 3, ΔE_c , ΔE_v , and ΔE_{CL} are the heterojunction conduction-band discontinuity, valence-band discontinuity, and core-level binding-energy differences at the interface, respectively. For convenience, an idealized flat-band diagram is shown in Fig. 3 which again assumes that $W \gg \lambda$ and ignores potential variations that may occur within a monolayer or two of an abrupt interface.

The heterojunction band discontinuity measurement differs from the E_F position measurement described in Sec. II. In addition to the ΔE_{CL} measurement, only accurate values of the bulk material constants ($E_{CL}^x - E_v^x$) for the semiconductors involved are needed and the actual E_F position at the interface does not need to be determined. From inspection of Fig. 3

$$\Delta E_v = (E_{CL}^x - E_v^y) - (E_{CL}^x - E_v^x) - \Delta E_{CL}. \quad (9)$$

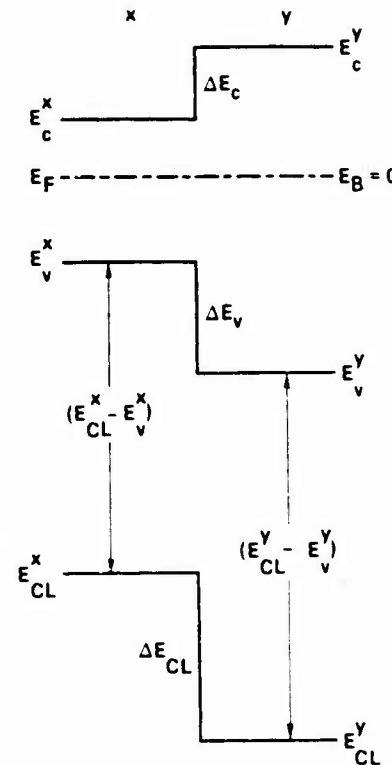


FIG. 3. Schematic energy-band diagram at an abrupt heterojunction interface.

The difference in band-gap energies, ΔE_g , of semiconductors x and y is $\Delta E_g = \Delta E_v + \Delta E_c$. An arbitrary E_F position is shown in Fig. 3; because only energy difference measurements are involved in the determination of ΔE_c , the electron spectrometer E_F position does not need to be calibrated for a heterojunction band discontinuity measurement.

IV. DETERMINATION OF $(E_{CL}^x - E_v^x)$ PARAMETERS

A key bulk semiconductor material parameter necessary to apply core-level photoelectron spectroscopy for semiconductor interface-potential measurements is $(E_{CL}^x - E_v^x)$; for AES and UPS studies E_{CL}^x may be replaced by E_{AES}^x and E_{VBF}^x , respectively. The width and possible complex structure of AES transitions will make it difficult to determine $E_{AES}^x - E_v^x$ parameters with high precision. Also, the precision of $E_{VBF}^x - E_v^x$ is ultimately limited by band dispersion considerations. Low E_v core levels will in general have insignificant band dispersion and $E_{CL}^x - E_v^x$ should be a well-defined quantity which is characteristic of a bulk semiconductor. In addition, these levels for a given semiconductor will in general have the narrowest linewidths (largest final-state lifetimes) and there is an advantage from the viewpoint of accurately measuring energy differences to keeping $E_{CL}^x - E_v^x$ relatively small. Thus in this section we will consider only the determination of outer core-level bulk semiconductor $E_{CL}^x - E_v^x$ parameters.

In general the precision of most $E_{CL}^x - E_v^x$ measurements has been limited to about $\pm 0.1 \text{ eV}$ for both SXPS and XPS measurements. The SXPS measurements are generally performed under extremely surface sensitive conditions. It is known⁴⁵ that many semiconductors undergo surface reconstruction at the vacuum interface and that core-level surface

chemical shifts of several tenths of an eV are common.⁴⁶ Thus even though the present energy resolution of most SXPS measurements is considerably better than most XPS measurements, the small λ involved in these measurements makes it necessary to carefully resolve surface and bulk electron signals for both core-level and valence-band emission which is one limitation on the precision of bulk semiconductor $E_{CL}^x - E_v^x$ parameter measurements by SXPS.

A primary difficulty with the XPS measurement of $E_{CL}^x - E_v^x$ has been the accurate determination of the E_v position in XPS spectra. The most frequently employed method involves extrapolation of the tangent line to the leading edge of the valence-band spectrum back to the energy axis and defines the slope intercept as E_v^x . It has been pointed out that because of the modest energy resolution usually available with the XPS technique, this procedure can lead to substantial uncertainties.⁴⁷ An alternative approach which largely overcomes the difficulty in determining the E_v position in XPS data has recently been suggested.⁴⁸ In essence the approach involves least-squares fitting XPS data in a limited region around the estimated position of E_v with an instrumentally broadened valence-band density of states (VBDOS) chosen so that

$$N_v(E) = \int_0^\infty n_v(E')g(E-E')dE', \quad (10)$$

where $n_v(E')$ is the theoretical VBDOS and $g(E)$ is the instrumental response function. The XPS spectral intensity $I(E)$ is assumed to have the form

$$I(E) = SN_v(E - E_v) + B, \quad (11)$$

where S is a scale factor, and B is a constant random-noise background. An example of this procedure is illustrated in Fig. 4 for XPS data collected from a GaAs(110) 1×1 surface where a nonlocal pseudopotential VBDOS⁴⁸ was used for $n_v(E')$. Similar analyses of Ge,⁴⁹ InAs,⁵⁰ and ZnSe (Ref. 51) XPS data have been reported. Factors which influence the precision for determining $E_{CL}^x - E_v^x$ bulk semiconductor parameters by this approach have recently been considered.⁴⁹ These factors include the presence of occupied surface states, band bending, surface chemical shifts, background effects associated with inelastic processes, instrumental line shape, and spectrometer calibration accuracy. It was concluded that $E_{CL}^x - E_v^x$ parameters could be determined for the 3d levels of Ge and GaAs with a precision of ≤ 0.026 eV.

Values of $E_{CL}^x - E_v^x$ for many semiconductors are needed if electron spectroscopy is to be widely applied for semiconductor interface potential measurements. These values are scattered through the literature for specific semiconductor core levels. In Table I, we have collected many of these values for elemental and compound semiconductors (only binary compound semiconductors with formula AB are considered); no attempt was made to obtain an exhaustive listing. No critical selection was applied in compiling this table and clearly there is considerable disagreement in results and uncertainty in many of the values. There is an obvious need to improve the precision with which many of these parameters are known if electron spectroscopy is to be widely used for accurate semiconductor interface potential measurements.

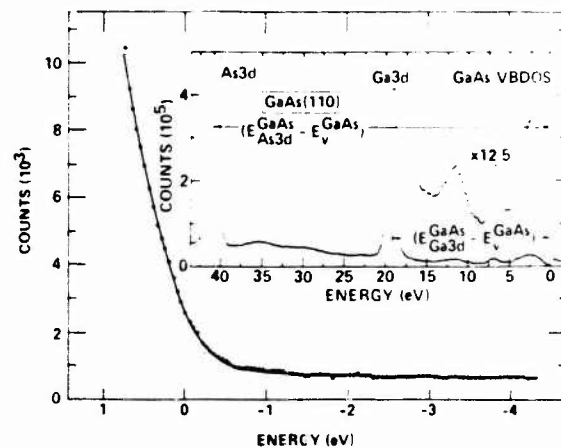


FIG. 4. Least-squares fit of instrumentally broadened theoretical VBDOS (solid curve) to XPS data (points) obtained with a GaAs(110) 1×1 surface. The inset shows the spectrum which contains both the valence-band and outer core-level data. The binding-energy scale is zero at the valence-band maximum.

The approach outlined above for determining the E_v position in XPS spectra of semiconductor samples could be utilized to determine core-level to E_F binding-energy differences for metallic reference samples. This would be useful for calibrating the E_F position of photoelectron spectrometers. The position of sharp core levels can be determined in XPS spectra with good precision (≤ 0.01 eV). If $E_{CL}^x - E_v^x$ parameters for bulk semiconductors are known with a precision of ≤ 0.026 eV and metallic core-level reference line binding energies are available with the same precision, it should be possible to make semiconductor interface-potential measurements and heterojunction band discontinuity measurements to an accuracy of ≈ 0.04 eV, a factor of 2–3 better than the reported ± 0.1 eV measurement accuracy reported for the majority of electron spectroscopic semiconductor interface-potential measurements.

The Au4f levels in metallic gold have frequently been used for photoelectron spectrometer calibration purposes.⁵⁴ Several studies^{34,36,37,52–54} have obtained E_B for Au4f_{7/2} of ≈ 84.0 eV with a scatter in results of about ± 0.1 eV. The need for electron spectroscopic reference standards which can be used for spectrometer energy-scale calibration purposes has been strongly emphasized.³⁴ As mentioned in Sec. II A, the accuracy with which the spectrometer E_F position can be calibrated is of equal importance to the accuracy with which the $E_{CL}^x - E_v^x$ bulk semiconductor parameters are known for semiconductor interface-potential measurement purposes.

V. CONCLUSIONS

Electron spectroscopy is an increasingly important technique for measuring abrupt semiconductor interface potentials and heterojunction band discontinuities by a direct contactless nondestructive method. Variations in potential near an abrupt semiconductor interface as well as interfacial chemical shifts indicate that advantages are to be gained by employing both large electron escape depths and semiconductor depletion widths. Well-resolved sharp semiconductor core-level spectra as opposed to broad valence-band and Auger spectra can simplify data interpretation. These con-

TABLE I. Values of $E_{\text{CL}}^x - E_c^x$ in eV for the outermost core levels [CL(A) and CL(B)] of several elemental and AB compound semiconductors. When available, error in the least significant digit is given parenthetically. A single column entry refers to the line center of the unresolved spin-orbit components; two entries in a column indicates resolution of the spin-orbit split components.

	Semiconductor x	CL(A)	CL(B)	$E_{\text{CL}(A)}^x - E_c^x$	$E_{\text{CL}(B)}^x - E_c^x$	Ref.
IV	Si	Si2p	...	99.0(2)	...	a
	Ge	Ge3d	...	29.57(3) 29.36(4) 29.1(1) 29.33(10)	...	b b c d
				29.91(4) 29.65(10) 29.86(10)	...	
					...	
III-V	AlAs	Al2p	As3d	73.2(1) 72.9	40.3(1)	e f
	AlSb	Al2p	Sb4d	73.40	31.90	33.00
	GaN	Ga3d	...	17.74(10)	...	g
	GaP	Ga3d	...	18.55(10)	...	h
				18.4 (1) 18.6 (2) 18.40	18.8 (1) 19.0 (2) 18.83	j k l
	GaAs	Ga3d	As3d	18.80(3) 18.9 (1) 18.9 (1) 18.82(15)	40.79(3) 40.8 (1) 40.9 (1) 40.76(15)	b m e i
				18.6 (2) 18.7 (2) 18.7 (1)	19.09(20) 19.1 (2) 19.28(10)	n k o
				18.60 18.63(4)	19.04 19.06(4)	41.07 41.18(4)
	GaSb	Ga3d	Sb4d	19.00(15) 18.6 18.8 (2) 18.70	31.58(15) 31.6 19.2 (2) 19.13	32.79(15) 32.7 ...
	InP	In4d	...	16.80(15) 17.1 (2)	31.67	32.92
IV-VI	InAs	In4d	As3d	17.09(15) 17.43(2)	40.30(15) 40.77(2)	i q
	InSb	In4d	Sb4d	16.9 (2) 17.31(10) 17.29(15)	17.72(20)	...
				17.15 17.1 (2)	31.45(15) 31.0	32.67(15) 32.25
				16.98(10) 17.15(5)	17.81(10) 18.00(5)	...
	ZnO	Zn3d	...	7.4 7.7(2) 8.81(15) 8.5(4) 7.5(2)	31.27(10)	32.52(10)
	ZnS	Zn3d	...	9.03(15)	...	i
	ZnSe	Zn3d	Se3d	9.20(15) 9.05(15) 8.6 9.20(15)	...	x y z i
				8.9(4) 8.90(2) 8.9	53.50(15)	v aa s
	ZnTe	Zn3d	Tc4d	9.40(15) 9.84(15) 9.1(4)	40.23(15)	41.70(15)
	CdS	Cd4d	...	9.64(15) 9.2(2) 10.0(4)	...	i bb v
II-VI	CdSe	Cd4d	...	10.04(15) 9.9(2) 10.7(4)	...	i bb v

TABLE I (cont.)

	CdTe	Cd4d	Te4d	10.3(2)	...	ee
				10.5(4)	...	v
				10.2	...	dd
				10.49(15)	39.50(15)	i
				10.0	40.94(15)	z
				10.65	...	v
	HgSe	Hg5d	...	7.4 (4)	9.2 (4)	...
	HgTe	Hg5d	Te4d	7.87(15)	9.64(15)	41.33(15)
				7.6 (4)	9.5 (4)	...
III-VI	GaSe	Ga3d	Se3d	19.39(10)	54.19(10)	54.82(10)
IV-VI	GeS	Ge3d	...	29.61(8)	30.16(8)	...
	SnS	Sn4d	...	23.80(8)	24.88(8)	...
	PbSe	...	Se3d	...	53.50(10)	i
	PbTe	...	Te4d	...	39.49(15)	40.95(15)

^aReference 13.^bReference 49.^cD. E. Eastman, J. L. Freeouf, and M. Erbudak, *AIP Conference Proceedings No. 20* (AIP, New York, 1974), p. 95. D. E. Eastman and J. L. Freeouf, *Phys. Rev. Lett.* **33**, 1601 (1974); W. D. Grobman, D. E. Eastman, and J. L. Freeouf, *Phys. Rev. B* **12**, 4405 (1975).^dM. Cardona, J. Tejeda, N. J. Shevchik, and D. W. Langer, *Phys. Status Solidi (b)* **58**, 483 (1973).^eR. Ludeke, L. Ley, and K. Ploog, *Solid State Commun.* **28**, 57 (1978).^fJ. R. Waldrop, S. P. Kowalczyk, R. W. Grant, E. A. Kraut, and D. L. Miller, *J. Vac. Sci. Technol.* **19**, 573 (1981).^gN. J. Shevchik, J. Tejeda, C. M. Penchina, and M. Cardona, *Solid State Commun.* **11**, 1619 (1972).^hJ. Hedman and N. Martensson, *Phys. Scr.* **22**, 176 (1980).ⁱL. Ley, R. A. Pollak, F. R. McFeely, S. P. Kowalczyk, and D. A. Shirley, *Phys. Rev. B* **9**, 600 (1974).^jT. C. Chiang and D. E. Eastman, *Phys. Rev. B* **21**, 5749 (1980).^kN. J. Shevchik, J. Tejeda, and M. Cardona, *Phys. Rev. B* **9**, 2627 (1974).^lD. E. Eastman, T.-C. Chiang, P. Heiman, and F. J. Himpel, *Phys. Rev. Lett.* **45**, 656 (1980).^mC. C. Chang, P. H. Citrin, and B. Schwartz, *J. Vac. Sci. Technol.* **14**, 943 (1977).ⁿD. E. Eastman and J. L. Freeouf, *Phys. Rev. Lett.* **33**, 1601 (1974).^oM. Cardona, C. M. Penchina, N. J. Shevchik, and J. Tejeda, *Solid State Commun.* **11**, 1655 (1972).^pC. Ance and A. Amamou, *Phys. Status Solidi (b)* **103**, 441 (1981).^qReference 50.^rD. E. Eastman and J. L. Freeouf, *Solid State Commun.* **13**, 1815 (1973).^sD. E. Eastman, J. Freeouf, and M. Erbudak, *J. Phys. (Paris) Colloq.* **34**, C6-37 (1973).^tW. Göpel, J. Pollman, I. Ivanov, and B. Reihl, *Phys. Rev. B* **26**, 3144 (1982).^uW. Ranke, *Solid State Commun.* **19**, 685 (1976).^vC. J. Veseley, R. L. Hengehold, and D. W. Langer, *Phys. Rev. B* **5**, 2296 (1972).^wR. A. Powell, W. E. Spicer, and J. C. McMenamin, *Phys. Rev. Lett.* **27**, 97 (1971).^xA. Ebina, T. Unno, Y. Suda, H. Koinuma, and T. Takahashi, *J. Vac. Sci. Technol.* **19**, 301 (1981).^yA. Ebina, Y. Suda, and T. Takahashi, *Int. J. Electron.* **52**, 77 (1982).^zD. E. Eastman, W. D. Grobman, J. L. Freeouf, and M. Erbudak, *Phys. Rev. B* **9**, 3473 (1974).^{aa}Reference 51.^{bb}J. L. Shay and W. E. Spicer, *Phys. Rev.* **169**, 650 (1968).^{cc}J. L. Shay and W. E. Spicer, *Phys. Rev.* **161**, 799 (1967).^{dd}J. A. Silberman, P. Morgan, I. Lindau, and W. E. Spicer, *J. Vac. Sci. Technol.* **21**, 142 (1982).^{ee}S. P. Kowalczyk, L. Ley, F. R. McFeely, and D. A. Shirley, *Solid State Commun.* **17**, 463 (1975).^{ff}A. Otto, L. Ley, J. A. Azoulay, T. Grandjean, R. Eymard, W. Braun, and M. Cardona, *Phys. Rev. B* **16**, 4429 (1977).

siderations suggest that high kinetic energy photoelectrons and moderately doped semiconductors should be employed when attempting to maximize measurement accuracy. With existing experimental techniques it is possible to measure outer core-level to valence-band maximum binding-energy differences for bulk semiconductors to a precision of ≤ 0.026 eV. This makes it possible to measure heterojunction valence-band discontinuities to ± 0.04 eV; the same precision should be attainable for semiconductor interface Fermi-level position measurements when metallic core-level reference line binding energies, which are suitable for spectrometer E_F calibration purposes, are accurately determined. At present the applicability of electron spectroscopy for high precision

semiconductor interface-potential measurement is limited to those few semiconductors for which core-level to valence-band maximum binding-energy differences are well known.

The use of electron spectroscopy for semiconductor interface-potential measurements should complement information obtained by more traditional I - V and C - V electrical measurements on semiconductor interfaces. Electron spectroscopy provides a means to determine and correlate directly semiconductor interface chemistry and potential (see, e.g., Refs. 55 and 56). It is possible to characterize a semiconductor interface by electron spectroscopy and subsequently analyze the same interface by I - V and C - V measurements after the overlayer thickness has been increased appropriate-

ly.^{57,58} Measurements of this type should provide insight into model dependent analysis of electrical measurements which are of direct interest to understanding semiconductor device performance.

ACKNOWLEDGMENT

This work was supported in part by ONR Contract No. N00014-76-C-1109.

- ¹K. Siegbahn, C. Nordling, A. Fahlman, R. Nordberg, K. Hamrin, J. Hedman, G. Johansson, T. Bergmark, S.-E. Karlsson, I. Lindgren, and B. Lindberg, *Nova Acta Regiae Soc. Sci. Ups.* **20** (1967).
- ²*Electron Spectroscopy*, edited by D. A. Shirley (North-Holland, Amsterdam, 1972).
- ³*Electron Emission Spectroscopy* edited by W. Dekeyser, L. Fiermans, G. Vanderkelen, and J. Vennik (Reidel, Dordrecht, Holland, 1973).
- ⁴*Electron Spectroscopy for Surface Analysis* edited by H. Ibach (Springer-Verlag, Berlin, 1977).
- ⁵*Electron Spectroscopy: Theory, Techniques, and Applications*, edited by C. R. Brundle and A. D. Baker (Academic, London, 1977-81), Vols. 1-4.
- ⁶*Photoemission and The Electronic Properties of Surfaces* edited by B. Feuerbacher, B. Fitton, and R. F. Willis (Wiley, New York, 1978).
- ⁷N. S. McIntyre, *Am. Soc. Test. Mater. Spec. Tech. Publ.* No. 643 (1978).
- ⁸*Photoemission in Solids*, edited by M. Cardona and L. Ley (Springer-Verlag, Berlin, 1978-9), Vols. I and II.
- ⁹C. C. Chang, *J. Vac. Sci. Technol.* **18**, 276 (1981).
- ¹⁰C. R. Helms, *J. Vac. Sci. Technol.* **20**, 948 (1982).
- ¹¹L. J. Brillson, *Surf. Sci. Rep.* **2**, 123 (1982).
- ¹²J. Auleytner and O. Hörsfeldt, *Ark. Fys.* **23**, 165 (1963).
- ¹³J. Hedman, Y. Baer, A. Berndtsson, M. Klasson, G. Leonhardt, R. Nilsson, and C. Nordling, *J. Electron Spectrosc. Relat. Phenom.* **1**, 101 (1972/73).
- ¹⁴I. Lindau and W. E. Spicer, *J. Electron Spectrosc. Rel. Phenom.* **3**, 409 (1974).
- ¹⁵M. P. Seah and W. A. Dench, *Surf. Interface Anal.* **1**, 2 (1979).
- ¹⁶G. Margaritondo, J. E. Rowe, and S. B. Christman, *Phys. Rev. B* **14**, 5396 (1976).
- ¹⁷W. E. Spicer, I. Lindau, P. Skeath, and C. Y. Su, *J. Vac. Sci. Technol.* **17**, 1019 (1980).
- ¹⁸P. Skeath, C. Y. Su, I. Hino, I. Lindau, and W. E. Spicer, *Appl. Phys. Lett.* **39**, 349 (1981).
- ¹⁹L. J. Brillson, C. F. Brucker, A. D. Katnani, N. G. Stoffel, R. Daniels, and G. Margaritondo, *J. Vac. Sci. Technol.* **21**, 564 (1982).
- ²⁰H. Gant and W. Mönch, *Appl. Surf. Sci.* **11/12**, 332 (1982).
- ²¹W. E. Pickett, S. G. Louie, and M. L. Cohen, *Phys. Rev. B* **17**, 815 (1978).
- ²²W. E. Pickett and M. L. Cohen, *Phys. Rev. B* **18**, 939 (1978).
- ²³D. J. Chadi, *Phys. Rev. B* **18**, 1800 (1978).
- ²⁴J. Pollmann, A. Mazur, and M. Schmeits, *Surf. Sci.* **99**, 165 (1980).
- ²⁵A. Hiraki, K. Shuto, S. Kim, W. Kammura, and M. Iwami, *Appl. Phys. Lett.* **31**, 611 (1977).
- ²⁶P. W. Chye, I. Lindau, P. Pianetta, C. M. Garner, and W. E. Spicer, *Phys. Rev. B* **17**, 2682 (1978).
- ²⁷J. R. Waldrop and R. W. Grant, *Appl. Phys. Lett.* **34**, 630 (1979).
- ²⁸A. McKinley, A. W. Parke, and R. H. Williams, *J. Phys. C* **13**, 6723 (1980).
- ²⁹L. J. Brillson, C. F. Brucker, A. D. Katnani, N. G. Stoffel, and G. Margaritondo, *J. Vac. Sci. Technol.* **19**, 661 (1981).
- ³⁰G. Margaritondo, A. D. Katnani, N. G. Stoffel, R. R. Daniels, and Te-Xiu Zhao, *Solid State Commun.* **43**, 163 (1982).
- ³¹W. E. Spicer, P. E. Gregory, P. W. Chye, I. A. Babalola, and T. Sukegawa, *Appl. Phys. Lett.* **27**, 617 (1975).
- ³²T. Grandke and M. Cardona, *Surf. Sci.* **92**, 385 (1980).
- ³³P. Zurcher, G. J. Lapeyre, J. Anderson, and D. Frankel, *J. Vac. Sci. Technol.* **21**, 476 (1982).
- ³⁴C. J. Powell, N. E. Erickson, and T. E. Madey, *J. Electron Spectrosc. Relat. Phenom.* **17**, 361 (1979).
- ³⁵C. J. Powell and A. Mandl, *Phys. Rev. B* **6**, 4418 (1972).
- ³⁶C. R. Anderson, R. N. Lee, J. F. Morar, and R. L. Park, *J. Vac. Sci. Technol.* **20**, 617 (1982).
- ³⁷C. J. Powell, N. E. Erickson, and T. Jach, *J. Vac. Sci. Technol.* **20**, 625 (1982).
- ³⁸J. R. Waldrop and J. S. Harris, *J. Appl. Phys.* **46**, 5214 (1975).
- ³⁹L. L. Kazmerski, P. J. Ireland, and T. F. Ciszek, *J. Vac. Sci. Technol.* **17**, 34 (1980).
- ⁴⁰M. J. Cohen, M. D. Paul, D. L. Miller, J. R. Waldrop, and J. S. Harris, Jr., *J. Vac. Sci. Technol.* **17**, 899 (1980).
- ⁴¹P. E. Gregory and W. E. Spicer, *Phys. Rev. B* **12**, 2370 (1975).
- ⁴²P. W. Chye, T. Sukegawa, I. A. Babalola, H. Sunami, P. Gregory, and W. E. Spicer, *Phys. Rev. B* **15**, 2118 (1977).
- ⁴³E. A. Kraut, R. W. Grant, J. R. Waldrop, and S. P. Kowalczyk, *Phys. Rev. Lett.* **44**, 1620 (1980).
- ⁴⁴W. Monch, R. S. Bauer, H. Gant, and R. Murschall, *J. Vac. Sci. Technol.* **21**, 498 (1982).
- ⁴⁵C. B. Duke, R. J. Meyer, and P. Mark, *J. Vac. Sci. Technol.* **17**, 971 (1980).
- ⁴⁶D. E. Eastman, F. J. Himpsel, and J. F. van der Veen, *J. Vac. Sci. Technol.* **20**, 609 (1982).
- ⁴⁷J. Olivier and R. Poirier, *Surf. Sci.* **105**, 347 (1981).
- ⁴⁸J. R. Chelikowsky and M. L. Cohen, *Phys. Rev. B* **14**, 556 (1976).
- ⁴⁹E. A. Kraut, R. W. Grant, J. R. Waldrop, and S. P. Kowalczyk (unpublished).
- ⁵⁰S. P. Kowalczyk, W. J. Schaffer, E. A. Kraut, and R. W. Grant, *J. Vac. Sci. Technol.* **20**, 705 (1982).
- ⁵¹S. P. Kowalczyk, E. A. Kraut, J. R. Waldrop, and R. W. Grant, *J. Vac. Sci. Technol.* **21**, 482 (1982).
- ⁵²F. R. McFeely, S. P. Kowalczyk, L. Ley, R. A. Pollak, and D. A. Shirley, *Phys. Rev. B* **7**, 5228 (1973).
- ⁵³K. Asami, *J. Electron Spectrosc. Relat. Phenom.* **9**, 469 (1976).
- ⁵⁴M. F. Ebel, *J. Electron Spectrosc. Relat. Phenom.* **8**, 213 (1976).
- ⁵⁵R. W. Grant, J. R. Waldrop, S. P. Kowalczyk, and E. A. Kraut, *J. Vac. Sci. Technol.* **19**, 477 (1981).
- ⁵⁶S. P. Kowalczyk, J. R. Waldrop, and R. W. Grant, *Appl. Phys. Lett.* **38**, 167 (1981).
- ⁵⁷L. J. Brillson, C. F. Brucker, A. D. Katnani, N. G. Stoffel, and G. Margaritondo, *Appl. Phys. Lett.* **38**, 784 (1981).
- ⁵⁸J. R. Waldrop, *Appl. Phys. Lett.* **41**, 350 (1982).

Band discontinuities and interface Fermi-level positions in Ge-GaAs(110) heterojunctions

Steven P. Kowalczyk, R. W. Grant, J. R. Waldrop, and E. A. Kraut

Rockwell International, Microelectronics Research and Development Center, Thousand Oaks, California 91360

(Received 29 January 1983; accepted 27 March 1983)

X-ray photoelectron spectroscopy (XPS) measurements were performed on (p)Ge-(p)GaAs(110) and (p)Ge-(n)GaAs(110) heterojunctions to investigate the possible influence of interface defect levels on valence-band discontinuities ΔE_v . These XPS experiments indicate that ΔE_v is independent of GaAs dopant type. Comparison of the present results with results from previous work shows that ΔE_v is independent of the GaAs(110) surface preparation method (thermal, sputter and annealed, or cleavage) and Ge dopant type. No evidence is found for the presence of an intrinsic dipole layer associated with interface defect levels.

PACS numbers: 73.40.Lq, 73.20. - r, 81.60. - j

I. INTRODUCTION

The emergence of molecular beam epitaxy and metal-organic chemical vapor deposition techniques as technologies for the fabrication of abrupt semiconductor-semiconductor (heterojunction) interfaces has stimulated much interest in the utilization of heterojunctions in advanced electronic design concepts because of their great design flexibility.^{1,2} The fundamental physical property and the one which is of crucial importance in device design application in a heterojunction system is the relative energy alignment of valence-band edges E_v and conduction-band edges E_c due to the difference in the band gaps E_g of the two semiconductor components of the heterojunction, which results in the valence-band discontinuities ΔE_v and conduction-band discontinuities ΔE_c at the heterojunction interface. The past five years has seen increasing application of surface sensitive spectroscopies to the study of such heterojunction interface problems as ΔE_v determination, interface abruptness, and interface chemistry. X-ray photoelectron spectroscopy (XPS) has been particularly useful for the determination of ΔE_v .³ A significant result of these spectroscopic studies has been the observation that ΔE_v (ΔE_c) can be significantly influenced by microscopic factors at the semiconductor-semiconductor interface. This has been clearly demonstrated by the manifestation of the nontransitive nature of ΔE_v ,⁴ and by the exhibition of ΔE_v dependence on crystallographic orientation (~0.20 eV),⁵ growth sequence (~0.25 eV),^{6,7} and growth parameters (~0.15 eV).⁷ During this same period considerable activity has been devoted to the Fermi-level pinning problem in Schottky barriers. There has emerged a consensus that Fermi-level pinning is induced by surface (interface) or near surface (interface) defects.^{8,9} Recent evidence has suggested that there is a single defect in both n- and p-type compound semiconductors which has multiple charge states.¹⁰⁻¹² The ubiquitousness of these defects at a wide variety of metal-semiconductor and oxide-semiconductor interfaces and the apparent dependence of heterojunction ΔE_v values on microstructural details has lead a number of researchers to suggest that surface (interface) defects may affect heterojunction band alignments. In fact a defect mechanism has been tacitly used to propose band alignments in the InAs-GaAs hetero-

junction system.^{13,14}

In this paper, XPS measurements of ΔE_v for Ge-GaAs(110) heterojunctions are reported for samples in which the doping type of the GaAs was varied. As noted above, Fermi-level pinning occurs at many GaAs interfaces. In particular, studies of the Ge-GaAs(110) interface have shown that two pinning levels are established in GaAs at 0.88 and 0.55 eV above E_v for n- and p-type material, respectively, even for submonolayer amounts of Ge evaporated onto cleaved GaAs(110) surfaces.¹⁵ If charge transfer across the interface occurs between defect levels associated with Fermi-level pinning, it might be expected that an interface dipole layer would form which could affect the magnitude of ΔE_v . The measurements reported here were performed to investigate this possibility.

II. XPS MEASUREMENTS

The details of the XPS technique for the determination of ΔE_v have been fully described elsewhere,^{3,16} only a brief exposition will be given here. A schematic energy-band diagram for the Ge-GaAs heterojunction system is given in Fig. 1 which illustrates the quantities necessary for the determination of ΔE_v by XPS. These are: (1) the Ga 3d core-level to valence-band maximum binding-energy difference for bulk GaAs ($E_{\text{Ga}3d}^{\text{GaAs}} - E_v^{\text{GaAs}}$), (2) the Ge 3d core-level to valence-band maximum binding-energy difference for bulk Ge ($E_{\text{Ge}3d}^{\text{Ge}} - E_v^{\text{Ge}}$), and (3) the core-level binding-energy difference $\Delta E_{\text{CL}} \equiv (E_{\text{Ge}3d}^{\text{Ge}} - E_{\text{Ga}3d}^{\text{GaAs}})$ across the interface. The first two quantities have been previously obtained by XPS measurements on single crystals of GaAs and Ge and have the values of 18.80 ± 0.03 eV and 29.57 ± 0.03 eV, respectively.¹⁶ The value of ΔE_{CL} is obtained from measurements reported here on *in situ* prepared heterojunctions with ~17 Å of Ge epitaxially grown on n- and p-type GaAs. The valence-band discontinuity is

$$\Delta E_v = (E_{\text{Ge}3d}^{\text{Ge}} - E_v^{\text{Ge}}) - (E_{\text{Ga}3d}^{\text{GaAs}} - E_v^{\text{GaAs}}) - \Delta E_{\text{CL}}.$$

The XPS measurements were performed with a HP5950A electron spectrometer. This system has been modified for ultrahigh vacuum (~ 5×10^{-10} Torr), for *in situ* film growth and substrate heating, and for low energy electron diffrac-

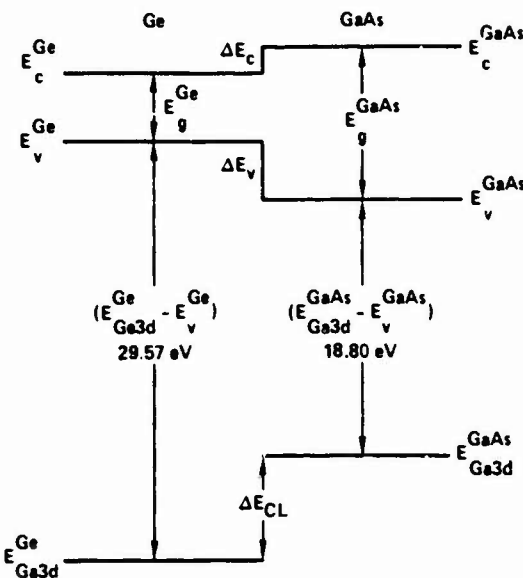


FIG. 1. Schematic energy-band diagram for the Ge-GaAs heterojunction system which indicates the quantities necessary for a XPS determination of ΔE_v and ΔE_c .

tion (LEED) analysis. The x-ray source is monochromatized $AlK\alpha$ ($h\nu = 1486.6$ eV) radiation.

III. GROWTH DETAILS

The substrates for the heterojunctions preparations were bulk grown n -(5×10^{16} cm $^{-3}$) and p -(2×10^{16} cm $^{-3}$) type GaAs crystals which had been wafered and polished to give (110) surfaces and 20 mil thickness (obtained from Crystal Specialties, Inc.). The n - and p -type substrates were simultaneously chemically etched with a freshly prepared 4:1:1 $H_2SO_4:H_2O_2:H_2O$ solution for ~ 1 min to remove polishing damage, mounted side by side on a Mo plate, and loaded into the spectrometer vacuum within several minutes of the chemical etch processing. The native oxide overlayer was removed by an ~ 10 s thermal treatment (~ 550 °C at $\sim 5 \times 10^{-10}$ Torr) in the XPS spectrometer sample preparation chamber.¹⁷ This process produced a clean (O and C free) GaAs surface as determined by XPS and the surface exhibited a 1×1 LEED pattern.

The heterojunctions were prepared *in situ* by simultaneous deposition of Ge from a resistively heated W wire-wound basket filled with high purity (50Ω cm) Ge onto n - and p -GaAs(110) substrates maintained at ~ 325 °C; this temperature is near the minimum necessary to achieve epitaxy. About 17 Å of Ge was deposited at this temperature. Epitaxy was confirmed by LEED and atomic cleanliness by XPS core-level spectra.

IV. RESULTS

A XPS spectrum in the Ge 3d-Ga 3d core-level region for a (p)Ge-(n)GaAs(110) heterojunction is shown in Fig. 2; similar data were obtained for (p)Ge-(p)GaAs(110). These core-level spectra were background subtracted by using a function which is proportional to the integrated photoelec-

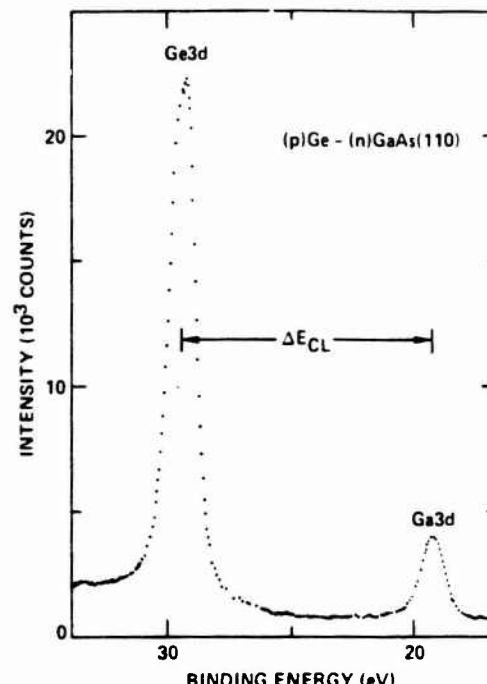


FIG. 2. XPS spectrum in the Ga 3d-Ge 3d core-level binding-energy region obtained from a (p)Ge-(n)GaAs(110) heterojunction.

tron peak area. The core-level peak position is defined as the center of the peak width at half peak height. Table I summarizes Fermi-level position, core-level splitting, and band discontinuity results for these experiments. The ΔE 's at 25 °C are 0.59 ± 0.05 eV and 0.54 ± 0.05 eV for the (p)Ge-(n)GaAs(110) and (p)Ge-(p)GaAs(110) heterojunctions, respectively. The Fermi-level pinning positions of the thermally cleaned n - and p -type surfaces were 0.69 ± 0.04 eV and 0.43 ± 0.04 eV, respectively, in good agreement with previous results.¹⁰ The Ge overlayers were determined to be degenerate p -type, presumably due to Ga doping from the GaAs substrate.

V. DISCUSSION

The ΔE_c values obtained for the (p)Ge-(p)GaAs and (p)Ge-(n)GaAs heterojunctions are identical to within the experimental error. These values can be compared with previously obtained values for Ge-GaAs heterojunctions fabricated on differently prepared surfaces. As can be seen from

TABLE I. Fermi-level positions, core-level splittings, and ΔE_c for (p)Ge-(n)GaAs(110) and (p)Ge-(p)GaAs(110) heterojunctions (in eV).

	(p)Ge-(n)GaAs(110)	(p)Ge-(p)GaAs(110)
E_F^{OAA} (surf) ^a	0.69 ± 0.04	0.43 ± 0.04
E_F^{OAA} (HJ) ^b	0.45 ± 0.04	0.39 ± 0.04
E_F^{Or} (HJ) ^c	-0.14 ± 0.04	-0.16 ± 0.04
ΔE_{CL}	10.18 ± 0.03	10.23 ± 0.03
ΔE_c (25 °C)	0.59 ± 0.05	0.54 ± 0.05

^aRelative to E_F^{OAA} .

^bThermally cleaned surface.

^cRelative to E_F^{Or} .

TABLE II. Comparison of ΔE_{CL} from several differently prepared Ge-GaAs(110) heterojunctions.

Heterojunction	ΔE_{CL} (eV)	GaAs surface prep.	Reference
(<i>p</i>)Ge-(<i>n</i>)GaAs(110)	10.18 ± 0.03	Thermal	This work
(<i>p</i>)Ge-(<i>p</i>)GaAs(110)	10.23 ± 0.03	Thermal	This work
Ge-(<i>p</i>)GaAs(110) ^a	10.21 ± 0.01	Sputter/anneal	3
(<i>n</i>)Ge-(<i>n</i>)GaAs(110)	10.26 ± 0.06	Cleaved	19

^aThe doping type of the Ge overlayer for these heterojunctions was not determined but is expected to be *p*-type [see, for example, R. A. Stull, C. E. C. Wood, K. Board, N. Dandekar, L. F. Eastman, and J. Devlin, *J. Appl. Phys.* **52**, 4062 (1981) and references therein].

Fig. 1, ΔE_{CL} is the most directly measured quantity for comparison. Table II lists ΔE_{CL} values obtained from this work on thermally cleaned GaAs(110) surfaces, and from previous work on sputtered/annealed^{3,18} and cleaved surfaces.¹⁹ The ΔE_{CL} values for these heterojunctions agree within experimental error. In addition there is no variation in ΔE_{CL} within experimental error for heterojunctions with (*n*)Ge overlayers on cleaved (*n*)GaAs(110) surfaces.¹⁹

The thermally cleaned *n*- and *p*-type GaAs surfaces are pinned at the positions noted in Table I. Following the growth of an ≈ 17 Å thick degenerately doped *p*-type Ge epilayer, the band bending at the *n*-GaAs(110) interface is substantially increased. The observed Fermi-level position at both the *n*- and *p*-type GaAs(110) interface with degenerately doped *p*-type Ge is substantially closer to E_v^{GaAs} than the GaAs pinning levels determined for the Ge-GaAs(110) interface by Mönch and Gant.¹⁵ This suggests that the GaAs surface is not pinned at the interface with degenerately doped Ge and that the donorlike levels associated with Fermi-level pinning of *p*-GaAs are fully ionized.

In summary, the results of this study when compared to previously published work indicate that for abrupt epitaxial Ge-GaAs(110) heterojunctions, ΔE_v is independent of dopant type for both GaAs and Ge and is independent of the GaAs(110) surface preparation technique (i.e., thermally

cleaned, sputtered/annealed, and cleaved). There is no evidence for the formation of an interfacial dipole layer associated with charge transfer across the interface between defect levels.

ACKNOWLEDGMENT

This work is supported by ONR Contract No. N00014-76-C-1109.

- ¹H. Kroemer, *Jpn. J. Appl. Phys.* **20**, S1 (1981).
- ²H. Kroemer, *Proc. IEEE* **70**, 13 (1982).
- ³E. A. Kraut, R. W. Grant, J. R. Waldrop, and S. P. Kowalczyk, *Phys. Rev. Lett.* **44**, 1620 (1980).
- ⁴J. R. Waldrop and R. W. Grant, *Phys. Rev. Lett.* **43**, 1686 (1979).
- ⁵R. W. Grant, J. R. Waldrop, and E. A. Kraut, *Phys. Rev. Lett.* **40**, 656 (1978).
- ⁶J. R. Waldrop, S. P. Kowalczyk, R. W. Grant, E. A. Kraut, and D. L. Miller, *J. Vac. Sci. Technol.* **19**, 573 (1981).
- ⁷S. P. Kowalczyk, E. A. Kraut, J. R. Waldrop, and R. W. Grant, *J. Vac. Sci. Technol.* **21**, 482 (1982).
- ⁸See, for example: W. E. Spicer, S. Egashira, I. Lindau, C. Y. Su, and P. R. Skeath, *Thin Solid Films* **89**, 447 (1982); and references therein.
- ⁹A. McKinley, G. J. Hughes, and R. H. Williams, *J. Phys. C* **15**, 7049 (1982); and references therein.
- ¹⁰R. W. Grant, J. R. Waldrop, S. P. Kowalczyk, and E. A. Kraut, *J. Vac. Sci. Technol.* **19**, 477 (1981).
- ¹¹H. Gant and W. Mönch, *Appl. Surf. Sci.* **11/12**, 332 (1982).
- ¹²J. R. Waldrop, S. P. Kowalczyk, and R. W. Grant, *Appl. Phys. Lett.* **42**, 454 (1983).
- ¹³J. M. Woodall, J. L. Freeouf, G. D. Petit, T. Jackson, and P. Kirchner, *J. Vac. Sci. Technol.* **19**, 626 (1981); J. M. Woodall and J. L. Freeouf, *ibid.* **19**, 794 (1981).
- ¹⁴S. P. Kowalczyk, W. J. Schaffer, E. A. Kraut, and R. W. Grant, *J. Vac. Sci. Technol.* **20**, 705 (1982).
- ¹⁵W. Mönch and H. Gant, *Phys. Rev. Lett.* **48**, 512 (1982).
- ¹⁶E. A. Kraut, R. W. Grant, J. R. Waldrop, and S. P. Kowalczyk, *Phys. Rev. B* (submitted).
- ¹⁷R. W. Grant, S. P. Kowalczyk, J. R. Waldrop, and W. A. Hill, in *The Physics of MOS Insulators*, edited by G. Lucovsky, S. T. Pantelides, and F. L. Galeener (Pergamon, New York, 1981), p. 202.
- ¹⁸J. R. Waldrop, E. A. Kraut, S. P. Kowalczyk, and R. W. Grant, *Surf. Sci.* (in press).
- ¹⁹W. Mönch, R. S. Bauer, H. Gant, and R. Murschall, *J. Vac. Sci. Technol.* **21**, 498 (1982).

**Semiconductor core-level to valence-band maximum binding-energy differences:
Precise determination by x-ray photoelectron spectroscopy**

E. A. Kraut, K. W. Grant, J. R. Waldrop, and S. P. Kowalczyk

Microelectronics Research and Development Center, Rockwell International, Thousand Oaks, California 91360

(Received 10 December 1982)

Angle-resolved core-level and valence-band x-ray photoelectron spectroscopy (XPS) data for GaAs(110), Ge(110), and Ge(111) surfaces are analyzed to determine core-level to valence-band maximum binding-energy differences to a precision of the order of the room-temperature thermal energy. A method for markedly improving the precision with which the position of the valence-band maximum in XPS data can be located is presented. This method is based on modeling the XPS valence-band spectrum in the vicinity of the valence-band maximum by an instrumentally broadened theoretical valence-band density of states and fitting this model to the experimental data by using the least-squares method. The factors which influence the attainable precision for determining core-level to valence-band maximum binding-energy differences are quantitatively discussed. These factors include the presence of occupied surface states, band bending, surface chemical shifts, background effects associated with inelastic processes, instrumental line shape, and spectrometer calibration accuracy. The spin-orbit-split components of the Ga, As, and Ge 3d core lines are resolved and binding energies of these components, measured relative to the valence-band maximum in GaAs and Ge, are reported.

I. INTRODUCTION

X-ray photoelectron spectroscopy (XPS) is well known for its usefulness in detecting the presence of specific elements by means of binding-energy measurements and for its ability to follow chemical-compound formation through observation of changes in binding energy (chemical shifts) and changes in photoelectron line shape.¹ A less frequently exploited use of XPS is to monitor the potential at a semiconductor interface.² In this way it becomes possible to make accurate determinations of band bending, Schottky-barrier heights, and heterojunction band discontinuities.³ Accurate XPS determination of the above quantities requires that experimental values of core-level to valence-band maximum binding-energy differences be known with a precision on the order of plus or minus the room-temperature thermal energy (0.025 eV). Recently we reported on a method of achieving this level of precision.³ The purpose of the present paper is to provide further important details, and to report new results for the binding energies of the spin-orbit-split components of the 3d core lines in Ge and GaAs measured relative to the valence-band maximum (E_v).

The application of XPS (and other photoelectron spectroscopies) to monitor semiconductor interface potentials depends on locating E_v relative to the Fermi level E_F at the interface. This application is illustrated in Fig. 1 for a vacuum-semiconductor interface. Near the interface the local charge-density distribution may differ from that deeper in the bulk semiconductor. Consequently, Poisson's equation predicts a spatially varying electrostatic potential which bends all of the bands or energy levels by an amount that depends only on the distance from the interface. This assumes that the energy band gap in the space-charge region is the same as it is deeper in the bulk semiconductor. For semiconductor x in Fig. 1, the energy

of a core-level E_{CL}^x , the valence-band maximum E_v^x , and the conduction-band minimum E_c^x are shown in the bulk (b) and at an interface (i). Binding energy E_B is measured with respect to E_F ($E_B = 0$). The band gap E_g^x , position of the Fermi level in the bulk relative to E_v^x , δ^x , band-bending potential V_{BB}^x , and depletion layer width W are also shown in Fig. 1.

It follows from Fig. 1 that the band-bending potential V_{BB}^x at the interface is given by

$$qV_{BB}^x = (E_{CL}^x - E_v^x) + \delta^x - E_{CL}^x(i), \quad (1)$$

where q is the electronic charge. The core-level to valence-band-edge binding-energy difference $E_{CL}^x - E_v^x$ and

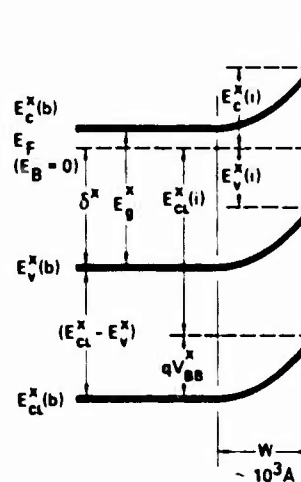


FIG. 1. Generalized energy-band diagram at an abrupt semiconductor-vacuum interface.

δ^x are material properties of semiconductor x . The photoelectron potential monitoring method consists of determining the band-bending potential V_{BB}^x from Eq. (1) by measuring $E_{CL}^x(i)$, given knowledge of the material parameters $E_{CL}^x - E_v^x$ and δ^x .

Core-level to valence-band maximum binding-energy differences can be measured by several photoelectron spectroscopies. Each technique has its own advantages and limitations. The presently available energy resolution of XPS may not be as good as some other photoelectron spectroscopies which utilize lower kinetic energy photoelectrons. However, the greater photoelectron escape depth typically associated with XPS measurements averages the photoelectron signal over many atom layers, which can be an advantage for minimizing complexities due to interface-chemical-shift and interface-potential variations. This paper focuses on optimizing the XPS

technique for high-precision $E_{CL}^x - E_v^x$ measurements.

In this paper we report binding energies of the 3d electrons in GaAs and Ge measured relative to E_v^x . For a semiconductor x of the zinc-blende type (e.g., GaAs), a schematic relation between the XPS spectrum, density of states, and energy bands is shown in Figs. 2(a)-2(c), respectively. Several previous measurements of the 3d binding energies in GaAs and Ge have been reported.⁴⁻⁷ In general, the precision of the previous measurements has been limited to about ± 0.1 eV. In this paper we shall examine, in detail, factors which affect the determination of $E_{CL}^x - E_v^x$ and of the spin-orbit-split components $E_{3d_{3/2}}^x - E_v^x$ and $E_{3d_{5/2}}^x - E_v^x$ shown in Fig. 2(a) to a precision on the order of the room-temperature thermal energy. The experimental procedure and results for GaAs and Ge are presented in Sec. II. Data analysis is discussed in Sec. III, and the paper is summarized in Sec. IV.

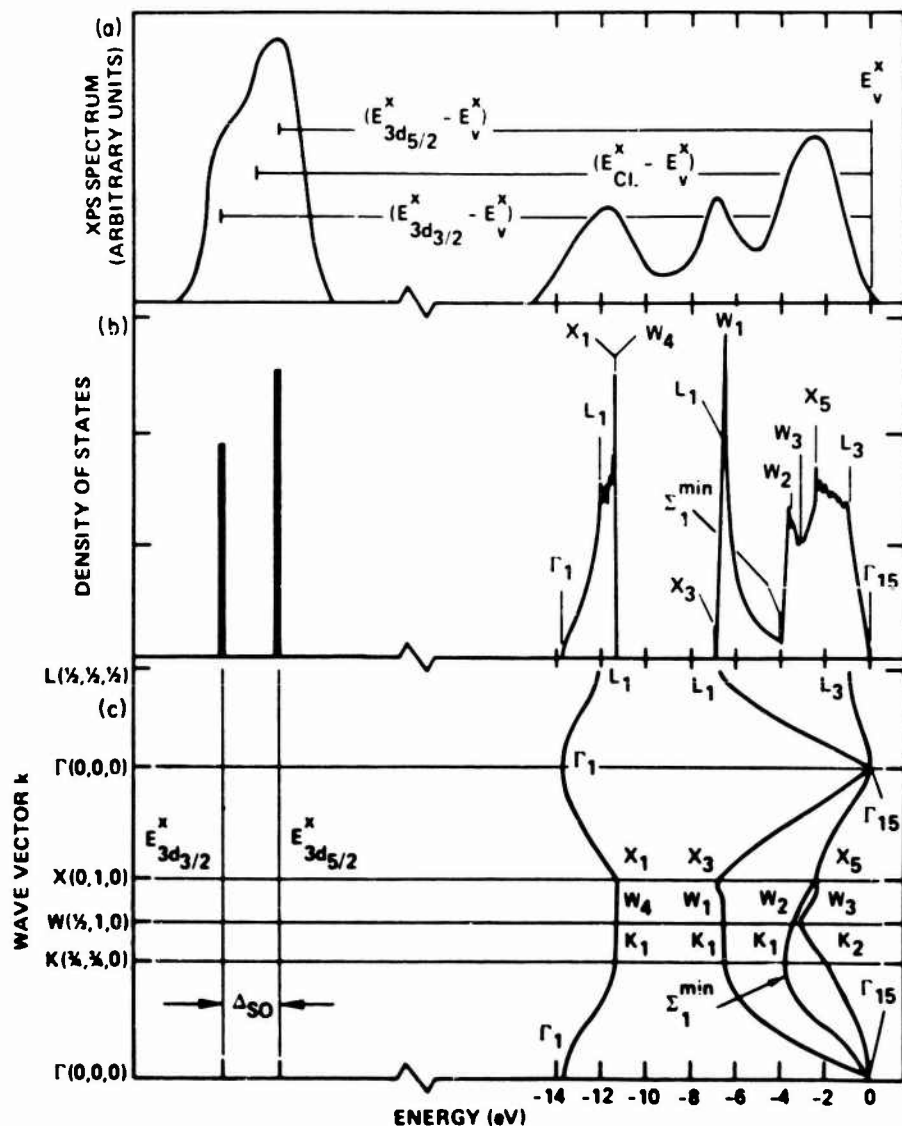


FIG. 2. (a) Schematic XPS core- and valence-band spectrum showing the valence-band edge E_v^x , the center E_{CL}^x of a 3d core level and its spin-orbit-split components $E_{3d_{3/2}}^x$ and $E_{3d_{5/2}}^x$. (b) Schematic zinc-blende valence-band density of states (VB DOS) and δ -function spin-orbit-split 3d core-level components. (c) Schematic zinc-blende valence-band structure and dispersionless spin-orbit-split (Δ_{SO}) 3d core-level components.

II. EXPERIMENTAL

To obtain high-precision $E_{\text{CL}}^x - E_v^x$ measurements, it was necessary to consider several experimental details. The important aspects of the experimental procedure and the experimental results are discussed in this section.

A. Spectrometer description

The electron spectrometer utilized for XPS measurements in this study was an ultrahigh-vacuum (UHV) modified Hewlett-Packard model 5950A, which employs a monochromatized $\text{Al}K\alpha$ ($h\nu = 1486.6$ eV) x-ray source. The average photoelectron kinetic energy excited from the GaAs and Ge valence bands and from the 3d core levels of Ga, Ge, and As corresponds to an escape depth of ~ 27 Å.⁸ The photoelectron-emission direction relative to the sample normal was kept fixed at 51.5° for all measurements so that the effective photoelectron escape depth was ~ 17 Å; thus the photoelectron signal was averaged over many atomic planes near the sample surface.

The bakable sample preparation chamber was equipped with a low-energy electron-diffraction (LEED) system and a rastered ion-sputter gun. Both ion pumps and cryo-pumps were used to achieve a base pressure of $\approx 1 \times 10^{-10}$ Torr. Titanium sublimation pumping was also employed to minimize reactive background gases. The sample holder had a heater and thermocouple arrangement, which was used to control the annealing temperatures of samples. All XPS measurements reported here were taken at or near room temperature.

The XPS spectrometer was equipped with a low-energy electron flood gun. Core-level spectra were taken with and without low-energy (~ 5 eV) electron illumination to test for sample charging due to x-ray illumination. No charging effects were observed for the samples used in this study.

The analyzer of the XPS spectrometer used in this work had a half-angle acceptance cone of $\sim 2^\circ$ so that data obtained with this instrument are angle resolved. This angular-resolution capability was utilized to test if the measured photoelectron spectrum in the vicinity of the valence-band maximum was affected by occupied surface-state contributions (see Sec. III A 2).

B. Spectrometer calibration

A key factor required to perform highly accurate XPS measurements is the precise calibration of the binding-energy scale. All XPS data reported herein were obtained by repeatedly scanning a 50-eV binding-energy interval until the desired statistical accuracy was obtained. To calibrate this 50-eV binding-energy interval, a precise measurement of the retarding voltage on the HP5950A XPS spectrometer electron-optics lens system was made. A high-impedance voltage-divider network was used for this measurement. The retarding lens voltage was first reduced by a precision 1000:1 voltage divider, and was then compared against a seven-place voltage calibrator with a sensitive null meter. The apparent binding energy of the $\text{Au}4f_{7/2}$ photoelectron peak from an Au calibration sample was monitored as a function of retarding lens voltage. By making several measurements of the $\text{Au}4f_{7/2}$ ph-

toelectron peak position as a function of the retarding lens voltage, it was found that the binding-energy scale could be routinely calibrated to 0.02%. No systematic ramp-voltage linearity deviation could be detected at this level of precision. The collection of valence-band spectra required long (typically ~ 12 h) counting times to obtain the desired statistical accuracy. The spectrometer energy scale was calibrated before and after these experiments to be sure that calibration variations larger than 0.02% were not present.

C. Sample selection and preparation

The single-crystal GaAs and Ge samples used in this study were oriented wafers cut from bulk-grown material. The GaAs wafers had (110) orientation, while both (111)- and (110)-oriented Ge wafers were studied. Laue back-reflection x-ray photography was used to confirm that the wafers were within 1° of the desired orientation. The orientation of low-index crystallographic axes was also determined, and it was possible to mount samples in the XPS spectrometer with a known angular orientation relative to the photoelectron emission direction of $\leq 2^\circ$.

As mentioned previously, the substantial escape depth of x-ray-excited outer core-level photoelectrons averages the photoelectron signal over many atom layers. For this reason it is desirable to use modestly or lightly doped semiconductors for study to avoid complications due to band bending within the photoelectron escape depth. The typical band-bending length for a 10^{17}-cm^{-3} -doped semiconductor is $\sim 10^3$ Å. As shown in Sec. III D 1, this band bending will not substantially affect the accuracy of the XPS ($E_{\text{CL}}^x - E_v^x$) determination. Thus $\sim 10^{17}\text{-cm}^{-3}$ doping represents a convenient doping-density upper limit in order to avoid XPS measurement complications of band bending. The GaAs samples used in this study were *n* type, $\sim 5 \times 10^{16}\text{ cm}^{-3}$; the Ge samples were undoped (slightly *n* type). It is, of course, desirable to select samples which have relatively low resistivity in order to avoid sample charging during the XPS measurements; for some semiconductors, this could set a useful lower limit on doping density.

Both the GaAs and Ge samples were chemically etched a few minutes prior to insertion into the XPS spectrometer. The GaAs etch was freshly prepared 4:1:1 ($\text{H}_2\text{SO}_4:\text{H}_2\text{O}_2:\text{H}_2\text{O}$); the Ge etch was dilute HF. The samples were quenched in H_2O and blown dry with N_2 . They were then attached to Mo-sample platens with In, which required heating in air to $\sim 160^\circ\text{C}$. After a bakeout procedure to achieve UHV, atomically clean and ordered surfaces were prepared by repeated sputtering and annealing cycles. The sputtering gas was Ar, and Ti sublimation pumping was used during sputtering to minimize reactive gases. The GaAs samples were sputtered with ion energies of ~ 600 eV and annealed at $\sim 575^\circ\text{C}$; Ge samples were sputtered at ~ 2 keV and annealed at $\sim 600^\circ\text{C}$. LEED measurements determined the surface ordering and removal of sputter damage. The GaAs(110) surfaces exhibited characteristic 1×1 patterns, while the Ge(111) surfaces had 2×8 patterns. The LEED pattern for the Ge(110) surfaces was complex and resembled the reported^{9,10} $c(8 \times 10)$ pattern characteristic of room-temperature Ge (110). XPS measurements before and after data collection

were used to determine the absence of detectable (≤ 0.1 monolayer) oxygen or carbon contamination.

D. XPS measurements

To minimize experimental difficulties associated with variations in apparent binding energies caused by spectrometer power-supply instabilities and sample position variations, the XPS data were collected by repeatedly scanning (~500 scans) a 50-eV binding-energy interval which contained both the core level of interest and the valence-band region until the desired statistical accuracy was obtained. The valence-band and core-level data were thus collected simultaneously from precisely the same spot (an area of $\sim 3 \text{ mm}^2$) on the sample. The ramp-voltage scan rate was 1 eV/s. This scan rate was found to be convenient in that it was slow enough to average out high-frequency power-supply noise, and yet fast enough to average out long-term power-supply voltage drifts. By always collecting the core-level and valence-band data simultaneously, instabilities in the spectrometer tended to have an equivalent effect on the apparent core-level and valence-band binding energies. Thus it was possible to always make energy-difference measurements rather than independent absolute determinations.

Several experiments were carried out to examine the reliability of this approach. The binding-energy difference between the Ga 3d and As 3d core levels was measured several times for GaAs(110) samples with various electron-emission directions. It was observed that the variation of the binding energy of a core level was less than ± 0.1 eV due to sample position variations, surface band-bending variations, spectrometer instability, etc.; the binding-energy difference between the two core levels was reproducible to better than ± 0.01 eV. In previous studies^{11,12} of Ge-GaAs heterojunctions, by using an identical measurement technique, it was also found from several measurements on the same sample that outer core-level binding-energy differences could be measured with a reproducibility of less than 0.01 eV and usually less than 0.005 eV.

A primary difficulty with the determination of E_v^x in XPS spectra is a minimization of valence-band spectral distortion due to occupied surface states in the vicinity of E_v^x . Our approach (see Sec. III A 2 for details) is to analyze and compare results for several sets of angle-resolved measurements. Because the XPS photoelectron cross section should depend on the orbital character of filled surface states,^{13,14} it should be possible to detect the presence or absence of these states by studying the angular variation of the XPS valence-band spectrum in the vicinity of E_v^x . In Fig. 3 a convenient polar-coordinate system is defined to relate the photoelectron emission direction $\vec{\epsilon}$ to crystallographic axes for (110) and (111) surfaces. The polar angle θ for all measurements was held at 51.5°, and only the azimuthal angle ϕ was varied.

1. GaAs

Six sets of angle-resolved XPS data were collected on (110)-oriented GaAs samples. The (110) plane was chosen for study as it is the cleavage plane, and considerable information regarding the surface geometry exists.^{15,16} It

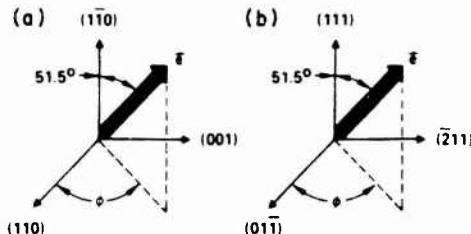


FIG. 3. Polar-coordinate systems relating photoelectron-emission direction $\vec{\epsilon}$ to crystallographic axes for (110) and (111) crystal surfaces (left and right, respectively). The azimuthal angle ϕ is in the plane of the crystal surface.

has been demonstrated that no detectable difference exists in the 1×1 LEED patterns for cleaved and sputter-annealed surfaces.¹⁷ The surface chemical shifts for the Ga 3d and As 3d photoelectron lines have been measured.¹⁸ Detailed analyses of the surface electronic structures have been carried out.¹⁹⁻²¹ The orbital character of the GaAs(110) surface states has been considered in detail.¹⁹ To assess the effect of surface-state contributions on the Ga 3d and As 3d to E_v^{GaAs} binding-energy difference measurements (see the analysis in Sec. III A 2), XPS data were collected for $\phi = 0^\circ, 35^\circ$, and 90° .

2. Ge

Six sets of angle-resolved XPS data were collected on (111)-oriented samples. Ultraviolet photoelectron spectroscopy (UPS)²² and electron-energy-loss spectroscopy (EELS)²³ measurements on (111) samples have indicated the presence of a surface state a few tenths of an eV below E_v^{Ge} . XPS data were collected for $\phi = 0^\circ, 30^\circ$, and 60° . Analyses of these data (Sec. III A 3) indicated that the surface state was substantially affecting the E_v^{Ge} determination. Thus four additional sets of XPS data were collected on (110)-oriented samples for $\phi = 0^\circ$ or 90° . Although the Ge(110) surface has been studied by LEED,^{9,24} and possible surface structures have been considered,²⁵ little is known about the electronic structure of this surface.

III. ANALYSIS OF XPS DATA

The objective of our XPS data analysis is the precise determination of $E_{\text{CL}}^x - E_v^x$ and the spin-orbit-split components $E_{3d_{3/2}}^x - E_v^x$ and $E_{3d_{5/2}}^x - E_v^x$ shown schematically in Fig. 2(a). This depends on locating the position of E_v^x in the XPS data with greater accuracy than has been generally attempted previously. We shall present a new method, based on fitting an instrumentally broadened theoretical valence-band density of states (VB DOS) to the XPS valence-band data in the region around E_v^x by using the method of least squares. Also in this section we discuss the analysis of the core-level energy positions, the resolution of the core-level spin-orbit-split components, and the limits of precision associated with the data analysis.

A. Location of E_v^x in the XPS data

The location of E_v^x in XPS data is complicated, even in the absence of occupied surface states, due to the slowly varying photoelectron signal in this energy region. For

semiconductors, methods such as extrapolating the tangent line to the leading edge of the photoelectron valence-band spectrum back to the energy axis and defining the slope intercept as E_v^x have been used.^{26,27} For metallic gold, the location of the inflection point in the XPS data has been used to define E_v^x (Refs. 28 and 29); while the inflection-point location method is appealing for metals with a partially filled valence band which has a slowly varying density of states near E_v , it is not appropriate for semiconductors. A major uncertainty is introduced into the determination of $E_{\text{CL}}^x - E_v^x$ for semiconductors by the extrapolation procedure used to locate E_v^x in the XPS data.

We have developed a method to obtain the position of E_v^x in XPS data by modeling a portion of the XPS valence-band spectrum in the region of E_v^x with an instrumentally broadened theoretical valence-band density of states $N_v(E)$, defined so that

$$N_v(E) = \int_0^\infty n_v(E') \sigma(E', h\nu) f(E') g(E - E') dE'. \quad (2)$$

In Eq. (2), $n_v(E')$ is a theoretical valence-band density of states. For Ge and GaAs data analyses we have employed the nonlocal pseudopotential VB DOS's of Cheikowsky and Cohen.³⁰ The next factor in Eq. (2) is the cross section or transition probability for photoionization

$$\sigma(E', h\nu) \propto |\langle \psi_f | P_{fi} | \psi_i \rangle|^2,$$

where P_{fi} is the transition operator between final- and initial-state wave functions ψ_f and ψ_i . In experiments reported here, $h\nu$ is 1486.6 eV, so that the density of available final states is sufficient for excitation of all initial states.

The factor $f(E')$ in Eq. (2) is the Fermi function and represents the effect of thermal broadening on the VB DOS. Since the integration is over the filled valence bands of a moderately doped semiconductor, the Fermi factor $f(E')$ is set equal to unity. The last factor in Eq. (2) is the instrumental resolution function $g(E)$ which is separately determined as discussed in Sec. III A 1.

To determine E_v^x from the XPS GaAs and Ge data, an energy interval extending from a few eV above E_v^x to ≈ 1 eV below E_v^x was analyzed. After setting $f(E')=1$, the remaining integral in Eq. (2) is recognized as a moving average of $n_v(E')\sigma(E', h\nu)$ over an interval roughly the full width at half maximum (FWHM) of the instrumental response function $g(E')$ and centered at energy E . If $\sigma(E', h\nu)$ is nearly constant when E' changes by no more than the FWHM of g , while $n_v(E')$ may vary by a large fraction over the same interval, then approximately:³¹

$$N_v(E) = \langle n_v \sigma \rangle \cong \langle n_v \rangle_E \langle \sigma \rangle_E. \quad (3)$$

The assumption that the photoelectric valence-band cross section varies more slowly than the VB DOS over the width of g is supported by both theoretical³²⁻³⁴ and experimental results.³⁵ Near E_v^x the orbital character of the wave functions is essentially p type and $\langle \sigma \rangle_E$ reduces to the constant cross section σ_p of p electrons. It follows from Eq. (3) that near E_v^x $N_v(E)$ is approximately

$$N_v(E) = \sigma_p \int_0^\infty n_v(E') g(E - E') dE'. \quad (4)$$

The position of E_v^x in the XPS data was determined by fitting $N_v(E)$ to the XPS valence-band data in the energy re-

gion around E_v^x by the method of least squares; thus E_v^x corresponds to $N_v(0)$. The fitting procedure involved three parameters, a scale factor S , the position of the valence-band edge E_v^x , and a constant random background B . The XPS spectral intensity $I(E)$ was assumed to have the form

$$I(E) = SN_v(E - E_v^x) + B. \quad (5)$$

In order to compare Eq. (5) with the experimental XPS data $I_{\text{XPS}}(E)$, both $N_v(E)$ and $I_{\text{XPS}}(E)$ were normalized so that the first peak below E_v^x corresponded to a peak height of unity. The parameters E_v^x , S , and B are then adjusted until the total error \mathcal{E} ,

$$\mathcal{E}^2 = \int_{E_{\min}}^{E_{\max}} [I_{\text{XPS}}(E) - I(E)]^2 dE, \quad (6)$$

is minimized for the fitting interval between E_{\min} and E_{\max} . In practice, E_v^x computed by minimizing Eq. (6) may be a function of E_{\max} . This complication will be discussed in relation to analyses of specific GaAs and Ge XPS data (Secs. III A 2 and III A 3). Finally we observe that when the experimental data $I_{\text{XPS}}(E)$ closely resemble the shape of the instrumentally broadened VB DOS $N_v(E)$ up to E_{\max} , the scale factor S in Eq. (5) can be replaced by $1 - B$ without sacrificing the quality of the fit.

1. Determination of the spectrometer response function

Our experimental results show that the shape of an experimental XPS spectrum around E_v^x is primarily controlled by $g(E)$. Therefore, the ability to determine an accurate analytic closed-form expression for the instrumental response function $g(E)$ plays an important role in determining precise values for the core-level to valence-band-edge binding-energy differences indicated in Fig. 2(a).

Experimentally observed Au 4f_{7/2} and Au 4f_{5/2} line shapes had FWHM of ~ 0.86 eV. Each of these lines $W_{\text{Au}4f_x}$ is related to $g(E)$ by

$$W_{\text{Au}4f_x}(E) = A_x \int_{-\infty}^{\infty} g(E - E') L(E') dE', \quad (7)$$

where A_x is a scale factor and $L(E')$ is a Lorentzian line shape (FWHM = 0.317 ± 0.010 eV),³⁶ which represents the inherent lifetime broadening of the Au 4f levels. An experimental characteristic of the gold 4f core levels is that after subtraction of a background function which is proportional to the integrated photoelectron peak area from the raw XPS data,³⁸ they are nearly symmetric and Gaussian around the peaks and Lorentzian in the tails. To represent the background-subtracted $W_{\text{Au}4f}(E)$ data analytically requires a function that is Gaussian in the core and Lorentzian in the tail. Voigt functions, formed by folding Gaussians with Lorentzians, have precisely this property, and have already been suggested as being useful for the analysis of experimental XPS line shapes.³⁷

In terms of the Voigt function

$$U(SE, b) = \frac{b}{S\pi^{3/2}} \int_{-\infty}^{\infty} \frac{e^{-S^2 x^2}}{(b/S)^2 + (E - x)^2} dx \quad (8)$$

of unit integrated area, the Au 4f spin-orbit-split doublet is represented as

$$W_{\text{Au}4f} = A_1 U(S(E - E_1), b) + A_2 U(S(E - E_2), b). \quad (9)$$

The parameters A_1 , A_2 , E_1 , E_2 , S , and b are obtained by fitting Eq. (9) to the background-subtracted XPS Au 4f core lines by using the method of least squares. A fit such as that shown in Fig. 4 is obtained each time a semiconductor core-level to valence-band-maximum binding-energy difference is measured in order to determine the instrumental response function $g(E)$ appropriate to the particular measurement in question.

The integral equation (7) for $g(E)$ can be solved exactly to yield the following closed-form analytic expression for the instrumental response function

$$g(E) = U(SE, b - K). \quad (10)$$

The parameters S and b in Eq. (10) are obtained from the least-squares fit in Eq. (9), and K is determined from the inherent (0.317 eV) (Ref. 36) linewidth (Γ_{FWHM}) of the lifetime-broadened Au 4f core levels through the relation

$$K = S(\Gamma_{\text{FWHM}})/2. \quad (11)$$

Phonon broadening of the Au 4f lines used to determine $g(E)$ was calculated following Citrin *et al.*³⁸ and was found to affect the $g(E)$ width by less than 0.01 eV; a similar result was reported by Citrin *et al.*³⁶

2. Results for GaAs

The Ga 3d and As 3d core-line centers (defined as the midpoint of the peak width at half of the peak height) were determined from the XPS data after a background function, which is proportional to the integrated photoelectron peak area, was subtracted to correct for the effect of inelastic photoelectron scattering. This procedure made it unnecessary to resolve spin-orbit splitting of the core lines to obtain high-precision peak positions. The position of E_v^{GaAs} was determined in the same spectrum by using the fitting procedure outlined in Sec. IIIA1.

Figure 5 shows the position of the E_v^{GaAs} measured relative to the center of the Ga 3d core level as a function of E_{max} for three angle-resolved sets of XPS measurements made on GaAs(110) surfaces. The azimuthal angles $\phi = 0^\circ$, 35° , and 90° are defined in Fig. 3. The least-squares analyses for the values of $E_v^{\text{GaAs}}(E_{\text{max}})$ and B , which mini-

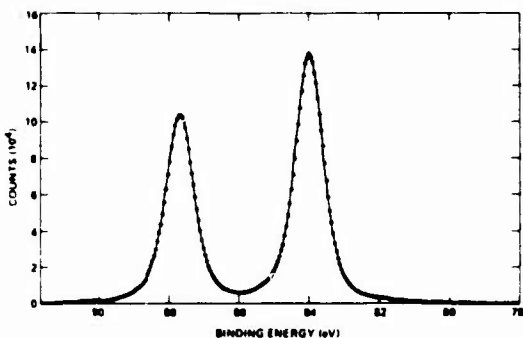


FIG. 4. Least-squares fit (solid curve) of the sum of two Voigt functions to the Au 4f_{5/2} and Au 4f_{7/2} background-subtracted (closed circles) Au 4f XPS spectrum.

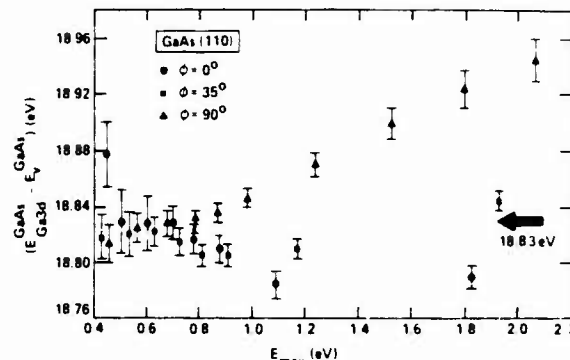


FIG. 5. Position of the GaAs valence-band maximum E_v^{GaAs} measured relative to the center of the Ga 3d core level as a function of the end point E_{max} of the fitting interval for azimuthal angles of 0° , 35° , and 90° defined in Fig. 3.

mize Eq. (6), were performed by using Marquardt's algorithm.³⁹ The error bars shown in Fig. 5 represent the 95% central confidence interval⁴⁰ for each least-squares value of $E_{\text{Ga}3d}^{\text{GaAs}} - E_v^{\text{GaAs}}(E_{\text{max}})$. Convergence to a common value of $E_{\text{Ga}3d}^{\text{GaAs}} - E_v^{\text{GaAs}} = 18.83$ eV occurs for $E_{\text{max}} \leq 1.0$ eV below E_v^{GaAs} .

The variation of $E_{\text{Ga}3d}^{\text{GaAs}} - E_v^{\text{GaAs}}$ with ϕ and with E_{max} can be explained in terms of occupied states associated with the GaAs(110) surface. Detailed analyses of the relaxed GaAs(110) surface electronic structure have been performed.¹⁹⁻²¹ Although the surface electronic structure is quite sensitive to precise details of the geometry, in general, the theoretical calculations place the highest-lying energy peaks in the local density of states between 0.5 and 1.5 eV below E_v^{GaAs} . Experimental results^{41,42} place the highest-lying surface-state peak at ≈ 1 eV below E_v^{GaAs} for the GaAs(110) surface. Thus for our spectrometer response function (see Sec. IIIA1) it might be expected that the XPS valence-band data within ≈ 1 eV of E_v^{GaAs} would not contain substantial surface-state contributions. The unique value of $E_{\text{Ga}3d}^{\text{GaAs}} - E_v^{\text{GaAs}}$ for $E_{\text{max}} \lesssim 1.0$ eV appears to confirm this view.

The orbital character of the GaAs(110) surface states has been considered in detail. Chadi's calculations¹⁹ indicate that the highest-lying surface state consistent with the 27° rotational relaxation model¹⁵ has a predominantly p_y -orbital character, while the bond relaxation model¹⁶ has a predominantly p_z character, with about equal amounts of p_x and p_y . In describing the p -derived orbital symmetries of the surface states, the \vec{x} direction is parallel to (110), the \vec{y} direction is parallel to (001), and the \vec{z} direction is parallel to (110).

Zunger⁴³ has pointed out that the upper As surface state has about 20% d character, and that there is a certain amount of arbitrariness in the assignment of atomic-orbital character to surface states. Experimental results^{44,45} suggest that the highest-lying surface states have predominantly p_z character (rather than p_x).

The photoelectron cross section σ is given following Gelius¹⁴ as

$$\sigma \propto |\langle p | PW(\vec{k}) \rangle|^2, \quad (12)$$

the square of the absolute value of the overlap between an orbital involved in the photoemission and the plane wave

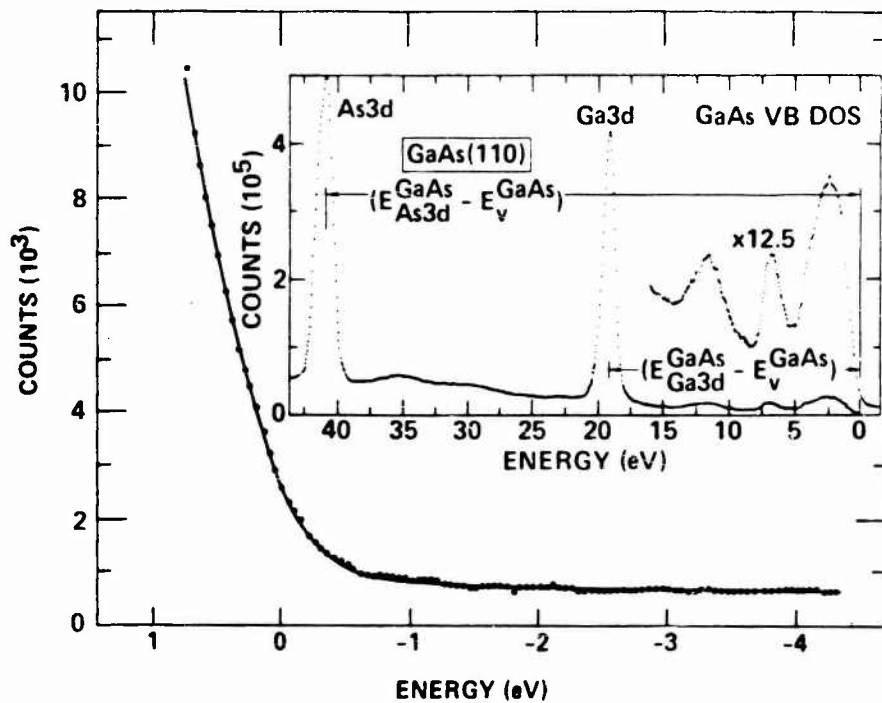


FIG. 6. Least-squares fit of the instrumentally broadened theoretical VB DOS (solid curve) to XPS data (dots) in the region of the valence-band maximum for GaAs. Inset shows the XPS spectrum which contains the VB DOS and the outermost core levels. The energy scale is zero at the valence-band maximum.

$PW(\vec{k})$ representing the free electron; \vec{k} denotes the wave vector for the photoelectron. Referring to Fig. 3, for $\phi=0^\circ$ and 90° , \vec{e} is orthogonal to \vec{y} and \vec{x} , respectively. Thus one would expect the maximum photoelectron cross-section contribution, Eq. (12), to the XPS valence-band data from predominately p_y -character surface states when $\phi=90^\circ$. This could account for the enhanced sensitivity of the $E_{\text{As}3d}^{\text{GaAs}} - E_v^{\text{GaAs}}$ determination to the fitting interval for $\phi=90^\circ$ data as noted in Fig. 5.

Figure 6 shows the least-squares fit of the instrumentally broadened $N_p(E)$ (solid curve) to XPS data (dots) in the region near E_v^{GaAs} . The inset in Fig. 6 shows the XPS spectrum which contains the valence band and the Ga 3d and As 3d core levels. The energy scale is zero at E_v^{GaAs} as discussed in Sec. III A. By analyzing six sets of GaAs(110) data as described here, the XPS measured values for $E_{\text{Ga}3d}^{\text{GaAs}} - E_v^{\text{GaAs}}$ and $E_{\text{As}3d}^{\text{GaAs}} - E_v^{\text{GaAs}}$ are 18.83 and 40.75 eV, respectively.

3. Results for Ge

The Ge 3d core line center was determined from XPS data in the same manner that the Ga 3d and As 3d line centers were determined (see Sec. III A 2). Also, the position of E_v^{Ge} was determined by the fitting procedure given in Sec. III A.

Figure 7(a) shows the results of analyzing three angle-resolved sets of data taken on the Ge(111) surface, and two additional sets of data for the Ge(110) surface. The azimuthal angle ϕ is defined in Fig. 3. The error bars are defined as in Fig. 5. UPS (Ref. 22) and EELS (Ref. 23) measurements on the Ge(111) 2×8 surface have indicated the presence of a high-lying surface state a few tenths of an eV below E_v^{Ge} . This surface state has been associated

with a dangling-bond state. Theoretical calculations⁴⁶ on the relaxed Ge(111) surface have placed a dangling-bond state, which has p_z -orbital character within 0.1 eV of E_v [the \vec{z} direction is parallel to (111)]. It could be anticipa-

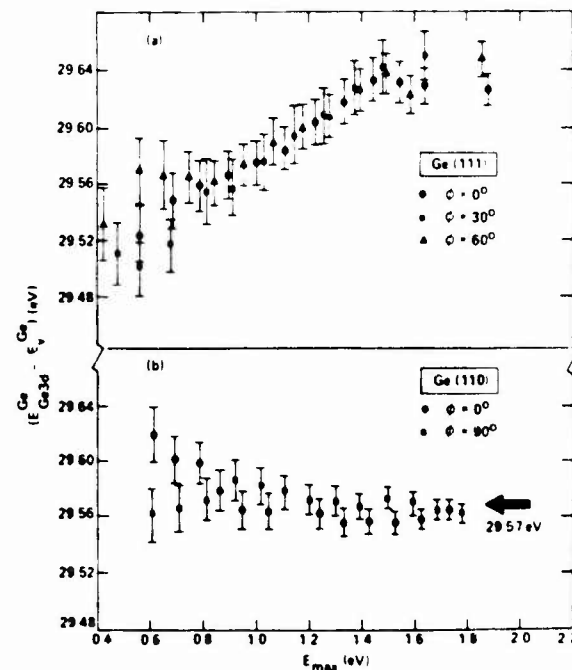


FIG. 7. Position of the Ge valence-band maximum E_v^{Ge} measured relative to the center of the Ge 3d core level as a function of the end point E_{max} of the fitting interval. Results are shown for azimuthal angles (Fig. 3) of 0° , 30° , and 60° on the (111) crystal face and 0° and 90° on the (110) crystal surface.

ed that this surface state would contribute substantially to the photoelectron signal in the vicinity of E_v^{Ge} , and that because of the p_z -orbital character of this state, variations of ϕ would have little effect on the ratio of surface to bulk emission in the photoelectron signal near E_v^{Ge} . The Ge(111) XPS data collected for $\phi=0^\circ$, 30° , and 60° and analyzed as shown in Fig. 7(a) seem to confirm this view. The analysis does not produce a satisfactory determination of $E_{\text{Ge}3d}^{\text{Ge}} - E_v^{\text{Ge}}$ because of the monotonic variation of $E_{\text{Ge}3d}^{\text{Ge}} - E_v^{\text{Ge}}$ with E_{max} .

In order to determine $E_{\text{Ge}3d}^{\text{Ge}} - E_v^{\text{Ge}}$, angle-resolved Ge(110) data were analyzed as shown in Fig. 7(b). The relatively constant value of $E_{\text{Ge}3d}^{\text{Ge}} - E_v^{\text{Ge}}$ independent of E_{max} and ϕ suggests that any filled Ge(110) surface states below E_v^{Ge} are either very weakly localized near the surface or lie well outside the energy interval analyzed, since it is unlikely that σ for such (110) surface states would be independent of ϕ .

Figure 8 shows a least-squares fit of $N_v(E)$ (solid line) to Ge(110) XPS data (dots) in the region of E_v^{Ge} . The inset in Fig. 8 shows the XPS spectrum containing the valence band and the Ge 3d core level. The energy scale is zero at E_v^{Ge} . By analyzing four sets of Ge(110) data, the XPS measured value for $E_{\text{Ge}3d}^{\text{Ge}} - E_v^{\text{Ge}}$ was 29.57 eV.

B. Surface chemical shifts

The chemical shifts of surface atoms relative to bulk binding energies have recently been measured for several semiconductors.^{18,47-49} In particular, for the GaAs(110) surface, it is observed¹⁸ that the surface Ga 3d level is shifted to larger binding energy by $\Delta E_B = 0.28$ eV, while

the As 3d level is shifted to smaller binding energy by $\Delta E_B = -0.37$ eV. For the Si(111) 2×1 surface, surface chemical shifts of $\Delta E_B = -0.59$ and $+0.30$ eV have been reported⁴⁷ for the Si 2p level. Both the GaAs(110) and Si(111) 2×1 surface measurements indicate that the surface chemical shifts are predominantly associated with initial-state charge transfer in the outermost atom layer. It has been emphasized⁵⁰ that sizable surface chemical shifts may influence XPS measured core-level binding energies.

The apparent shift of the XPS measured $(E_{\text{CL}}^* - E_v^*)_{\text{XPS}}$ from the bulk value due to surface chemical shifts can be estimated with good accuracy if knowledge of these shifts is available. A small correction can then be applied to obtain the bulk $(E_{\text{CL}}^* - E_v^*)_b$ values. We have used the measured¹⁸ GaAs(110) surface chemical shifts to estimate corrections to our Ga 3d and As 3d XPS binding-energy measurements. The electron escape depth λ has been measured in Ge for an electron kinetic energy E_k of 1228 eV as $\lambda(1228 \text{ eV}) = 24.2 \pm 2 \text{ \AA}$ (Ref. 8), for $E_k > 200$ eV, it was found that $\lambda \propto E_k^{0.56}$. Extrapolating this result to $E_k = 1450$ eV, which is more appropriate for the Ga 3d, Ge 3d, and As 3d levels studied in this work, yields $\lambda(1450 \text{ eV}) = 26.6 \pm 2.2 \text{ \AA}$. This result is in good agreement with an earlier, although less precise, measurement of $\lambda(1404 \text{ eV}) = 29 \pm 4 \text{ \AA}$ which was obtained for amorphous Ge.⁵¹ The GaAs(110) interplanar spacing is 2.00 \AA , and the photoelectron-emission direction relative to the surface normal is 51.5° . Assuming an ideally flat surface, approximately $11.4 \pm 0.9\%$ of the Ga 3d and As 3d photoelectron signals originate from the surface layer. The apparent

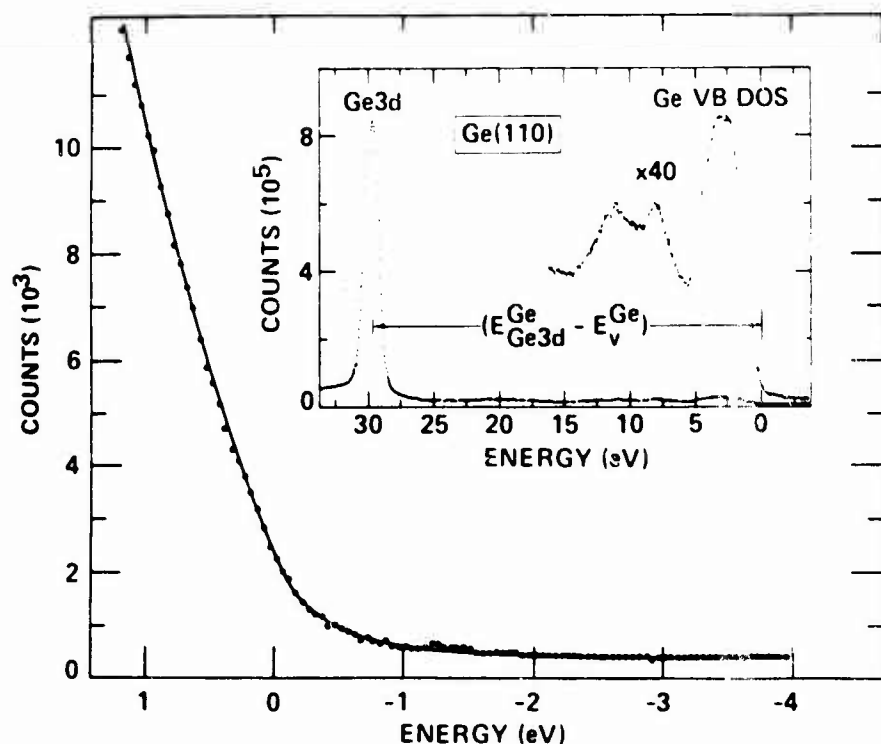


FIG. 8. Least-squares fit of the instrumentally broadened theoretical VB DOS (solid curve) to XPS data (dots) in the region of the Ge valence-band maximum. Inset shows the XPS spectrum which contains the VB DOS and the Ge 3d core level. The energy scale is zero at the valence-band maximum.

shift in the Ga 3d and As 3d core levels caused by the surface chemical shifts of $\Delta E_s = +0.28$ and -0.37 eV, respectively, was estimated by summing the experimentally observed line shapes with a second component, which was shifted in energy by the appropriate surface chemical shift, and had an intensity scaled to represent 11.4% of the total signal. The estimated shifts of the Ga 3d and As 3d line centers due to surface chemical shifts are $+0.030$ and -0.035 eV, respectively. When these shifts are subtracted from the measured $(E_{CL}^x - E_v^x)_{XPS}$ values, the $(E_{CL}^x - E_v^x)_b$ values for GaAs are 18.80 and 40.79 eV for $(E_{Ga\ 3d}^{GaAs} - E_v^{GaAs})_b$ and $(E_{As\ 3d}^{GaAs} - E_v^{GaAs})_b$, respectively.

Surface chemical shifts have not yet been studied on Ge(110) surfaces, however, the magnitudes of surface chemical shifts observed on Ge(111) surfaces⁴⁸ are similar to those observed on the GaAs(110) (Ref. 18) and Si(111) surfaces.⁴⁷⁻⁴⁹ If surface chemical shifts on the Ge(110) surface are predominantly associated with initial-state charge transfer, one might expect that the major effect on the XPS-measured Ge 3d photoelectron line would be a small-line broadening with a very modest line-center shift. The Si 2p surface chemical shifts measured on the Si(111) 2×1 surface⁴⁷ may be a somewhat analogous situation; from a simple first moment type of argument, one can estimate a centroid shift of -0.017 eV for the Si 2p line for our experimental arrangement.

The surface chemical-shift correction to $(E_{CL}^x - E_v^x)_{XPS}$ is not very sensitive to the exact photoelectron line shape. From a first-moment calculation, one would estimate apparent Ga 3d and As 3d line centroid shifts of $+0.032$ and -0.042 eV for our experimental geometry. This suggests that a surface chemical-shift correction can be made with good accuracy (assuming that these shifts are known for a particular surface).

C. Resolution of spin-orbit-split core-level to valence-band-edge binding-energy differences

The operational definition of the core-level binding energy as the energy corresponding to the midpoint of the peak width at half the core-level peak height is convenient because core lines are prominent in XPS spectra and the line centers are easy to locate accurately. However, the width of the core level is not only dependent on intrinsic broadening mechanisms such as lifetime broadening and phonon broadening, but is also dependent on the broadening introduced by the spectrometer response function.

In order to eliminate the effect of spectrometer broadening and to obtain instrument-independent core-level to E_v

binding-energy differences, it is necessary to refer binding-energy measurements to the $3d_{3/2}$ and $3d_{5/2}$ spin-orbit-split components of the 3d core levels. These instrumentally independent core-level to E_v binding-energy differences should be true semiconductor bulk properties, and should be more easily compared with other experimental results.

In order to resolve the spin-orbit-split $3d_{3/2}$ and $3d_{5/2}$ core-line components, it is assumed that the instrumentally broadened experimental 3d core line $W_{x\ 3d}^x(E)$ is representable as a linear combination $\tilde{W}_{x\ 3d}^x(E)$ of two Voigt functions, $U(SE, b)$, defined in Eq. (8) and separated from one another by the spin-orbit splitting Δ_{so} .

$$\tilde{W}_{x\ 3d}^x(E) = A_1 U(S(E - E_1), b_1) + A_2 U(S(E - E_2), b_2) \quad (13)$$

where

$$\Delta_{so} = (E_1 - E_2) \quad (14)$$

The parameters A_1 , A_2 , E_1 , S , b_1 and b_2 are determined by the method of least squares³⁹ by adjustment until the total error given by

$$\delta^2 = \int_{E_{\text{initial}}}^{E_{\text{final}}} [W_{x\ 3d}^x(E) - \tilde{W}_{x\ 3d}^x(E)]^2 dE \quad (15)$$

is minimized. The integration interval $E_{\text{final}} - E_{\text{initial}}$ in Eq. (15) is large enough to include nearly the entire instrumentally broadened core line. Figures 9(a)–9(c) show typical least-squares fits of Eq. (13) to Ga 3d, Ge 3d, and As 3d core lines, respectively. The line center is defined as zero energy in the figure. The intensity ratio $I_{\pm} = I_{\frac{1}{2}}/I_{\frac{5}{2}}$ has a theoretical value $[2 \times (\frac{1}{2}) + 1]/[2 \times (\frac{5}{2}) + 1]$ equal to 0.67 in approximate agreement with the intensity ratio determined from the individual spin-orbit-split line components which are also shown in Fig. 9.

The spin-orbit splittings Δ_{so} used to analyze these data are given in Table I and were determined from other data such as XPS results or in the case of As 3d from interpolation between other high-resolution electron spectroscopy data.^{7,18} The binding energies for the spin-orbit-split components relative to the line centers for Ga 3d and As 3d core lines in GaAs and for the Ge 3d core line in Ge are also given in Table I.

D. Precision analysis

In this section we consider factors which affect the precision of XPS core-level binding-energy measurements.

TABLE I. Binding energies of spin-orbit components relative to line centers in eV

Core level	Spin-orbit splitting	Binding energy relative to line center
Ga 3d _{3/2} (GaAs)	0.43	-0.17
Ga 3d _{5/2} (GaAs)		+0.26
Ge 3d _{3/2} (Ge)	0.55	-0.21
Ge 3d _{5/2} (Ge)		+0.34
As 3d _{3/2} (GaAs)	0.71	-0.30
As 3d _{5/2} (GaAs)		+0.41

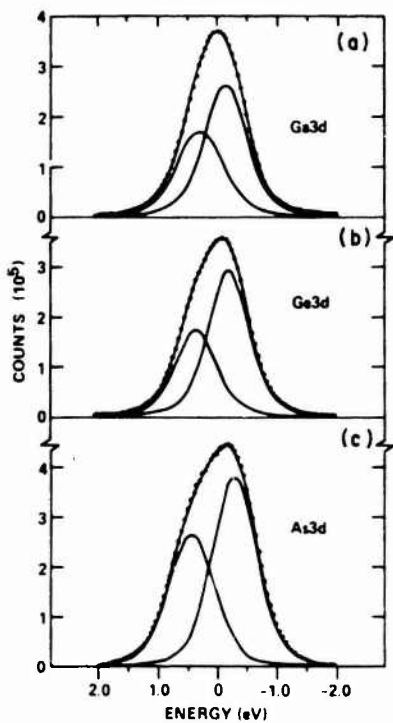


FIG. 9. Resolution of the spin-orbit-split Ga, Ge, and As $3d_{3/2}$ and $3d_{5/2}$ core-level components by means of a least-squares fit of the sum of two Voigt functions to the background-subtracted 3d-core line shapes.

1. Band bending

Free-surface band bending could affect the accurate XPS determination of core-level to valence-band maximum binding-energy differences for heavily doped materials. When the surface Fermi-level pinning position is known, it would be possible to minimize this complication by a judicious choice of bulk doping density. In general, this complication should be more severe for wide-band-gap than for narrow-band-gap semiconductors.

For n -type GaAs, a typical surface band bending is 0.8 eV.^{52,53} Therefore, as a worst-case estimate for the effect of band bending on the core-level to E_b^x binding-energy difference, a simple calculation was carried out to determine the shift of the Ga 3d core-level center for a surface potential $V_s = 0.8$ V, a doping density $N_D = 1 \times 10^{17} \text{ cm}^{-3}$, a dielectric constant $\epsilon_r = 12$, and an escape depth equal to 26.6 Å.⁴ In the depletion approximation, the potential, $V(x)$, within a surface-depletion region of width W , is given by

$$V(x) = E_m [x - (x^2/2W)], \quad (16)$$

where the maximum electric field at the surface is $|E_m| = qN_D W/\epsilon_r$, and $W = (2\epsilon_r V_s / qN_D)^{1/2}$; q is the electronic charge. For our measurements the electron-emission direction relative to the sample surface normal was 51.5°; this angle decreases the effective sampling depth and its effect was included in the calculation. Assuming an ideally smooth surface, photoelectrons generated at a depth x below the surface are attenuated exponentially as

$$I(x) = I_0 \exp(-x/\lambda \cos\theta), \quad (17)$$

where I_0 is the unattenuated intensity emitted from the surface at $x=0$. Thus the envelope of the core line $M(E)$ which is shifted in energy due to band bending is given by

$$M(E) = \int_0^\infty m(E - V(x)) \exp(-x/\lambda \cos\theta) dx, \quad (18)$$

where $m(E)$ is the core-level line shape observed at the surface. The calculations utilized the experimentally observed XPS Ga 3d line shape for $m(E)$. For the conditions specified above, the total shift of the line center was 0.014 eV. Thus for the moderate doping densities of the samples utilized herein, band bending affects the observed core-level center by less than 0.01 eV. A smaller shift in the observed E_b^x would also be expected due to band bending. Because the two shifts would be in the same direction, they would tend to cancel.

2. Accuracy of the instrumental response function

The method used to determine g was outlined in Sec. IIIA1. The typical precision in the least-squares procedure used to model the Au 4f line shapes for the purposes of determining g produced an uncertainty in the Voigt-function FWHM of about 0.01 eV. The instrumental response function is determined by deconvolving a Lorentzian curve with $\Gamma_{\text{FWHM}} = 0.317 \pm 0.010$ eV (Ref. 36) (determined by the Au 4f final-state lifetime) from the Voigt function used to model the Au 4f line shape. An uncertainty in the deconvolved Lorentzian curve of 0.01 eV would produce an additional uncertainty in the FWHM of the instrumental response function of about 0.006 eV leading to a total uncertainty in the FWHM of the instrumental response function of ≈ 0.012 eV.

3. Choice of the theoretical VB DOS

As a test of the sensitivity of the core-level to valence-band-maximum binding-energy determinations to the particular theoretical (VB DOS) $n_v(E)$ used in Eq. (4), computations were performed for both local⁵⁴ and nonlocal³⁰ pseudopotential VB DOS's. The latter includes the effects of spin-orbit splitting of the valence band, and also represents valence bandwidths more accurately.³⁰ Computational results show that the difference between local⁵⁴ and nonlocal³⁰ pseudopotential VB DOS's in Eq. (4) amounts to less than a 0.01-eV change in the apparent position of E_b^x . The effect of the spin-orbit splitting at the valence-band edge, which amounts to 0.34 and 0.29 eV in GaAs and Ge, respectively,⁵⁵ was not resolvable in the experiments reported here.

4. Effects of background subtraction

A background function which was proportional to the integrated photoelectron peak area was subtracted from all core-level peaks to remove approximately the contribution from inelastically scattered photoelectrons from the XPS spectra. It was found that this correction shifted the apparent E_b^x position by ≤ 0.01 eV. The effect of background on the E_b^x determination was also investigated by subtracting a similar background function from the XPS

valence-band data. By determining E_v^x (with the procedure outlined in Sec. III A) from XPS valence-band data both with and without the background correction applied, it was observed that the apparent E_v^x position was only shifted by ~ 0.005 eV due to background effects.

5. Precision limits

In Secs. III D 1–III D 4 several factors which affect the limits of precision on XPS $E_{CL}^x - E_v^x$ measurements have been discussed. These factors are now combined to obtain precision limits for the experimentally measured binding-energy differences reported in this paper.

As noted in Sec. II D, the precision in determining a core-level center from the experimental data was about 0.005 eV. Possible effects of band bending within the XPS sampling depth were shown (Sec. III D 1) to introduce an uncertainty of less than 0.01 eV in the apparent core-level position. The background-subtraction procedure used in analyzing the core-level data produced an apparent energy shift of ≤ 0.01 eV (Sec. III D 4), which provides an estimate of the uncertainty caused by background effects. Combining these three uncertainties leads to an uncertainty in determining the core-level center from XPS data of ≤ 0.015 eV. To remove approximately the effect of surface chemical shifts from the XPS-measured core-level center position, a correction was applied (see Sec. III B). If we assume that the accuracy of the surface chemical-shift determination¹⁸ is ± 0.05 eV and consider the uncertainty in λ of ± 2.2 Å (see Sec. III B), the uncertainty in the surface chemical-shift correction is less than 0.006 eV. Thus the total uncertainty in determining the core-level center for bulk material is ≤ 0.016 eV.

Uncertainty in g affects the uncertainty in the determination of E_v^x from the experimental data. By fitting data near E_v^x with theoretical functions obtained by folding VB DOS's with Voigt-function approximations to g which spanned the range of uncertainty in g (see Sec. III D 2), it was determined that the uncertainty in g produced a 0.014-eV uncertainty in determining E_v^x . The choice of theoretical density of states in the valence-band-edge modeling procedure was shown to introduce a variation in the apparent E_v^x position of less than 0.01 eV (Sec. III D 3). The precision of the least-squares-fitting procedure used to locate E_v^x in the experimental data was typically 0.005 eV, and the estimated uncertainty due to background effects is ~ 0.005 eV (Sec. III D 4). Thus the total uncertainty in determining the position of E_v^x in the experimental data is ≤ 0.019 eV.

By combining the uncertainties in determining the core-level center and E_v^x from the experimental data, the uncertainty in the $E_{CL}^x - E_v^x$ values is estimated as ≤ 0.025 eV. The spectrometer energy scale is calibrated to 0.02% (Sec. II B). The uncertainty in this calibration introduces an uncertainty in determining $E_{CL}^x - E_v^x$ which increases with increasing core-level binding energy. The As 3d core level had the largest binding energy of core levels studied in this work, and therefore provides a worst-case estimate. Including the uncertainty due to spectrometer calibration leads to a total uncertainty in the core-level to E_v^x binding-energy difference of ≤ 0.026 eV.

The curve-fitting procedure used to determine the energy positions of the core-level spin-orbit components is discussed in Sec. III C. The precision of the fitting procedure was less than 0.01 eV. The uncertainty in the magnitude of the spin-orbit splitting for Ga 3d, Ge 3d, and As 3d core levels is about ± 0.05 eV (Refs. 7 and 18) and thus the uncertainty of each spin-orbit-split component relative to the line center would be ~ 0.035 eV. The total uncertainty in determining the spin-orbit components relative to the line center is therefore about 0.036 eV. Combining this uncertainty with the uncertainty in the measurement of the line-center position leads to a total uncertainty for the spin-orbit components to E_v^x binding-energy differences of ≤ 0.044 eV.

IV. SUMMARY

A procedure has been developed to measure semiconductor core-level to valence-band maximum binding-energy differences with greater precision than has been previously attempted. This procedure involves analyzing an XPS spectrum in which both the core-level and valence-band data have been collected simultaneously. The position of E_v^x in the XPS spectrum is determined by least-squares-fitting a theoretical VB DOS, which has been broadened by the instrumental response function to data in a limited energy region near E_v^x . The instrumental response function is determined from analysis of XPS-measured Au 4f core-level data. The effects of occupied surface states on the measurements are determined by analyzing angle-resolved data obtained from samples with known crystallographic orientations. The spin-orbit-split components of particular core levels are resolved by employing the method of least squares.

Core-level to E_v^x binding-energy differences have been determined for Ga 3d and As 3d in GaAs, and for Ge 3d in Ge. The experimental results and limits of precision are

TABLE II. Core-level to E_v^x binding-energy differences in eV. The absolute value of the uncertainty in the least significant figure is indicated in parentheses.

Semiconductor surface	Core level	$(E_{CL}^x - E_v^x)_{XPS}$	$(E_{CL}^x - E_v^x)_b$	$(E_{M_{3/2}}^x - E_v^x)_b$	$(E_{M_{3/2}}^x - E_v^x)_b$
GaAs(110)	Ga 3d	18.83(3)	18.80(3)	18.63(4)	19.06(4)
	As 3d	40.75(3)	40.79(3)	40.47(4)	41.18(4)
Ge(110)	Ge 3d	29.57(3)	29.57(3) ^a	29.36(4)	29.91(4)

^aThe Ge 3d surface chemical shifts for the Ge(110) surface are unknown. From the argument given in Sec. III B there should be little difference between the XPS measured and bulk values of $E_{CL}^{Gr} - E_v^{Gr}$.

summarized in Table II. This table includes the XPS-measured values of the core-level center to E_v^x binding-energy differences ($E_{CL}^x - E_v^x$)_{XPS} and the corresponding bulk semiconductor values ($E_{CL}^x - E_v^x$)_b, which have been corrected for surface chemical-shift effects. Also included in the table are the bulk semiconductor values of binding energies for the spin-orbit-split components of the core levels relative to E_v^x .

The value of ($E_{Ga3d}^{GaAs} - E_v^{GaAs}$)_{XPS} is in good agreement with previous literature that reported results of 18.9 ± 0.1 (Refs. 4 and 6) and 18.82 ± 0.15 eV.⁵ The value of ($E_{Ge3d}^{Ge} - E_v^{Ge}$)_{XPS} is in rather poor agreement with the previously reported result of 29.0 ± 0.1 eV.⁶ The binding energies of the Ga 3d and As 3d spin-orbit-split components relative to E_v^{GaAs} have recently been measured¹⁸ as $E_{Ga3d_{5/2}}^{GaAs} - E_v^{GaAs} = 18.60$ eV, $E_{Ga3d_{3/2}}^{GaAs} - E_v^{GaAs} = 19.04$ eV, $E_{As3d_{5/2}}^{As} - E_v^{As} = 40.37$ eV, and $E_{As3d_{3/2}}^{As} - E_v^{As} = 41.07$ eV. Considering the precision limits of the experiments, these results are in very good agreement with the results reported here. Earlier reported⁷ binding energies for the spin-orbit-split components of Ge 3d relative to E_v^{Ge} are $E_{Ge3d_{5/2}}^{Ge} - E_v^{Ge} = 29.1$ eV, and $E_{Ge3d_{3/2}}^{Ge} - E_v^{Ge} = 29.65$ eV;

these values are not in as good agreement with our present results. Although the origin of the discrepancy cannot be identified with certainty, the earlier measurements were obtained on Ge(111) surfaces, and the occupied surface-state emission may have complicated the determination of E_v^{Ge} . We note from our data in Fig. 7 that if Ge(111) data were analyzed only in a small interval near E_v^{Ge} , a substantially lower $E_{Ge3d}^{Ge} - E_v^{Ge}$ would be obtained.

We have previously discussed³ the applications of photoelectron spectroscopy for determining semiconductor band bending, Schottky-barrier heights, and heterojunction band discontinuities, and we will not repeat that discussion here. As additional core-level to E_v^x binding-energy differences for several semiconductors become available with good precision, the capability of XPS and other photoelectron spectroscopies to monitor interface potential could find wide applications.

ACKNOWLEDGMENT

This research was supported in part by the U.S. Office of Naval Research Contract No. N00014-76-C-1109.

- ¹K. Siegbahn, C. Nordling, A. Fahlman, R. Nordberg, K. Hamrin, J. Hedman, G. Johansson, T. Bergmark, S.-E. Karlsson, I. Lindgren, and B. Lindberg, in *ESCA-A Atomic, Molecular, and Solid State Structure Studied by Means of Electron Spectroscopy* Uppsala, 1967 [Nov. *Acta R. Soc. Sci. Ups. Ser. IV.* **20** (1967)].
- ²J. Auleyiner and O. Hornfeldt, *Ark. Fys.* **23**, 165 (1963).
- ³E. A. Kraut, R. W. Grant, J. R. Waldrop, and S. P. Kowalczyk, *Phys. Rev. Lett.* **44**, 1620 (1980).
- ⁴C. C. Chang, P. H. Citrin, and B. Schwartz, *J. Vac. Sci. Technol.* **A14**, 943 (1977).
- ⁵L. Ley, R. A. Pollak, F. R. McFeely, S. P. Kowalczyk, and D. A. Shirley, *Phys. Rev. B* **9**, 600 (1974).
- ⁶M. Cardona, C. M. Penchina, N. J. Shevchik, and J. Tejeda, *Solid State Commun.* **11**, 1655 (1972).
- ⁷D. E. Eastman and J. L. Freeouf, *Phys. Rev. Lett.* **33**, 1601 (1974).
- ⁸H. Gani and W. Mönch, *Surf. Sci.* **105**, 217 (1981).
- ⁹B. Z. Olshansky, S. M. Repinsky, and A. A. Shklyav, *Surf. Sci.* **64**, 224 (1977).
- ¹⁰D. Haneman, *Adv. Phys.* **31**, 165 (1982).
- ¹¹R. W. Grant, J. R. Waldrop, and E. A. Kraut, *Phys. Rev. Lett.* **40**, 656 (1978).
- ¹²R. W. Grant, J. R. Waldrop, and E. A. Kraut, *J. Vac. Sci. Technol.* **A15**, 1451 (1978).
- ¹³See, e.g., V. G. Aleshin and Yu. N. Kucherenko, *J. Electron Spectrosc.* **9**, 1 (1976).
- ¹⁴U. Gelius, in *Electron Spectroscopy*, edited by D. A. Shirley (North-Holland, Amsterdam, 1972), p. 311.
- ¹⁵S. Y. Tong, A. R. Lubinsky, B. J. Mrstik, and M. A. Van Hove, *Phys. Rev. B* **17**, 3303 (1978).
- ¹⁶A. Kahn, E. So, P. Mark, and C. B. Duke, *J. Vac. Sci. Technol.* **A15**, 580 (1978).
- ¹⁷P. Skeath, W. A. Saperstein, P. Pianetta, I. Lindau, and W. E. Spicer, *J. Vac. Sci. Technol.* **A15**, 1219 (1978).
- ¹⁸D. E. Eastman, T.-C. Chiang, P. Heimann, and F. J. Himpel, *Phys. Rev. Lett.* **45**, 656 (1980).
- ¹⁹D. J. Chadi, *Phys. Rev. B* **18**, 1800 (1978).
- ²⁰D. J. Chadi, *J. Vac. Sci. Technol.* **A5**, 1244 (1978).
- ²¹J. R. Chelikowsky and M. L. Cohen, *Solid State Commun.* **29**, 267 (1979).
- ²²T. Murotani, K. Fujiwara, and M. Nishijima, *Phys. Rev. B* **12**, 2424 (1975).
- ²³R. Ludeke and A. Koma, *Phys. Rev. B* **13**, 739 (1976).
- ²⁴F. Jona, *IBM J. Res. Dev.* **9**, 375 (1965).
- ²⁵D. Haneman, in *Surface Physics of Phosphors and Semiconductors*, edited by C. G. Scott and C. F. Reed (Academic, London, 1975), p. 1.
- ²⁶D. E. Eastman, W. D. Grobman, J. L. Freeouf, and M. Erbudak, *Phys. Rev. B* **9**, 3473 (1974).
- ²⁷R. Ludeke, L. Ley, and K. Ploog, *Solid State Commun.* **28**, 57 (1978).
- ²⁸D. A. Shirley, *Phys. Rev. B* **5**, 4709 (1972).
- ²⁹G. Aeppli, D. E. Eastman, R. W. Johnson, R. A. Pollak, and H. J. Stoltz, *J. Electron Spectrosc.* **14**, 121 (1978).
- ³⁰J. R. Chelikowsky and M. L. Cohen, *Phys. Rev. B* **14**, 556 (1976).
- ³¹E. A. Kraut, *Rev. Geophys.* **1**, 401 (1963).
- ³²V. V. Nemoshkalenko, V. G. Aleshin, and Yu. N. Kucherenko, *J. Electron Spectrosc.* **13**, 361 (1978).
- ³³V. V. Nemoshkalenko, V. G. Aleshin, and Yu. N. Kuchesenko, *Solid State Commun.* **20**, 1155 (1976).
- ³⁴T. Jarlborg and A. J. Freeman, *Phys. Lett.* **74A**, 349 (1979).
- ³⁵R. G. Cavell, S. P. Kowalczyk, L. Ley, R. A. Pollak, B. Mills, D. A. Shirley, and W. Perry, *Phys. Rev. B* **7**, 5313 (1973).
- ³⁶P. H. Citrin, G. K. Wertheim, and Y. Baer, *Phys. Rev. Lett.* **41**, 1425 (1978).
- ³⁷G. K. Wertheim, M. A. Butler, K. W. West, and D. N. E. Buchanan, *Rev. Sci. Instrum.* **45**, 1369 (1974).
- ³⁸P. H. Citrin, G. K. Wertheim, and Y. Baer, *Phys. Rev. B* **16**, 4256 (1977).
- ³⁹D. W. Marquardt, *J. Soc. Indust. Appl. Math.* **11**, 431 (1963).
- ⁴⁰R. L. Kelly *et al.*, *Rev. Mod. Phys.* **52**, S36 (1980).
- ⁴¹J. A. Knapp and G. J. Lapeyre, *J. Vac. Sci. Technol.* **A13**, 757

- (1976).
- ⁴²R. Ludeke and L. Ley, *Proceedings of the 14th International Conference on the Physics of Semiconductors, Edinburgh, 1978*, edited by B. L. H. Wilson (IOP, Bristol, 1978), Chap. 28, p. 1069.
- ⁴³A. Zunger, Phys. Rev. B **22**, 959 (1980).
- ⁴⁴G. P. Williams, R. J. Smith, and G. J. Lapeyre, J. Vac. Sci. Technol. **15**, 1249 (1978).
- ⁴⁵A. Huijser, J. van Laar, and T. L. van Rooy, Phys. Lett. **65A**, 337 (1978).
- ⁴⁶K. C. Pandey and J. C. Phillips, Phys. Rev. Lett. **32**, 1433 (1974).
- ⁴⁷S. Brennan, J. Stöhr, R. Jaeger, and J. E. Rowe, Phys. Rev. Lett. **45**, 1414 (1980).
- ⁴⁸F. H. Himpsel, D. E. Eastman, P. Heimann, B. Reihl, C. W. White, and D. M. Zehner, Phys. Rev. B **24**, 1120 (1981).
- ⁴⁹F. J. Himpsel, P. Heimann, T.-C. Chiang, and D. E. Eastman, Phys. Rev. Lett. **45**, 1112 (1980).
- ⁵⁰D. Chadwick and M. A. Karolewski, J. Electron Spectrosc. **24**, 181 (1981).
- ⁵¹J. Szajman, J. G. Jenkin, J. I. Egang, and R. C. G. Leckey, J. Electron Spectrosc. **14**, 41 (1978).
- ⁵²R. W. Grant, J. R. Waldrop, S. P. Kowalczyk, and E. A. Kraut, J. Vac. Sci. Technol. **19**, 477 (1981).
- ⁵³W. E. Spicer, I. Lindau, P. Skeath, and C. Y. Su, J. Vac. Sci. Technol. **17**, 1019 (1980).
- ⁵⁴J. Chelikowsky, D. J. Chadi, and M. L. Cohen, Phys. Rev. B **2**, 2786 (1973).
- ⁵⁵F. Herman, C. D. Kuglin, K. F. Cuff, and R. L. Kortum, Phys. Rev. Lett. **11**, 541 (1963).

VALENCE-BAND DISCONTINUITIES FOR ABRUPT (110), (100), AND (111) ORIENTED Ge-GaAs HETEROJUNCTIONS

J.R. WALDROP, E.A. KRAUT, S.P. KOWALCZYK and R.W. GRANT

Rockwell International, Microelectronics Research and Development Center, Thousand Oaks, California 91360, USA

Received 30 September 1982; accepted for publication 10 November 1982

Valence-band discontinuities, ΔE_v , have been derived from XPS data on abrupt Ge-GaAs interfaces for five different crystallographic orientations. The ΔE_v values for epitaxial Ge layers grown on (111)Ga, (100)Ga, (110), (100)As, and (111)As GaAs substrates are 0.48, 0.55, 0.56, 0.60 and 0.66 eV, respectively.

1. Introduction

Considerable electron spectroscopic evidence has been reported which shows that semiconductor heterojunction band discontinuities depend on microscopic details of interface structure [1-8]. Much of this evidence has been reviewed in these proceedings [9-11] and will not be repeated here. It has previously been pointed out [1,2,6] that crystallographic orientation is among those factors which influence the magnitude of the band discontinuities of Ge-GaAs heterojunctions. In our initial X-ray photoelectron spectroscopy (XPS) study of Ge-GaAs heterojunctions [1,2], we reported relative changes in valence-band discontinuity with crystallographic orientation because the core-level binding energies required to determine absolute values were not known with good precision. These binding energies have now been determined [12,13] and in this brief contribution we report absolute values of valence-band discontinuities for five different crystallographically oriented Ge-GaAs interfaces.

2. Summary of experimental details

Only a summary of the XPS experiment and sample preparation are given here; additional information may be found in ref. [2]. The ΔE_v measurement by XPS is illustrated with a schematic energy-band diagram in fig. 1. The quantities E_c , E_v , ΔE_c , ΔE_v , $E_{\text{Ge}3d}^{\text{GaAs}}$, and $E_{\text{Ge}3d}^{\text{Ge}}$ are the conduction-band

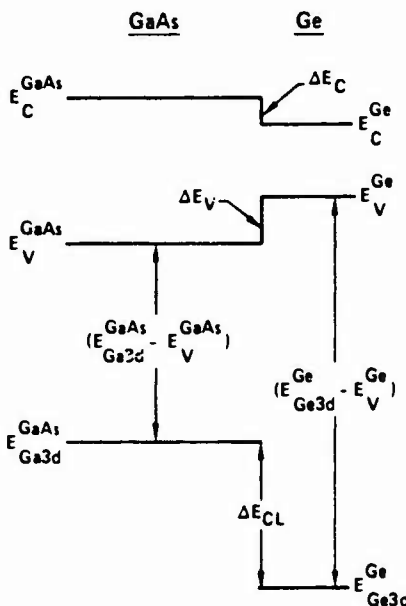


Fig. 1. Schematic energy-band diagram which illustrates the XPS determination of ΔE_v for an abrupt Ge-GaAs heterojunction.

minimum, the valence-band maximum, the conduction-band discontinuity, the valence-band discontinuity, the Ga 3d binding energy in GaAs, and the Ge 3d binding energy in Ge; $\Delta E_{C1} = E_{Ge3d}^{Ge} - E_{Ga3d}^{GaAs}$. From inspection of the figure it is clear that

$$\Delta E_v = (E_{Ge3d}^{Ge} - E_v^{Ge}) - (E_{Ga3d}^{GaAs} - E_v^{GaAs}) - \Delta E_{C1}. \quad (1)$$

A HP 5950A XPS spectrometer which employs Al K α ($h\nu = 1486.6$ eV) radiation was used for the measurements. GaAs substrates with (110), (100) and (111) orientations were all cut from the same boule of $\approx 10^{15}$ cm $^{-3}$ p-type material. The substrate orientation was confirmed with Laue back reflection X-ray photography. Following chemical lapping, each substrate was etched in freshly prepared 3:1:1 H₂SO₄:H₂O₂:H₂O prior to insertion into the XPS vacuum system. The substrates were cleaned by sputtering with 750 eV Ar⁺ ions and annealed at $\approx 460^\circ\text{C}$ to remove sputter damage. The (110)Ga surface was obtained by slowly increasing the annealing temperature until the $\alpha(8 \times 2)$ LEED pattern was observed. Surface cleanliness was assessed by XPS and the removal of sputter damage was confirmed by low energy electron diffraction (LEED). Prior to growth of Ge epitaxial layers, the room temperature GaAs substrate LEED patterns were (110) (1 \times 1), (111)Ga (2 \times 2), (111)As (1 \times 1)

Table 1
Ge epitaxial layer thickness, Ge 3d-Ga 3d binding energy differences, and valence-band discontinuities for various Ge-GaAs interfaces

Substrate surface	Ge layer thickness (Å)	$\Delta E_{\text{Cl}}^{\text{a})}$ (eV)	$\Delta E_v^{\text{b})}$ (eV)	$(\Delta E_v)_{\text{Av}}$ (eV)
(111)Ga (2×2)	13	10.27	0.50	0.48
	20	10.31	0.46	
(100)Ga c(8×2)	22	10.22	0.55	0.55
(110) (1×1)	14	10.20	0.57	0.56
	17	10.21	0.56	
(100)As -	14	10.17	0.60	0.60
(111)As (1×1)	13	10.11	0.66	0.66
	18	10.10	0.67	

^{a)} Error limits are ± 0.01 eV.

^{b)} Error limits are ± 0.04 eV.

and (100)Ga c(8×2); the (100)As LEED pattern was either c(2×8) or (2×4).

Very thin (≈ 20 Å thickness) epitaxial layers of Ge were grown at ≈ 1 Å/s deposition rates under ultra high vacuum (UHV) conditions on GaAs substrates at a growth temperature of $\approx 340^\circ\text{C}$ [14]; the Ge overlayer thicknesses are given in table 1. Samples were cooled to near room temperature within minutes after growth and LEED was used to confirm the epitaxy of the Ge overlayers. The XPS measured ΔE_{Cl} values for five different crystallographically oriented Ge-GaAs interfaces were previously reported in ref. [1] and are reproduced in table 1.

Several epitaxial growth and diffusion studies of Ge-GaAs interfaces under UHV conditions have been reported in the past few years [3,6,8,15-22]. There appears to be a fairly narrow growth temperature range from about 300 to 350°C [3,15] in which abrupt rather than interdiffused junctions can be prepared. Also, for slow growth rates (≤ 1 Å/min), As (and even traces of Ga) are found to segregate on the growing Ge surfaces [8]. These studies tend to confirm the conclusion that the interfaces which we studied were abrupt.

3. ΔE_v results

To determine ΔE_v from eq. (1) and the measured values of ΔE_{Cl} given in table 1 (from ref. [1]), it is necessary to know $(E_{\text{Ge}3d}^{\text{Ge}} - E_v^{\text{Ge}})$ and $(E_{\text{Ga}3d}^{\text{GaAs}} -$

E_v^{GaAs}) in bulk Ge and GaAs respectively. The primary difficulty in determining precise values for these quantities is the determination of the E_v position in XPS data. A mathematical method to accomplish this determination has been reported [12]. Kraut et al. [13] have very recently refined this method by considering, among other things, the GaAs(110) (1 × 1) surface chemical shift results of Eastman et al. [23]. These surface chemical shift results were used to correct the XPS measured values of $(E_{\text{Ga}3d}^{\text{GaAs}} - E_v^{\text{GaAs}})$ and $(E_{\text{As}3d}^{\text{GaAs}} - E_v^{\text{GaAs}})$ to obtain the bulk values of 18.80 ± 0.03 and 40.79 ± 0.03 respectively. Although surface chemical shifts have not yet been measured on Ge(110) surfaces, it is argued [13] that if these shifts are predominately associated with initial state charge transfer, they should have little effect on the XPS measured value of $(E_{\text{Ge}3d}^{\text{Ge}} - E_v^{\text{Ge}}) = 29.57 \pm 0.03$ eV.

The above values of $(E_{\text{Ga}3d}^{\text{GaAs}} - E_v^{\text{GaAs}})$ and $(E_{\text{Ge}3d}^{\text{Ge}} - E_v^{\text{Ge}})$ are combined with the measured ΔE_{Cl} values given in table 1 to calculate ΔE_v from eq. (1) for the eight individual interfaces (five different crystallographic orientations) and the results are listed in table 1. Average valence-band discontinuity values, $(\Delta E_v)_{\text{Av}}$, for the different crystallographic orientations are also listed in the table.

4. Discussion

There has been considerable discussion in these proceedings [9–11] about microscopic interface contributions to ΔE_v values. It is important to note from table 1 that for Ge-GaAs interfaces prepared under as nearly identical conditions as possible the ΔE_v results have small variation. This is best demonstrated by the reproducibility of the ΔE_{Cl} values rather than the ΔE_v values; the ΔE_v values include the uncertainty of $(E_{\text{Ga}3d}^{\text{GaAs}} - E_v^{\text{GaAs}})$ and $(E_{\text{Ge}3d}^{\text{Ge}} - E_v^{\text{Ge}})$. The only significant variation is observed for the two interfaces formed on the GaAs (111)Ga (2 × 2) surface; here the difference is only 0.04 eV. As the various electron spectroscopic techniques for determining band discontinuities continue to be refined and the precision of the measurements improve, it is quite probable that sample preparation dependent differences in measured values of Ge-GaAs(110) heterojunctions will exist. The reproducibility of the ΔE_{Cl} results shown in table 1 for Ge layers grown on (111)Ga, (110) and (111)As GaAs surfaces indicates that it will be possible to systematically study the effects of such sample preparation factors as growth temperature, growth rate, annealing, doping, and substrate preparation on the magnitude of ΔE_v .

Values of ΔE_v for epitaxial Ge-GaAs(110) heterojunctions have been reported by two other groups; the results are 0.42 ± 0.1 eV [8] and 0.25 eV [24] (the error limits derived from fig. 3 of ref. [24] appear to be $\approx \pm 0.07$ eV). The ΔE_v results reported here agree with the results of Mönch et al. [8]; it remains

to be seen if growth dependent variations can account for the substantially lower result reported in ref. [24]. Bauer and Mikkelsen [6] have studied the Ge-GaAs(100) interface and have concluded that ΔE_v is independent of the starting As surface stoichiometry to within ± 0.1 eV or better. In addition they find that ΔE_v is over 0.1 eV greater than that determined for the Ge-GaAs(110) interface. Referencing this latter result to the $\Delta E_v = 0.42 \pm 0.1$ eV Ge-GaAs(110) determination by Mönch et al. [8] mentioned above, gives ΔE_v , Ge-GaAs(100) > 0.52 eV. The ± 0.1 eV independence of ΔE_v for Ge-GaAs(100) interfaces on initial surface stoichiometry is completely consistent with our results as is the estimated lower limit of ΔE_v .

As a final point we mention the need for information on interface chemical shifts. When electron spectroscopic heterojunction measurements which involve core-level binding-energy differences are used to determine ΔE_v from eq. (1), the results will clearly be affected by the chemical shifts associated with interface bonds. This possible complication has been noted by Margaritondo et al. [25]. For the Ge-GaAs heterojunction one might expect this effect to be small due to the similarity of the electronegativities of the elements involved. The recent results of Mönch et al. [8] support this conjecture. They observe that the difference in binding energies between the As 3d and Ga 3d core levels for a clean, cleaved GaAs (110) surface increases by 0.15 eV at a 1.5 monolayer coverage of Ge due to the removal of the GaAs free surface reconstruction. We have reanalyzed our data associated with the Ge-GaAs(110) interfaces mentioned in table 1. Our XPS measured binding-energy difference on the clean GaAs(110) (1×1) surface is 21.92 ± 0.01 eV which yields a Ga 3d to As 3d binding-energy separation of 21.99 ± 0.02 eV for bulk GaAs when surface chemical shift corrections are made [13]. The Ga 3d to As 3d binding-energy difference observed when there is a Ge overlayer of ≈ 15 Å thickness present is 22.01 ± 0.05 eV [26]. This binding-energy difference agrees with the bulk value of 21.99 ± 0.02 eV mentioned above and confirms the observations of Mönch et al. [8] when the different escape depths of the two experiments are considered. The fact that the Ga 3d to As 3d binding-energy difference observed for the Ge-GaAs(110) heterojunctions is the same to within experimental error as the bulk GaAs value, supports the previously mentioned expectation that interface chemical shifts at the Ge-GaAs heterojunction should be small (smaller than for the reconstructed GaAs(110) free surface). Thus although there is a clear need for future work to obtain information on interface chemical shifts in general, there is no evidence that these shifts will substantially affect the Ge-GaAs heterojunction ΔE_v analysis.

Acknowledgment

This work was partially supported by the US Office of Naval Research Contract No. N00014-76-C-1109.

References

- [1] R.W. Grant, J.R. Waldrop and E.A. Kraut, Phys. Rev. Letters 40 (1978) 656.
- [2] R.W. Grant, J.R. Waldrop and E.A. Kraut, J. Vacuum Sci. Technol. 15 (1978) 1451.
- [3] R.S. Bauer and J.C. McMenamin, J. Vacuum Sci. Technol. 15 (1978) 1444.
- [4] J.R. Waldrop and R.W. Grant, Phys. Rev. Letters 43 (1979) 1686.
- [5] J.R. Waldrop, S.P. Kowalczyk, R.W. Grant, E.A. Kraut and D.L. Miller, J. Vacuum Sci. Technol. 19 (1981) 573.
- [6] R.S. Bauer and J.C. Mikkelsen, Jr., J. Vacuum Sci. Technol. 21 (1982) 491.
- [7] S.P. Kowalczyk, E.A. Kraut, J.R. Waldrop and R.W. Grant, J. Vacuum Sci. Technol. 21 (1982) 482.
- [8] W. Monch, R.S. Bauer, H. Gant and R. Murschall, J. Vacuum Sci. Technol. 21 (1982) 498.
- [9] G. Margaritondo, Surface Sci. 132 (1983) 000.
- [10] R.S. Bauer, Surface Sci. 132 (1983) 000.
- [11] H. Kroemer, Surface Sci. 132 (1983) 000.
- [12] E.A. Kraut, R.W. Grant, J.R. Waldrop and S.P. Kowalczyk, Phys. Rev. Letters 44 (1980) 1620.
- [13] E.A. Kraut, R.W. Grant, J.R. Waldrop and S.P. Kowalczyk, Phys. Rev. in press.
- [14] Our sample temperature was measured by a thermocouple attached to the sample heater. The initially reported (refs. [1] and [2]) growth and annealing temperatures have been reduced by 20% as an approximate correction for the temperature drop between the thermocouple and sample surface; see also J. Vacuum Sci. Technol. 19 (1981) 477.
- [15] R.Z. Bachrach and R.S. Bauer, J. Vacuum Sci. Technol. 16 (1979) 1149.
- [16] W. Monch and H. Gant, J. Vacuum Sci. Technol. 17 (1980) 1094.
- [17] G. Margaritondo, N.G. Stoffel, A.D. Katnani and L.J. Brillson, Appl. Phys. Letters 37 (1980) 917.
- [18] H.M. Clearfield, D.G. Welkie and M.G. Lagally, J. Vacuum Sci. Technol. 18 (1981) 802.
- [19] C.A. Chang, W.-K. Chu, E.E. Mendez, L.L. Chang and L. Esaki, J. Vacuum Sci. Technol. 19 (1981) 567.
- [20] R.S. Bauer, Thin Solid Films 89 (1982) 419.
- [21] R.A. Stall, C.E.C. Wood, K. Board, N. Dandekar, L.F. Eastman and J. Devlin, J. Appl. Phys. 52 (1982) 4062.
- [22] J.M. Ballingall, R.A. Stall, C.E.C. Wood and L.F. Eastman, J. Appl. Phys. 52 (1982) 4098.
- [23] D.E. Eastman, T.-C. Chiang, P. Heimann and F.J. Himpsel, Phys. Rev. Letters 45 (1980) 656.
- [24] P. Perfetti, D. Denley, K.A. Mills and D.A. Shirley, Appl. Phys. Letters 33 (1978) 667.
- [25] G. Margaritondo, A.D. Katnani, N.G. Stoffel, R.R. Daniels and Te-Xiu Zhao, Solid State Commun. 43 (1982) 163.
- [26] The precision of this measurement is degraded by the presence of intense Ge loss peaks in the energy vicinity of the As 3d line.